PHD

The influence of level and rate of pre-strain on creep deformation in 1Cr. Mo. V. steel.

Hodgson, B. J. R.

Award date:
1970

Awarding institution:
University of Bath

The Influence of Level and Rate of Pre-Strain on Creep Deformation in 1Cr.Mo.V. Steel

Submitted by

B.J.R. Hodgson A.C.T., A.I.M.

for the Degree of Doctor of Philosophy

of Bath University of Technology

1970

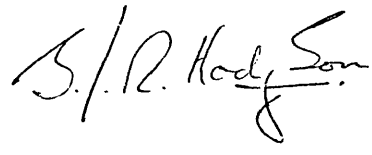

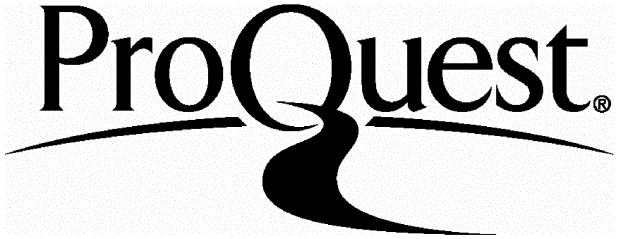

PREFACE

The work contained in this thesis was performed by the author during the period 1967 to 1970 whilst a student of Bath University of Technology and employed by the Central Electricity Generating Board.

This thesis is the author's own work except where duly acknowledged in the text. No part of it has been submitted in support of an application for another degree to this or any other University.

INDEX

SUMMARY

The response of the creep behaviour of 1Cr.Mo.V. steel to both rapid and slow loading or pre-straining has been examined at 550°C and at stresses between 180 N/mm^2 and 270 N/mm^2.

In the ferrite-pearlite condition the creep rate has been shown to exhibit a dependence on particle spacing which is in turn dependent upon the rate of initial loading or pre-straining. A general expression for the creep rate is given by the equation

$$\dot{\varepsilon}_s = K.\sigma^{12}.\lambda^{2.5}$$

where $\dot{\varepsilon}_s$ is the steady state creep rate, K is a constant, σ is the applied stress and λ the interparticle spacing of second phase precipitates.

The high activation energy of $\sim$ 100 kcal/mol is attributed to both the climb distance for dislocations to move past particles and to the mechanism by which they climb. The mechanism is probably a stress dependent one such as the operation of Bardeen-Herring sources.

A previously assumed equivalence of creep strain and prior plastic strain has been shown to be invalid.

Slow initial loading results in a considerable loss of creep resistance. The decrease in properties is not so severe if a slow pre-strain is given but increasing the amount of pre-strain does not overcome the adverse effects of slow deformation.

Rapid initial loading gives the best properties; pre-straining rapidly occasions a decrease of creep resistance which is inversely proportional to the amount of pre-strain.

A nominally constant strain to failure was obtained for both slowly and rapidly loaded tests. In this respect the material may be

considered to consist of a ductile matrix in which the deformation rate but not quantity is determined by second phase particles.

SYMBOLS

σ	stress
$\dot{\varepsilon}$	strain rate
ε	strain
t	time
T	temperature, qualified where necessary by ^{o}C or ^{o}K
T_m	melting temperature in ^{o}K
R	gas constant
Q	activation energy
ρ	density
E	Young's modulus

Subscripts

c	creep
t	tertiary
f	failure
p	plastic
E	elastic
s	steady state

1. INTRODUCTION

1.1 Background to the Research

The C.E.G.B. has a total of 742 steam turbine generating sets which are capable of delivering 46,000 MW. Many of these sets are old, small but reliable and the trend is continually to produce equally reliable larger generating sets culminating in the latest giants, Figures 1 and 2. These new sets, of which there are a mere 16, constitute about 1/6th of the total generating capacity. By the end of 1973 these large 'sets' will produce nearly half of the 67,000 MW then available.

Obviously the failure of one of these is of far greater importance than the failure of a small set and it would be completely unrealistic to assume 100% reliability. Furthermore the expected life is a quantity which needs to be known to enable the Board's capital investment programme to be formulated intelligently and in such a manner that future demands can be met.

Thus the expected life as a whole and the integrity of its individual components is now, more than ever, a major cause for concern in the Board. The justification for this concern is that the large generators cannot be regarded simply as physically larger since this would imply a straightforward assessment of importance based on the size factor. In pure economic terms this is valid but hand in hand with increasing size goes increasing temperature. From the standpoint of material behaviour the most significant change in design parameter is not in size but in the steam temperatures at the turbine inlet of 565°C compared to the previous temperatures of 450°C or less. Thus the possible deformation modes of the Cr.Mo.V. type steels used now include those dependent upon self-diffusion and a fresh approach is required to predicting the service behaviour of these materials.

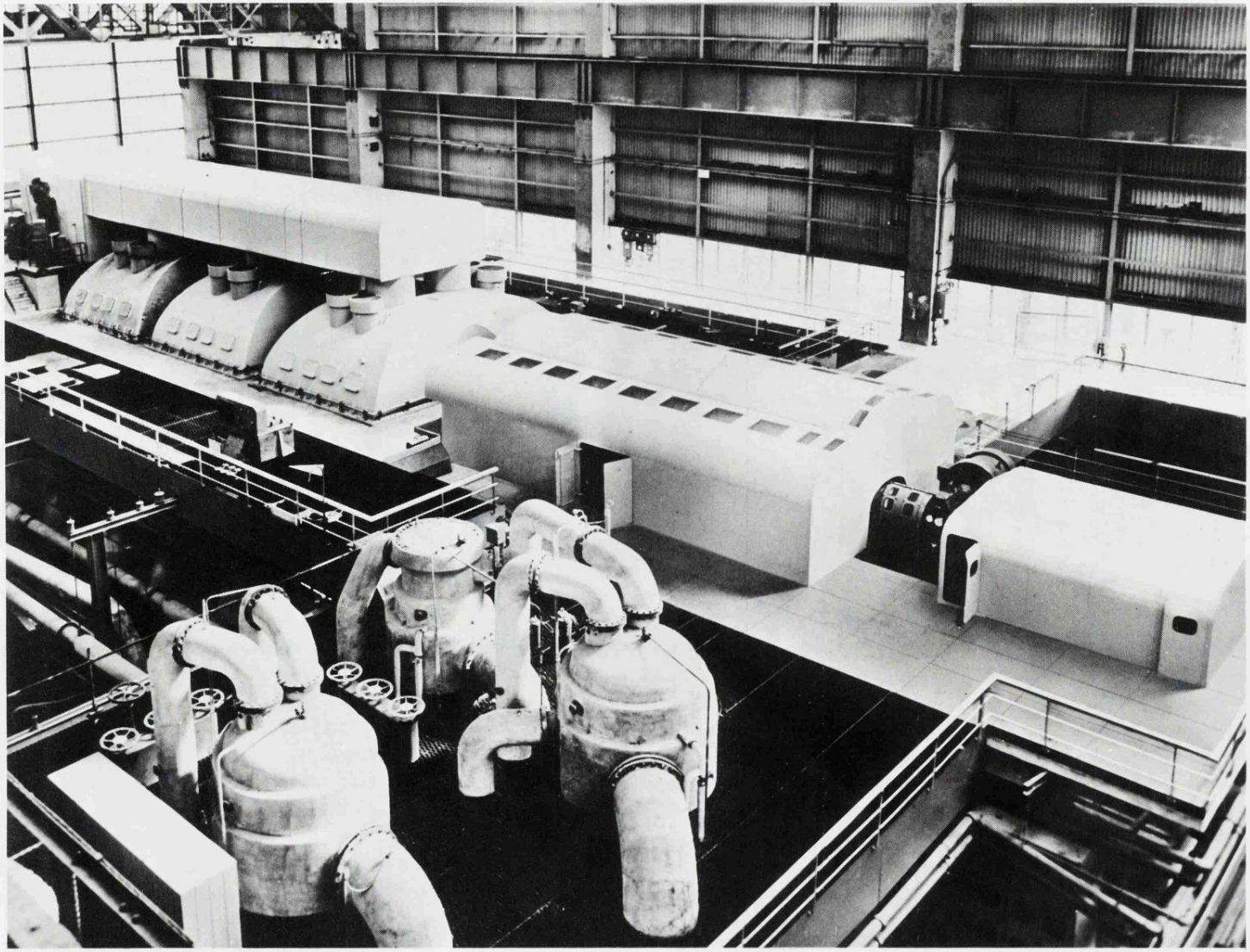

FIGURE 1 GENERAL VIEW OF A 500 MW TURBINE

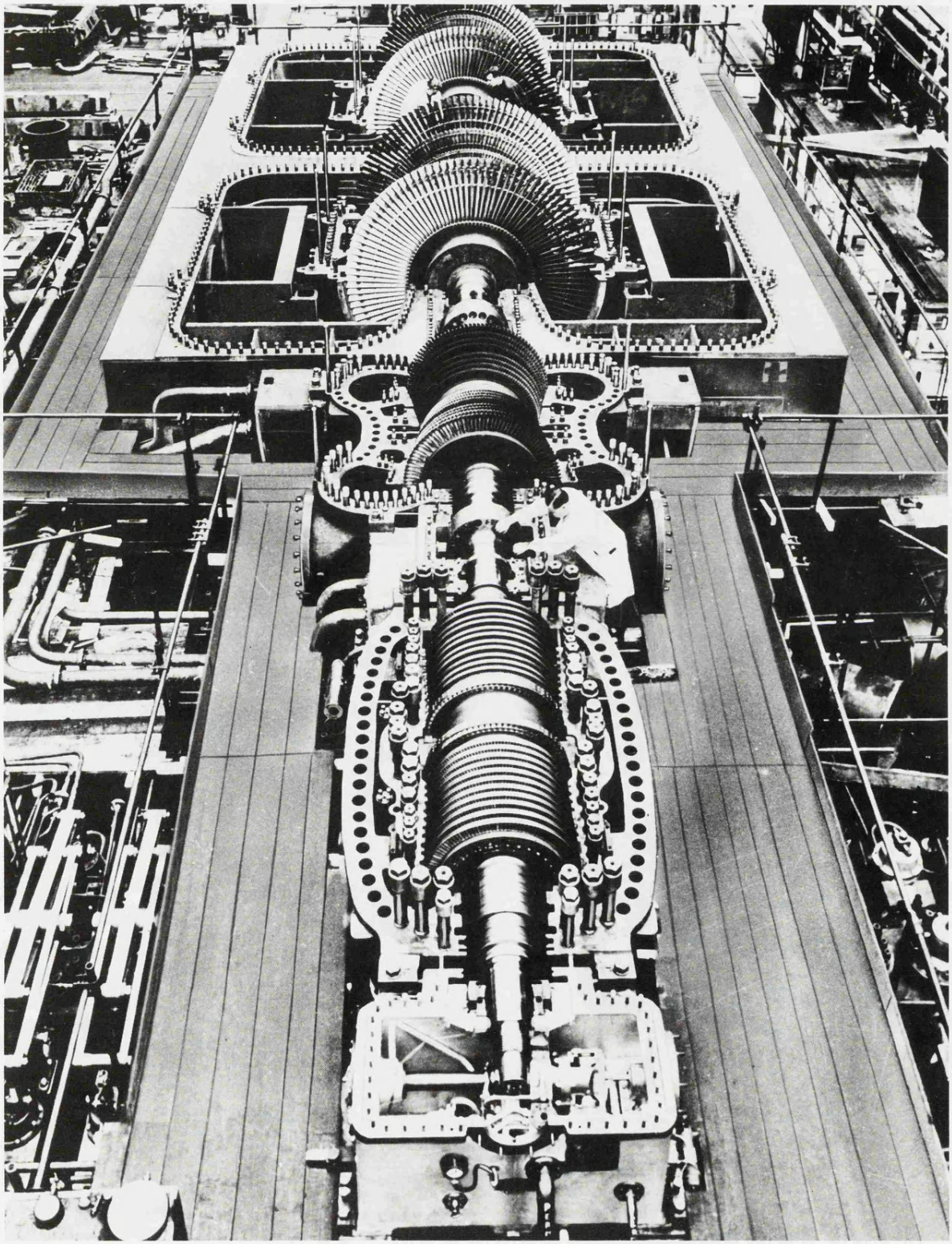

FIGURE 2 500 MW TURBINE ROTOR AND CASING

Part of the research effort is therefore directed towards predicting service behaviour which is a complex problem soluble largely by computer programs since the large sets are, it is hoped, still in the early part of their lives and running experience is limited.

The stress analysts are obliged to make many assumptions when attempting these predictions which are based on limited temperature and stress/strain data. Computation of the stress/strain patterns in non-axysymmetric components such as casings and even axysymmetric parts such as rotors poses severe analytical problems because of the dearth of operating data.

The materials scientist can play a vital role in these circumstances by examining some of the assumptions which are made. In general this type of work falls into the category of cumulative damage and materials behaviour, a wide subject and one which has been approached in many ways by a great many people. The outcome of this work is that there are a multitude of empirical laws which are of use in a limited way and a wide variety of papers describing the results of specific tests. As yet there is no reliable way of summing damage such as creep plus fatigue plus hold times in uniaxial let alone multiaxial regimes.

The work described in this thesis was designed to give information on quite small but important facets of cumulative damage to aid the stress analyst.

1.2 Objectives

The objectives are fourfold and may be simply stated thus:

1. to test the equivalence of plastic strain and creep strain,
2. to examine the effect of loading rate on creep behaviour,
3. to define the cause(s) of any loading rate dependence of creep behaviour, and

4. to put the results of this research into the form most likely to aid design and service behaviour predictions pertinent to commercial applications of 1Cr.Mo.V. steel.

1.3 Selection of the Experimental Method

Initially this was not the choice of the author since the question "Are plastic strain and creep strain equivalent?" had already been posed and the creep machine and associated hydraulics was already in existence.

The author's first task was to commission the machine using existing specimens. Originally the hydraulic ram connected to the specimen stringer (described in 2.2) was controlled and programmed by a mechano-electrical analogue device. During commissioning the control mechanism for the hydraulics was replaced by a totally electrical system, described in Appendix 1. The parameters of this unit were defined by problems associated with the rig and with flexibility of control.

Nevertheless, the basic system of a creep machine capable of being used as a sophisticated tensile testing machine was quite logical and it is not easy to think of an equally effective alternative system.

The selection of 550^{o}C as the test temperature was realistic since it approximated to the highest operating temperatures of generating plant. This leads to higher and therefore more viable laboratory creep rates commensurate with practical conditions. The choice of 270 N/mm^2 as the stress for the pre-strain tests and for the upper limit of stress in the loading rate tests, was simply to keep test times as short as possible. Previous work by Myers (1968)[54] had shown that results could be extrapolated with confidence down to the upper limit of plant stresses at about 120 N/mm^2. Thus it was considered that the

use of high stress was justified since only one creep machine was available for these tests.

When the loading rate tests were initiated it was decided to use the same temperature and to use a range of stresses from that used for pre-strain to upper plant stresses. The aim was to be able to correlate both sets of tests and to link up with plant conditions. The modifications carried out on the rig during service were all designed to nullify specific problems or to answer specific questions. Examples are the temperature compensation of the extensometry to nullify ambient temperature changes and electronic modifications to smooth the ram operation.

1.4 Some Aspects of the Microstructural Dependence of Creep Rate

1.4.1 General

The effect of pre-strain and pre-strain rate upon creep rate is not a discrete one but rather a manifestation of much wider influences.

The creep rate at temperatures from ~ 0.4 to ~ 0.9 Tm may be described by an expression such as $\dot{\varepsilon} = f(\sigma).f(T).f(S)$ where σ and T have the usual meaning and f(S) is a function of structure. Taking these functions individually the first two are adequately described by the expressions

$$\dot{\varepsilon} = C.\sigma^{n} \qquad (1)$$

and

$$\dot{\varepsilon} = A.e^{-Q/RT} \qquad (2)$$

where A and C are constants. The unknowns in each of these equations are readily obtained by converting them into the standard $y = mx + c$ form by taking logs or plotting on log-log axes. Thus standard creep data over a range of stresses and temperatures provide all the

information necessary to obtain the dependence of creep rate on these parameters.

However no expression describes the overall dependence of creep rate upon the structure. Attempts have been made to fit equations to structural parameters but these have limited scope and application. In practice it is rare to have an engineering material in which the second phase, precipitate, solute etc. have predictable form, spacing and distribution. Add grainsize, subgrain size, dislocation density to these variables and the reasons for large tolerances and safety factors are not hard to envisage. The steel used in the tests described in this thesis is receiving a great deal of attention from both manufacturers and users all over the world because of its variable properties. Commercially it is attractive but properties vary very widely even though more and more stringent specifications are evolved. In a large turbine rotor the structure can vary from ferrite/pearlite right through the range of bainites, the range of creep properties is shown in Figure 3. Even if one structure is tested the results of creep tests may have a wide spread. Figure 4 shows a set of results obtained from one batch of material tested by three test houses of repute, the variation is immediately apparent. The effect of varying the structure by testing different batches from differing production routes will be to magnify these 'errors'. The stress analyst faced with the problem of predicting the life of a component must therefore use results from the limits of reliable data. This may well produce widely differing predictions but at present such a state of affairs must be accepted and not ignored. If it is commercially worthwhile to predict the life of components then it follows that predictable microstructures are desirable and the cost of (a) understanding and (b) producing these materials should be accepted.

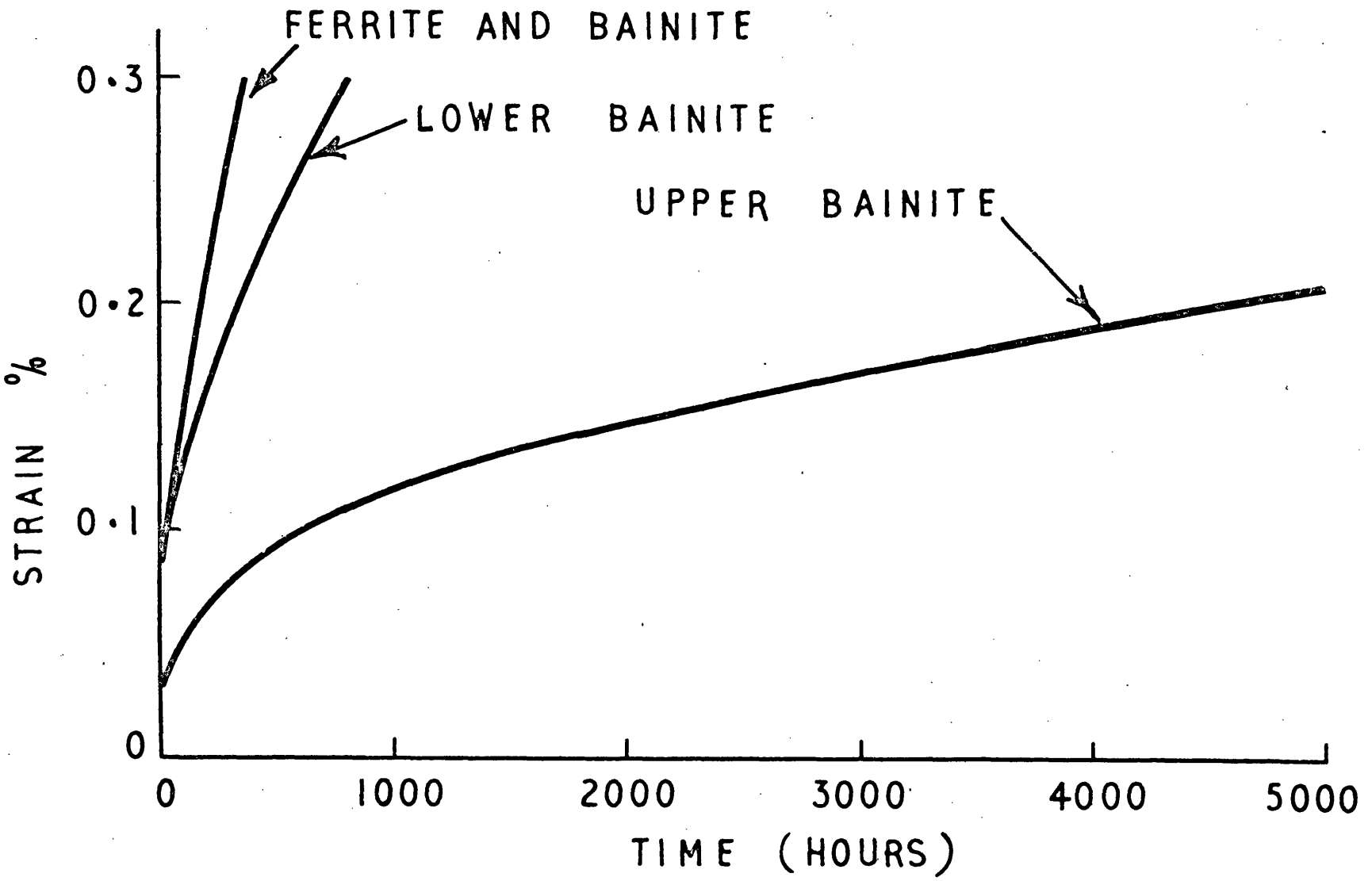
FERRITE AND BAINITE
LOWER BAINITE
UPPER BAINITE
STRAIN %
0·3
0·2
0·1
0
0
1000
2000
3000
4000
5000
TIME (HOURS)

FIGURE 3

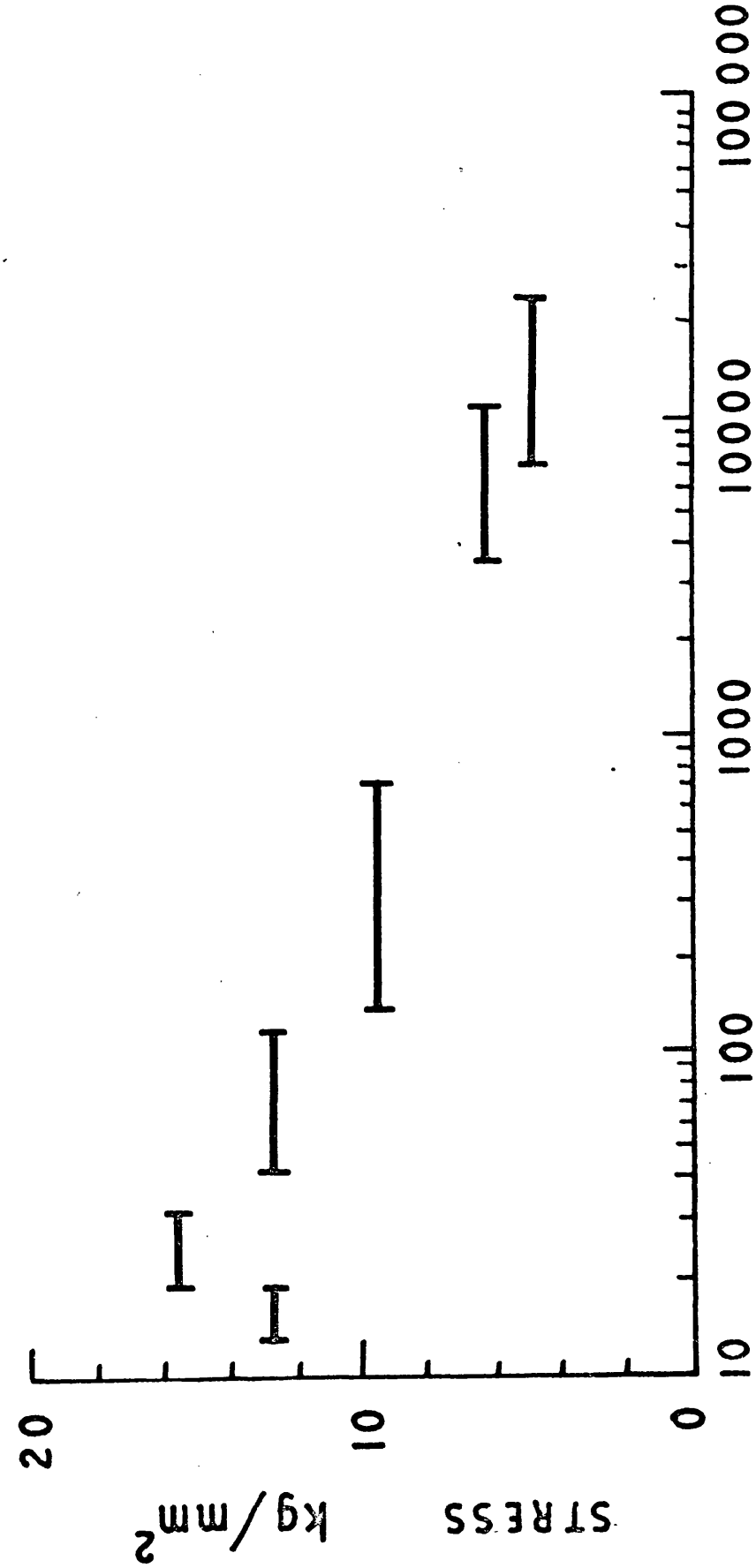
STRESS kg/mm²
20
10
0
10
100
1000
10000
100 000
TIME FOR 1·0% CREEP, HOURS.

FIGURE 4

A great deal of work has been completed in recent years which is leading to an understanding of the role of structure in creep. Some approaches examine the mechanisms in general, others investigate the parameters relevant to specific materials. However, most researches have underlying common themes such as recovery, grain boundary movements and the role of diffusion. An appreciation of facets such as these is essential in determining the cause(s) of the pre-strain and pre-strain rate effects discussed in later sections since creep behaviour is directly dependent on them. In the following sub-sections only those aspects pertinent to the later sections will be discussed.

1.4.2 Rate controlling factors

The Bailey-Orowan relationship $\dot{\varepsilon} = r/h$ (where r is the recovery rate and h the work hardening coefficient) is widely accepted as a simple but generally accurate statement of the relationship between the major parameters in creep. Mitra and McLean (1967)[50], using stress reduction tests, showed that this relationship held for secondary creep rates in nickel and aluminium. A feature of this work was that having established a sub-grain size and dislocation density proportional to the initial stress a stress reduction resulted in a tendency to negative creep rates. This arises not only, as here, because of a stress reduction but in other types of test as well where a structure has been established by prior workhardening. The reason in both types is that the sub-structure has a smaller sub-grain size and greater dislocation density than would have arisen under constant load conditions hence recovery must occur. This is a logarithmic process and under creep conditions it is unlikely that it will ever proceed to completion. In fact in their case recovery was very limited, resulting in a lower creep rate than would have been achieved with constant load conditions. The inverse relationship between sub-grain size and workhardening has also been described by Ham (1967)[33] and Hodgson (1967, 1968)[35][37] in

other regimes. Sidey and Wilshire (1969)[64] have also reported work on the Bailey-Orowan relationship. In this case two alloys were used, one was Ni.20%Cr. and the other Nimonic 80A.

Ni.20%Cr., obeyed the relationship but confirmation was not readily obtained for Nimonic 80A. The implication is nevertheless that the relationship holds. They also deduce that the high creep resistance of the complex Nimonic alloy is due to retardation of recovery by the Ni_3 (Al, Ti) precipitate.

The role of precipitates is a major one in creep resistant alloys and deservedly receives a lot of attention. Many investigators are concerned with the form and type of precipitate, often complex, and the conditions of nucleation and growth. This approach is essential in order to understand the behaviour of a particular material or family of materials in the light of theoretical considerations of the effect of particle spacing and size upon creep properties. Some authors such as Garafalo et al. (1961)[22] describe the dependence of secondary creep strain in an austenitic steel as due to grainboundary carbides resisting migration of the boundaries. This is a general effect in such steels and in sophisticated alloys such as the Nimonic series. In the latter alloys there is a much greater effect from matrix precipitates such that together with the more massive carbides exists the fine dispersion of Ni_3 (Ti, Al) which imparts the major proportion of the creep strength. In the 1Cr.Mo.V. steels the role of the Ni_3 (Ti, Al) is taken by vanadium carbide commonly reported as V_4C_3. The carbides in this steel are varied and complex, most are stable and precipitate during transformation on the γ grain boundaries. Some confusion exists as to the exact stage at which V_xC_y is formed. Norton and Strang (1969)[57], Murphy and Branch (1969)[53], Bates and Ridal (1963)[6] and Prnka (1969)[60] state that it forms during

transformation and not during tempering; Jusko and Gut (1966)[41], Goldhoff and Beattie (1965)[32], report precipitation of this and other carbides during creep. Buchi et al. (1965)[9] also claim that vanadium carbide is formed during transformation but only in the upper knee of the CCT diagram at the γ-α interface - they do add however that copious FeC_3 suppresses V_xC_y formation. Myers et al. (1968)[55] reporting on creep behaviour of the material in the martensitic, bainitic and pearlitic condition indicated a belief that V_xC_y forms at high temperatures and is stable during short term tests. All of these workers except Myers et al., agree that it is the dispersion of vanadium carbide that determines the creep strength. Myers et al. found a high activation energy (95 kcal/mol) for the material under creep conditions above stress levels of 2 tsi. Whilst they agree with the other workers that V_xC_y spacing and creep strength have an inverse relationship they conclude that up to their maximum stress of 18 tsi a solute drag model applies. This is an unexpected result on a low alloy steel and is considerably at variance with the widely accepted models of recovery creep based on diffusion controlled climb and also of cross slip. Their results were well documented and analysed so that the activation energy obtained must be assumed correct. The solute-drag hypothesis is worth considering a little further. Discontinuous yielding occurs in some vanadium containing α steels and some niobium containing γ steels at lower temperatures. The proposal is that there is an interaction between these elements and dislocations for which a model was derived by Russel et al. (1968)[62]. Pinning of dislocations in the 1Cr.Mo.V. steel is considered to be due to carbon/vanadium pairs. Obviously this relies markedly upon the diffusion of vanadium and this is possible since the value of $\sim$ 60 kcal/mol is favourable. The proposal begins to break down at high strain rates, as

might be expected, since re-pinning of dislocations is dependent upon the vanadium migration rate. Other work which lends credence to the concept of 'solute' pinning is that of Goldhoff and Beattie (1965)[32] in which they calculate that the diffusion velocity of molybdenum in α iron is high enough at low creep rates to account for the precipitation of Mo_2C on dislocations in 1Cr.Mo.V. steels. The proposal here is that the ductility trough experienced at secondary creep rates of $\sim 10^{-8}$ cm/cm/hr may be explained by Mo_2C pinning of dislocations. The calculated diffusion velocity of molybdenum was an order higher than that of the dislocations. The choice of the solute drag model of Myers et al. was prompted by the rejection of the recovery model due to small inter-particle spacing and the high activation energy for creep. It is pertinent to question the relevance of their method for calculating inter-particle spacing. The use of planar analysis based on an area count is not necessarily the best, particularly when the carbides are of variable size. Assuming sphericity is something that has to be resorted to in the circumstances because of the shape complexity but a volumetric assessment may well have resulted in a smaller spacing value. From the work of Prnka (1969)[60] and his review of particle spacing computing methods, the value of spacing quoted by Myers may be too big by λ/d where λ is the spacing and d the particle diameter, Westmacott et al. (1966)[69]. Hirschorn and Ansell (1965)[34] state a preference for a volumetric analysis and Kocks (1966)[42] criticises the simple models pointing out that errors of 20% can arise in many cases. Prnka compared volumetric and planar methods directly and as shown by Figure 5 there is at least a 20% difference. Since Prnka's material is very similar to Myers' this is a valid point. It is very easy to unwittingly dogmatise when dealing with a parameter such as structure under these circumstances.

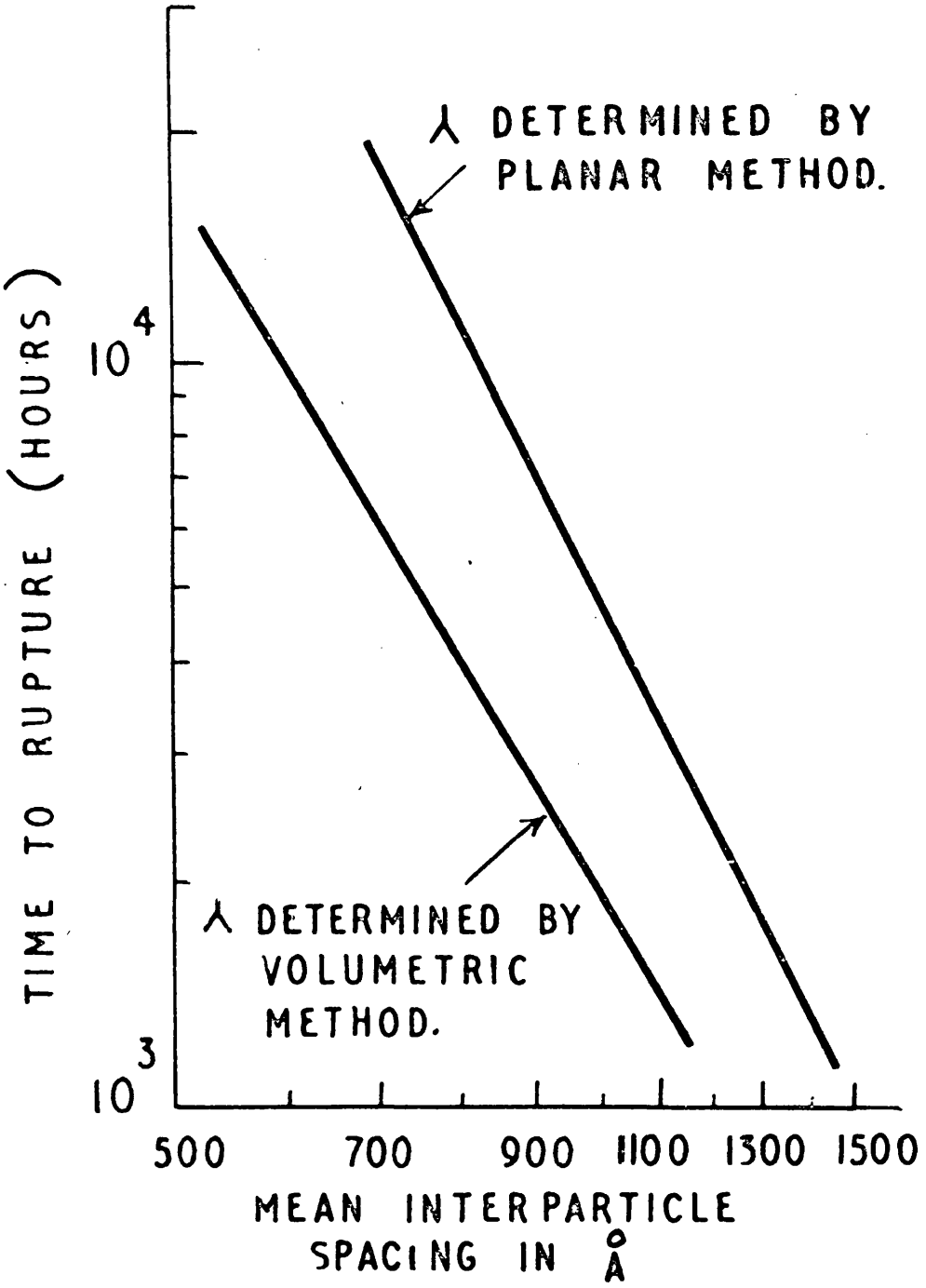

VANADIUM CARBIDE SPACINGS IN LOW ALLOY CR. MO. V. STEEL (PRNKA AND FOLDYNA)

FIGURE 5

Unfortunately, once a decision to accept one assumption as opposed to another is made it often becomes necessary to build upon this as though it were fact. In this way, from identical basic information, differing analyses can arise leading to quite different conclusions. In this case it strengthens Myers' initial argument that the stress to bow dislocations between particles was higher than the applied stress.

The departure from recovery creep mechanisms in Myers' work is unusual and should not let attention be drawn away from the importance of this aspect of creep rate dependence. The fact that at stresses up to 18 tsi, which is high for operational stresses in this material, the activation energy for creep remained at 95 kcal/mol is also unusual. A much more common value is in the region of 60 kcal/mol which corresponds to the value for the diffusion of vacancies and is quoted for recovery creep.

It has already been stated that dislocation interaction with 'defects', such as precipitates, imparts creep strength and that strength is inversely proportional to the defect-defect spacing. Commonly, the type of defects imparting strength are carbides and second phase particles. These are relatively easy to control in terms of size and distribution and the normal assessment of their role is to force dislocations either to bow between and leave loops or to prevent bowing leading to cross-slip, climb or cutting of particles. Another type of defect is simply the dislocation. McLean (1968)[47] points out that a fine dislocation network is the only glide resistance which is virtually unaffected by temperature. The elastic interaction between dislocations is certainly a very effective means of strengthening but as McLean remarks, maintaining a stable network is difficult. The rate controlling mechanism in creep therefore controls the frequency with which dislocations are released from pinning positions. Or in the case of

dislocation/dislocation interaction the rate at which jogs are permitted to climb or run out to the ends of dislocation segments. In recovery the rate controlling factor is the vacancy flux which appears in the steady state creep rate equation as D, viz

$$\dot{\varepsilon}_s = A\sigma^n D \qquad (3)$$

where D is the diffusion coefficient and A, n are constants. Usually D is included in the single constant of proportionality. McLean (1966)[46] discusses steady state creep and emphasises the tri-dimensionality of dislocation networks when considering the opposing mechanisms of recovery and hardening. Also discussed is the inhomogeneity of deformation, in practice slip occurs spasmodically but at a large number of points giving the overall impression of homogeneity. Thus the creep rates experienced in the majority of engineering materials depend directly upon recovery mechanisms and inversely upon those factors which impede recovery.

1.4.3 Creep failure

There are two main ways of approaching this topic, one from a mechanistic aspect and the other from an empirical aspect. Mechanistically it is satisfying to be able to define the process or processes leading to failure. In general such data are not directly applicable to either engineering design or service behaviour predictions. In the long term, work to define failure mechanisms may enable the producer and fabricator to market a material with a more predictable behaviour. Hence such research must logically be justified and in some areas has already been practically vindicated. One such instance is the modifying of the composition and heat treatments of 1Cr.Mo.V. steel for use in steam turbines. These modifications have not, it is true, arisen from a study of failure but of the general creep process in this

material and have led to a retardation of this process and hence, failure. The consideration of failure as an entity is a mistake which will be discussed later.

Empirically, creep data can be treated to give expressions relating stress, temperature, creep rate, total strain and the time to reach a particular stage of creep. It is very difficult to give scientific reasons for the success of such expressions but the engineer asks for little more than a quantitative expression which fits the material he is considering. There is ample justification for using these expressions but the limitations are not always appreciated. Woodford (1969)[72] successfully demonstrates this and shows that at low stress the index is not unity, as often stated, because the creep strain rates measured are rarely minima. They should be taken at constant strains for all stresses if the complete test curve is not available. Representative 'n' values will only be obtained at constant structure. For constant stress tests the strain rate must be measured at constant strain and in constant load tests only after the minimum creep rate is known to have been reached. Woodford's analysis is shown to be viable for long term 1Cr.Mo.V. tests by Marshall (1970)[49] and demonstrates the danger of examining linear plots of ε vs. t and, when the creep rate apparently becomes linear, assuming that secondary creep has commenced. Tests on this steel show that at low stresses the creep rate may be a primary rate for extremely long times, certainly up to five years at some operating conditions.

Many expressions have been derived to link the various creep parameters. One of the most straightforward of these, used by Monkman and Grant (1956)[51] and discussed at length by Garafalo (1965)[21] is

$$(\dot{\varepsilon}_s \times t_f) = \text{constant} = K \qquad (4)$$

It was apparently first recognised about forty years ago by H.J. French and has recently been used frequently. The origins of this expression lie with the basic creep curve and are easier to visualise than expressions and parameters based on stress-rupture data. Figure 6, essentially that given by Garafalo, is the basis of the expression. Inspection shows that

$$\dot{\varepsilon}_s = \frac{(\varepsilon_4 - \varepsilon_1)}{t_f} \qquad (5)$$

and if $(\varepsilon_4 - \varepsilon_1)$ is essentially constant with stress then equation (5) holds. Equation (4) is somewhat rigid however and both Marshall (1970)[49] and the author have shown that the slope of - 1 predicted by the equation is not necessarily found in practice. It is suggested that

$$(\dot{\varepsilon}_s^m \times t_f) = K \qquad (6)$$

is more satisfactory.

Most authors plot log t_f vs. log $\dot{\varepsilon}_s^m$ and in the form

$$\log t_f = K - m \log \dot{\varepsilon}_s \qquad (7)$$

the value of m is found to be between - 0.8 and - 1 for the low alloy Cr.Mo. steels in general. Often the term t_f is replaced by t_t and equally good fits are obtained.

By using different portions of Figure 6 other relationships can be derived thus

$$t_f = A(t_2 - t_1)^{\alpha} \qquad (8)$$

for the duration of secondary creep and

$$t_f = B(t_2)^{\beta} \qquad (9)$$

for the onset of tertiary. Remarkably good agreement is reached for these equations by Garafalo[21].

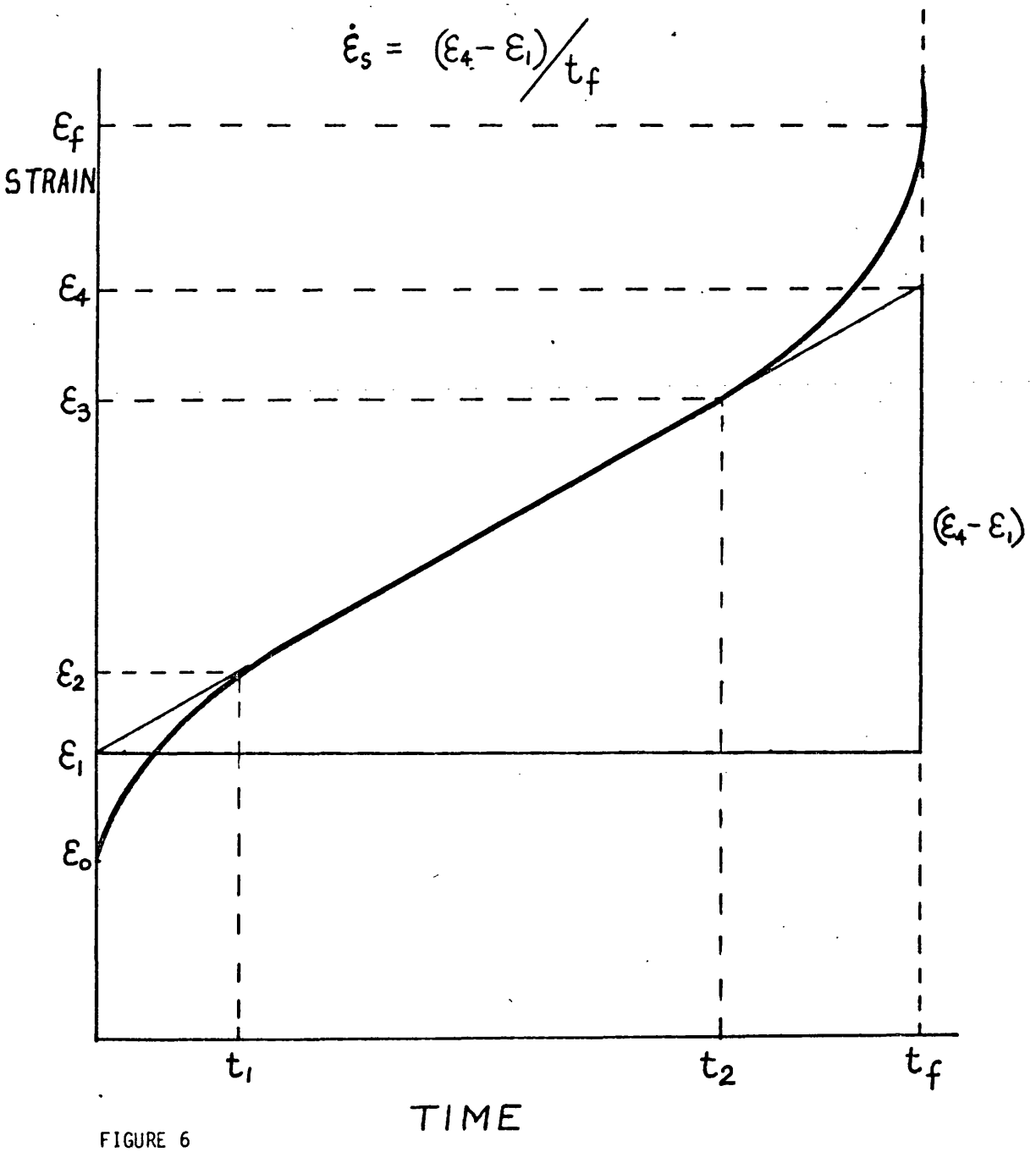
$\dot{\varepsilon}_s = (\varepsilon_4 - \varepsilon_1)/t_f$
ε_f
STRAIN
ε_4
ε_3
$(\varepsilon_4 - \varepsilon_1)$
ε_2
ε_1
ε_o
t_1
t_2
t_f
TIME

FIGURE 6

The point has already been made that the basis for these equations is easier to visualise than most. It is also true to say that it is easier to establish links between these equations and the underlying mechanisms. There are conflicting schools of thought on the failure modes operating in creep and one of these, the nucleation and growth of grainboundary cavities by ledge formation and grain-boundary sliding, is exemplified by the work at University College, Swansea. They find that several nickel alloys and pure nickel obey these relationships. Some of their work and that of the opposing school will be discussed later but references relevant to the present topic are Davies and Wilshire (1968)[18] for a nickel 0.1% palladium alloy, Davies et al. (1961)[13] on a nickel 0.1% gold alloy, Davies et al. (1963)[14] on pure nickel and nickel-gold, also Evans and Wilshire (1967)[20] on nickel-chromium.

Other references are Dennison et al. (1967)[19], Davies et al. (1964)[11] and the results of Woodford (1969)[72] which give good agreement when fitted to the equation. These last researches were made on Ni.20%Cr., Au, and steel. Thus the relationship holds for pure gold and nickel, dilute solid solutions, Ni.20%Cr. alloy (Swansea work), austenitic steel (Garafalo) and low alloy Cr.Mo. and Cr.Mo.V. steels (Berkeley work).

In the opening paragraph of this sub-section it was intimated that the consideration of failure as an entity was a mistake. Very rarely in high temperature regimes is failure a catastrophic or sudden phenomenon, more often it is a process which originates very early in life. Hodgson (1968)[37] has shown that in high temperature, high-strain fatigue, failure commences at $\sim$ 10% of life, Ratcliffe and Greenwood (1965)[61] show that cavity growth in creep of a Mg.Al. alloy commences virtually at the beginning of creep, Evans and Wilshire

(1967)[20] agree using a dilute Ni.Cr. alloy. Evans and Wilshire showed that a stress independence of the product ($t_f \times \dot{\varepsilon}_s$) occurs in a pre-strained Ni.1%Cr. alloy. They assume this to be proof that nucleation of cavities is specifically by ledge formation. It can certainly be accepted that nucleation occurs early in life, during primary creep. The results also show that nucleation is time dependent since rapid pre-strain at creep temperature fails to achieve the same effect. Evans and Wilshire are somewhat confusing in this respect since they write at first of ledges forming during initial extension and during primary creep. Yet if ledge formation is completely suppressed by pre-strain it follows that they do not form during instantaneous extension. The stress independence of the product may well be due to a change in the values of (t_f) in the pre-strained condition to account for the nucleation time required. Analysis of their results (which were not given) might give some indication of the time dependence of nucleation and whether it is modified by the sub-grain structure developed by pre-strain. It will be demonstrated in a later section (1.5) that the value of ($\dot{\varepsilon}_s$) may be changed also. Their results are also critically assessed in the Discussion, Chapter 4. In creep, failure is associated with the nucleation, growth and subsequent linking of voids by cracks. The process is the subject of a controversy since the origin and development of the voids is claimed on the one hand to be due to accumulation of vacancies and on the other to grainboundary sliding. Other work combines the two mechanisms.

Davies, Wilshire and co-workers at Swansea are the main supporters of the theory that during loading and primary creep the bulk of cavities are nucleated. The nucleation process is thought to be one of sliding occurring at suitably oriented grainboundary 'ledges'. These ledges may be schematically described by Figure 7 taken from Davies and

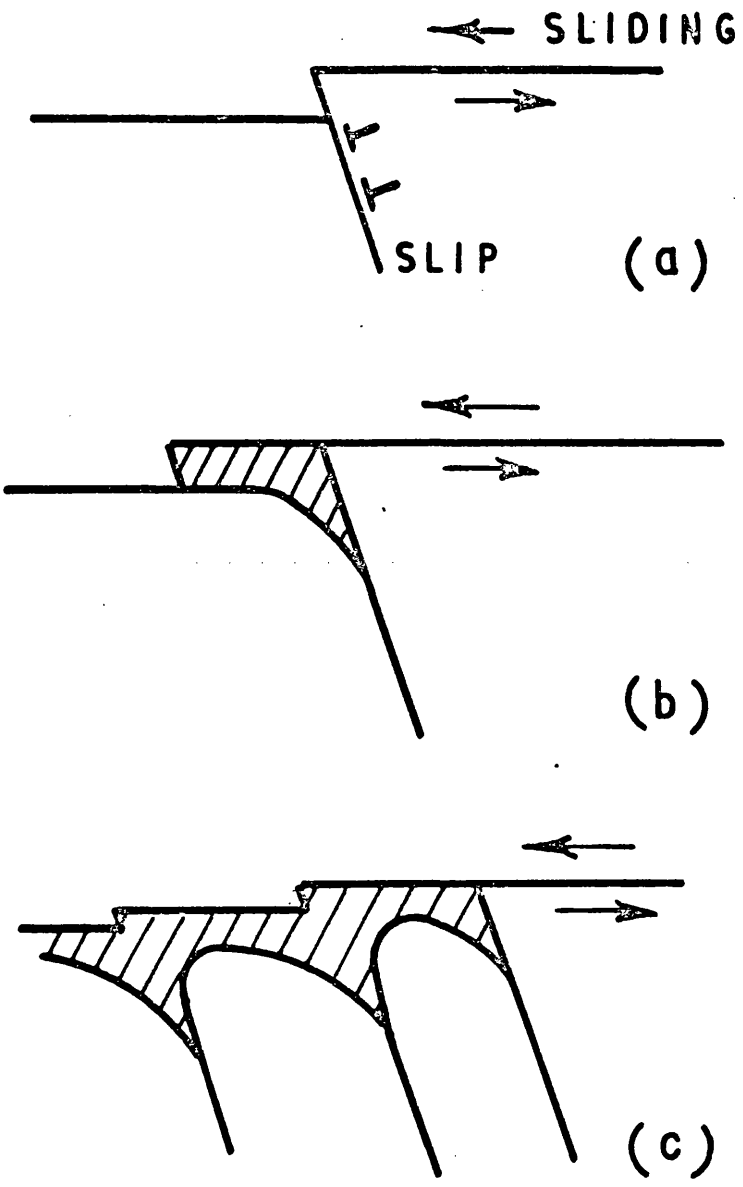

ILLUSTRATING THE COMBINATION OF GRAIN BOUNDARY SLIDING AND CRYSTAL SLIP THAT COULD GIVE RISE TO CAVITIES. (DAVIES AND WILLIAMS)

FIGURE 7

Williams (1969)[15], the ledge shown may only be a few atomic spacings high and is assumed to be caused by slip on the plane shown. Once the ledge is formed any grainboundary sliding will give rise to decoherency in the plane of the ledge and it is believed that dislocations running into the 'cavity' formed will stabilise it. 'Zener cracking' can then enlarge the cavity as though it was a portion of a triple point. The last diagram in the figure shows the linking up of cavities. Growth of cavities is always assumed to be due to sliding at the grainboundaries. This process is now thought to be achieved by dislocation movement, Ishida and McLean (1967)[40], due to dislocations reaching the boundary and then cross-slipping and climbing along the boundary emitting vacancies and finally reaching the cavity. Ishida and McLean introduce this process to partially explain the inadequacies of diffusion growth theory since they are of the opinion that dislocations contribute deformation in the grain matrix and vacancies for cavity growth when in the boundary. Thus cavities grow at a rate proportional to creep rate and not diffusion rate. Davies and Williams refer to the dislocation movement but ignore the vacancy contribution. They describe cavity growth as a process of dislocations entering the cavity and the Burgers vector component in the plane of the boundary causing sliding whilst the component at right angles to this causes widening of the cavity. Growth of cavities solely by sliding and dislocation action is also propounded by Davies and Williams (1969)[16] in which they perform compression tests on cavitated copper at 90^{o} and 180^{o} to the stress axis and find that cavities continue to grow in the 90^{o}, high temperature condition. Similar results were obtained by Davies and Dutton (1966)[12]. Conclusions were reached to the effect that this supported a sliding growth mechanism. The resolved stress causing sliding must be inferred to be similar to that in tension both in sign

and value at 90°. Hence had conditions previously favoured vacancy flow along a stress gradient, conditions would not have changed for this mechanism either. Furthermore, it would not be unexpected that in their room temperature test, again in compression at 90° to the tensile stress axis, cavities ceased to grow by a vacancy mechanism. Hence these results do no more than show that compression at 90° to tension has a similar effect and that cavities grow (a) at elevated temperature, (b) under an applied stress. Bowring et al. (1968)[8] point out that the rate of cavity growth is much lower in an alloy than in a pure metal even though the diffusion coefficients are essentially the same. Lower creep rates also occur with alloy additions, which favours strain controlled cavity growth proposals. These observations are valid and should be borne in mind. In an earlier paper Davies and Wilshire (1965)[17] performed very similar tests in order to contend the vacancy growth proposal of Hull and Rimmer (1959)[39]. Davies contradicts the results of his earlier paper in his paper[16] but draws the same conclusion from both even though comparable materials and tensile creep strains were used. The creep rates vary by a factor of five due to stress differences. However, since Davies et al. only subscribe to one model for cavity growth it may be assumed that the opposed conclusions would not be ascribed to this small variation. In the 1965 paper[17] compressive tests at 180° fail to close the voids produced in tension and the conclusion reached is that 'little reduction in void size can therefore take place by grainboundary sliding under compression'. In the 1969 paper[16] compression at 180°C to the tensile stress produced 'extensive sintering ... so that very few cavities could be detected'. The conclusion in both cases was that the results favoured the sliding mechanism and disproved the vacancy growth model.

The 'vacancy growth' school was essentially founded when Hull and Rimmer[39] developed their model. This was prompted by the reports of other workers whose observations were of voids, coalescence of voids and demonstration of vacancy accumulation at grainboundaries under creep conditions. Later work which supports their hypothesis is that of Ratcliffe and Greenwood[61], Gittins (1967)[28] and Gittins and Williams (1969)[29]. The latter work was in a fatigue regime but they report that grainboundary cavities in high purity copper shrink during annealing as if they were spherical voids emitting vacancies. Since voids produced by creep should behave in the same way it is a useful observation of a damage removal process. Ratcliffe and Greenwood found that in a dilute magnesium-aluminium alloy, void nucleation and growth could be entirely suppressed by imposing a hydrostatic pressure equal to the creep stress. The creep curves with zero and applied hydrostatic pressure are shown in Figure 8. Their calculations showed that void growth could be accounted for by vacancy diffusion. Gittins[28] concluded that cavities in copper are nucleated continuously in creep and that they grow by vacancy diffusion. Stability is deemed to be imparted by gas in the voids. Speight and Harris (1967)[65] and Boettner and Robertson (1961)[7] also support the growth of cavities by vacancy condensation.

Whilst it may well be true that there are materials which in practice cavitate purely by either sliding or by vacancy accumulation there is no valid reason put forward to date which disproves a combined theory. Both schools of thought have extremely credible facets. It would therefore be appropriate to conclude this section with a review of those workers who are more liberal in their analyses.

Langdon (1968)[44] and Price (1968)[59] both subscribe to the view that grainboundary sliding does occur early in creep. Their assessment

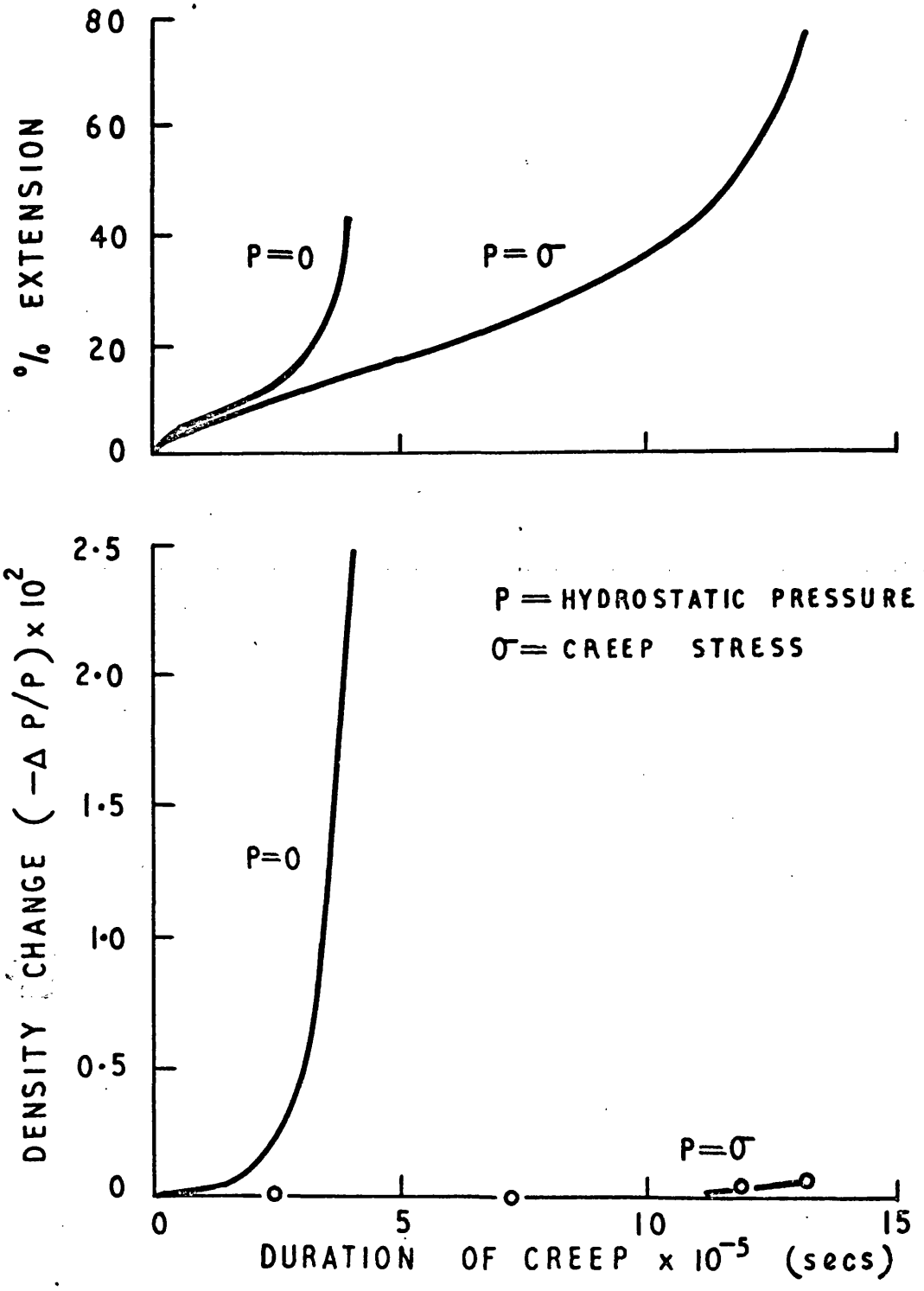

THE EFFECT OF HYDROSTATIC PRESSURE ON CREEP IN MAGNESIUM. (RATCLIFFE AND GREENWOOD)

FIGURE 8

does not depart essentially from Gibbs' (1968)[24] critical and definitive treatment of the inter-relation between grain-matrix deformation and grainboundary sliding. As he points out in his summary, grainboundary sliding must be accompanied by other grain deformation processes if coherency conditions are to be satisfied. The model proposed by Ishida and McLean[40] is most pertinent at this stage and as stated earlier they propose that dislocations run out from the matrix into the boundary. Once in the boundary it is proposed that they move along it, emitting vacancies which can be absorbed by cavities. Thus grain deformation and vacancies are contributed which can resolve the problem of explaining why the diffusion rate is not high enough for cavity growth by vacancy movement. Cavities therefore grow at a rate proportional to the creep rate. A similar hypothesis is expounded by Thölen and Hyman (1968)[66]. Gittins and Williams[29] widen the hypothesis of Gittins[28] and suggest that at high strain rates cavities are produced by grainboundary sliding but at low strain rates by absorbing vacancies. Boettner and Robertson (1961)[7] also support the growth of cavities by vacancy condensation while McMahon (1968)[48] does little more than quote the opposing views and underline the uncertainties. This does serve, however, to point out the lack of proof for a unilateral process. Finally, Woodford (1969)[74][75] in a well contrived analysis brings considerable weight to the hypothesis that cavities nucleate by sliding but grow by diffusion.

There is no cogent reason why grainboundary sliding should cease after nucleation of cavities and it is highly probable that the process will eventually be described as a continuous process of sliding plus vacancy absorbtion. The contribution of each could well depend upon the ratio of stress to temperature. The implication being that sliding

is favoured by high stress and vacancy 'condensation' favoured by high temperature or low stress and temperatures above $\sim$ 0.5 Tm.

1.5 The Effect of Pre-Strain on Creep Behaviour

Williams and Lindley (1969)[71] conclude from a review of the literature that the influence of pre-strain on creep life depends on the balance between workhardening (strengthening, increasing life) and grainboundary damage (weakening, decreasing life). This is a generalisation of course but does indicate the important effects.

One of the early papers on this subject by Sherby et al. (1954)[63] examined the proposals made by Wood and co-workers between 1948 and 1952 on creep mechanisms. Their conclusions embody not only structure effects per se but the effect of instantaneous strain because this varies with stress and temperature and is a part of creep even though the rate is high. Cold pre-straining of aluminium test pieces resulted in increased creep strength. As the temperature of pre-strain was increased, creep rates increased and presumably creep ductility to judge from their strain vs. time plots.

Most of the work subsequent to that of Sherby may conveniently be divided into low and high temperature pre-strain, the latter usually at the test temperature.

General agreement is reached that cold pre-strain reduces ductility due to the strengthening imparted. Gindin et al. (1966)[27] found that strengthening occurs up to the temperature at which diffusion occurs. Work on G19, Barr et al. (1967)[4], Type 318(18/8) steel, Barr et al. (1964)[5] and on Al.20%Zn., Williams (1968)[70], all showed effects associated with precipitates. Cracking of the precipitates occurred in G19[4] and the Al.Zn.[70] and triple point cracking associated with precipitates was observed in Type 316[5]. However, triple point cracking was reduced in the Al.Zn.[70]. The effect of subsequent heat

treatment was to remove the effect of pre-strain in Type 316[5] but only partially so in G19[4]. Zozyrskiy et al. (1966)[43] found that as creep stress increases the effect of pre-strain decreases. Davies et al. (1961)[13] point out that instantaneous creep strain values must be exceeded before the effect is seen on a dilute Ni.Au. alloy. They find a decrease in the product ($\dot{\varepsilon}_s$ x t_f) but show that the sum of the plastic and creep strains equals the non-prestrained value which implies equivalence. It should be noted that they are careful to avoid recrystallisation, if this occurred the results could be affected due to the annealing effect of the moving boundaries. In a later paper (1963)[14] the same workers found that graingrowth during a test decreased the creep resistance of pre-strained material. This work includes pre-strains at - 196°, 20° and 500°C on Ni and dilute Ni alloy and they find that a given pre-strain has a magnitude of effect which is inversely proportional to the temperature of application. The result of permitting recovery to occur is to increase the product ($\dot{\varepsilon}_s$ x t_f) but a decrease is observed for pre-strained material in the absence of graingrowth. Thus pre-strain reduces the ductility and creep rate.

The work of Evans and Wilshire[20] has already been discussed and there is evidence that pre-strain at the creep temperature has an effect but it is not stated how the creep rate and time to failure change. From their results either the rate or the time or both, are decreased. Their results are shown in Figure 9 and, as previously stated, critically appraised in the Discussion, Chapter 4.

Goldhoff (1962)[30], a meticulous investigator, has unfortunately only produced this one paper involving pre-strain. The work has a great deal of factual information and a refreshing lack of assumption. The material is Cr.Mo.V. steel but as he points out (1967)[31] small

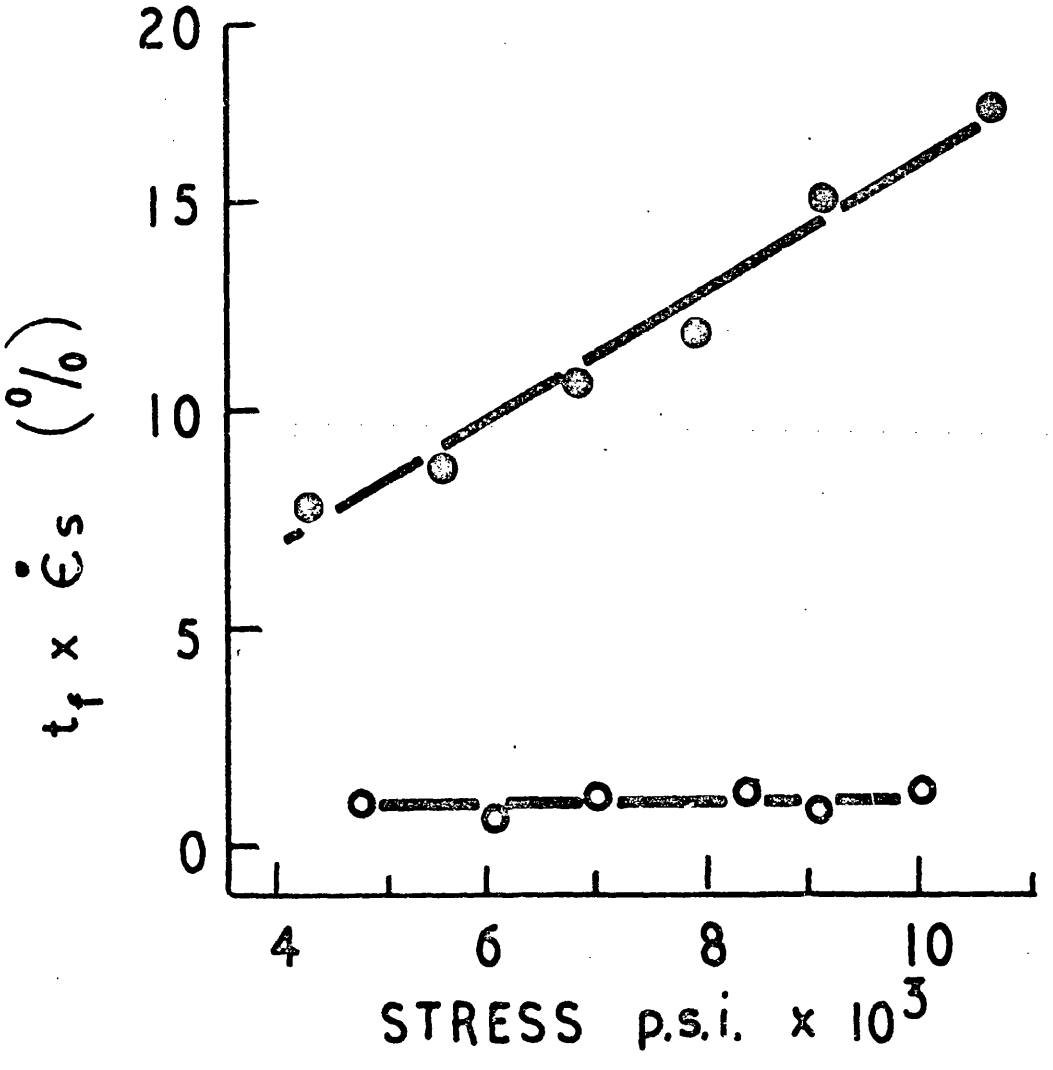

EVANS AND WILSHIRE'S PLOT TO SHOW THE STRESS DEPENDENCE OF $[t_f \times \dot{\epsilon}_s]$

FIGURE 9

variations in composition and different heat treatments produce a material with fundamentally changed properties. This material only approximates in some conditions to that used in the work reported in this thesis. He shows that pre-strain increases the creep strength and reduces ductility in one heat treated condition but in another has little effect upon strength. Widely varied results arise due to heat treatment. Ductility varies with both treatments and pre-strain. An important aspect is the structure dependence of the effects achieved by pre-straining.

Research by Voorhees et al. (1962)[67] showed that for several alloys creep rates were increased by pre-strain in contrast to Goldhoff's results. Lower rupture times were recorded, the plot of stress vs. rupture time lying parallel to the non pre-strained plot but displaced to lower time values.

1.6 The Effect of Pre-Strain Rate upon Creep Behaviour

There is a dearth of information on this topic. Many workers have reported tests in which deformation was controlled by the rate of applying stress as in a tensile test. This type of test is not relevant to the conditions which apply in this research since the rate controlling process in creep will be principally defined by temperature dependent factors and the load is constant. That is to say, the deformation process occurring in the present work will be thermally activated but may be stress aided. The stresses occurring under the conditions used in the author's tests are, in any case, less than that at the yield point. Goldhoff observes[30] that rapid pre-straining decreased the time to failure in Cr.Mo.V. steel and slow pre-straining increased this moderately in one heat treated condition.

In the remaining conditions the steel was strengthened by pre-

strain but more so in the slowly pre-strained condition.

The only other reference in the literature is that of Hodgson (1969)[38] and this will be discussed in a later chapter.

2. EXPERIMENTAL DETAILS

2.1 The Materials Used in the Tests

The material used was a low alloy Cr.Mo.V. steel. This type of steel has found a very wide field of use throughout the world. Compositions very similar to the one used here are specified for generating plant in Japan, U.S.A., U.S.S.R. and Europe. Detail changes in composition and heat treatment result, however in a wide range of properties. In the U.K., where generating sets are now becoming much larger and running at temperatures up to about 0.4 Tm, much more stringent specifications are in use than heretofore. In the last five years or so a great deal of work has been carried out in the laboratories of the steel producers, generating set manufacturers and of the C.E.G.B. to determine optimum composition and heat treatment for the material. One of the greatest difficulties which arises is that of obtaining a uniform structure in such massive components as, for example, the low pressure (LP) rotor of a modern set. The rotor is forged as a single component comprising both shaft and turbine discs. The differing cross sections present great problems even in a 'through-hardening' steel such as this, Figure 3 shows the range of structures and creep rates that occur in a turbine rotor forging. The latest specifications call for a V, C ratio of $1\frac{1}{2}$:1 or 2:1 to ensure that a fine dispersion of vanadium carbide is present because this has been shown to be responsible for the creep resistance by several groups of workers (references 6, 9, 36, 41, 60). Rationalisation of the heat treatment in parallel with the more stringent composition specification has led to the following recommended composition and heat treatment. The composition of the material used in the tests described in this thesis is also given.

TABLE 1

	C	Mn	Cr	Mo	Ni	V
Optimised composition	.28	.7	1.0	.7	.7	.35
Material used for tests	.29	.74	1.06	1.0	.7	.35

N.B. Mo is thought to stabilise the vanadium carbide by maintaining partial coherency between the carbide and the matrix. The vanadium carbide takes up to 40% Mo into solution. If the Mo content exceeds this, molybdenum carbide forms and coherency is lost and growth of the molybdenum carbide occurs. This is incoherent and denudes the matrix of vanadium carbide. Mo must not exceed the V content by more than X3. The test material should therefore be acceptable in the light of the optimised composition.

TABLE 2

Heat Treatment (experimental and manufacture)	
Austenitise at 1,000°C Cool to 675°C at 50°C per hour. Hold for 70 hours. Air cool.	This gives a fine ferrite pearlite which, because of the small grain-size prevents excessive grainsize in the final treatment.
Austenitise 975°C. Oil quench. Temper 700°C for 20 hours, furnace cool.	

The experimental material is in fact part of the excess produced for the West Burton Power Station, LP Rotor and several workers have

received an allocation. The material used by the author was in the form of 7.5 cm square,forged billets, about 1.2 m in length.

In view of the fact that creep tests can take thousands of hours in the upper bainite region it was decided to test the material in the ferrite-pearlite condition. The heat treatment used was the first half of the rotor treatment quoted above. This produced a fine ferrite-pearlite structure with a small grainsize of between 1 μm and 15 μm as shown by Figure 10. Three heat treatment batches were used in these tests, Batch 1 for pre-strain, Batch 2 for loading rate dependence and Batch 3 for temperature dependence and repeat tests for confirmation of results.

2.2 The Creep Plasticity Rig

The test equipment received this title because the initial requirement was for a high sensitivity creep machine which incorporates facilities for pre-straining specimens at the test temperature.

A general view is shown in the photograph Figure 11 and a schematic layout is given in Figure 12. The basic creep machine is a Mand high sensitivity frame and furnace. Temperature control is by a platinum resistance thermometer and a proportional controller driving a three zone furnace. Each zone can be balanced with respect to the others by Variac variable transformers. Temperatures are held to $\pm 1\frac{1}{2}^{o}C$ over the gauge length and are measured by three chromel-alumel thermocouples spot welded to the specimen. The gauge length is shielded from direct radiation from the furnace wall by asbestos tape.

Since chromel-alumel thermocouples can be up to $10^{o}C$ in error due to drift and an order-disorder change at about $475^{o}C$, the couples are made from specially stabilised wire. The finished couples are calibrated for the test temperature in a constant temperature bath.

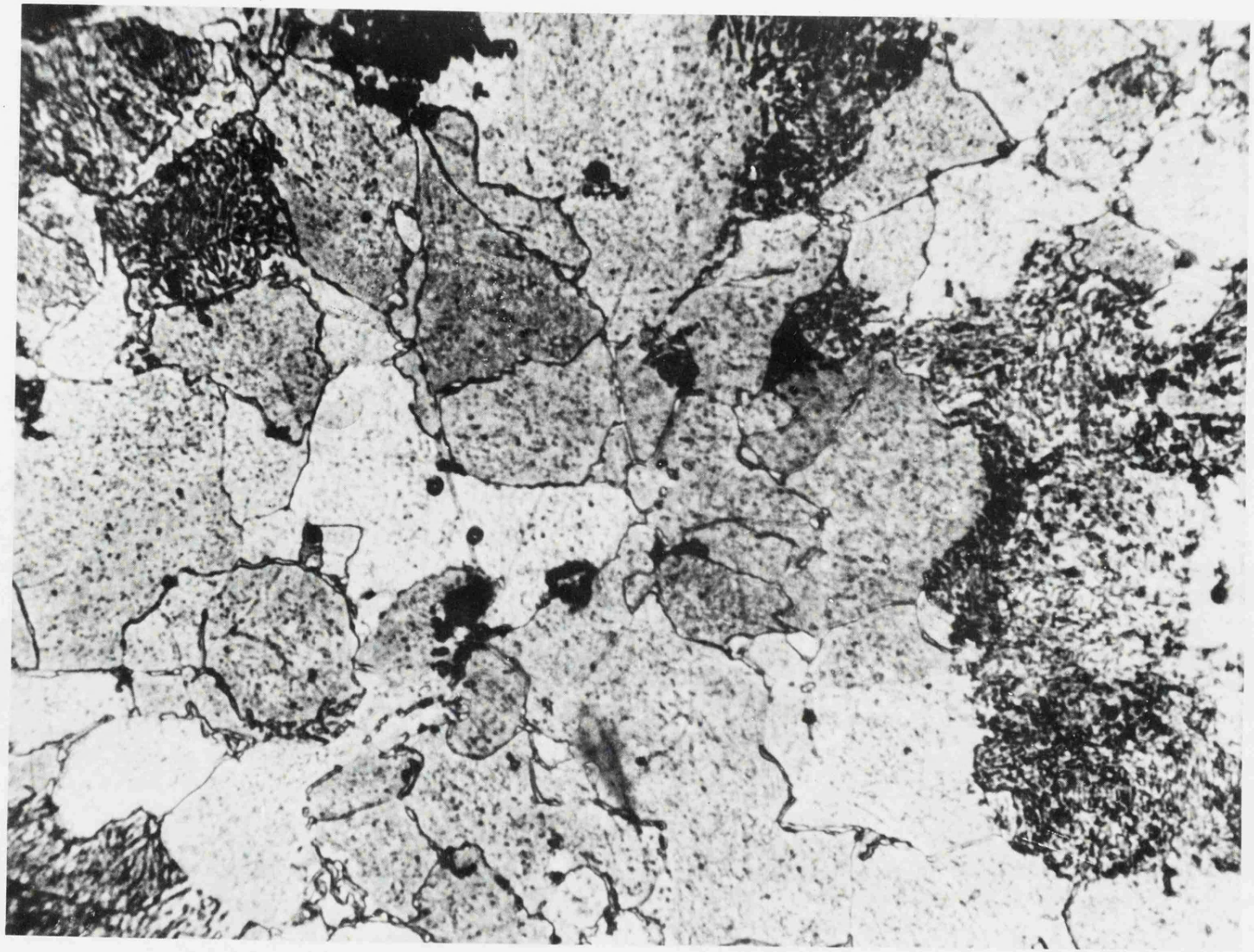

FIGURE 10 MICROSTRUCTURE PRIOR TO TEST. X 1,000

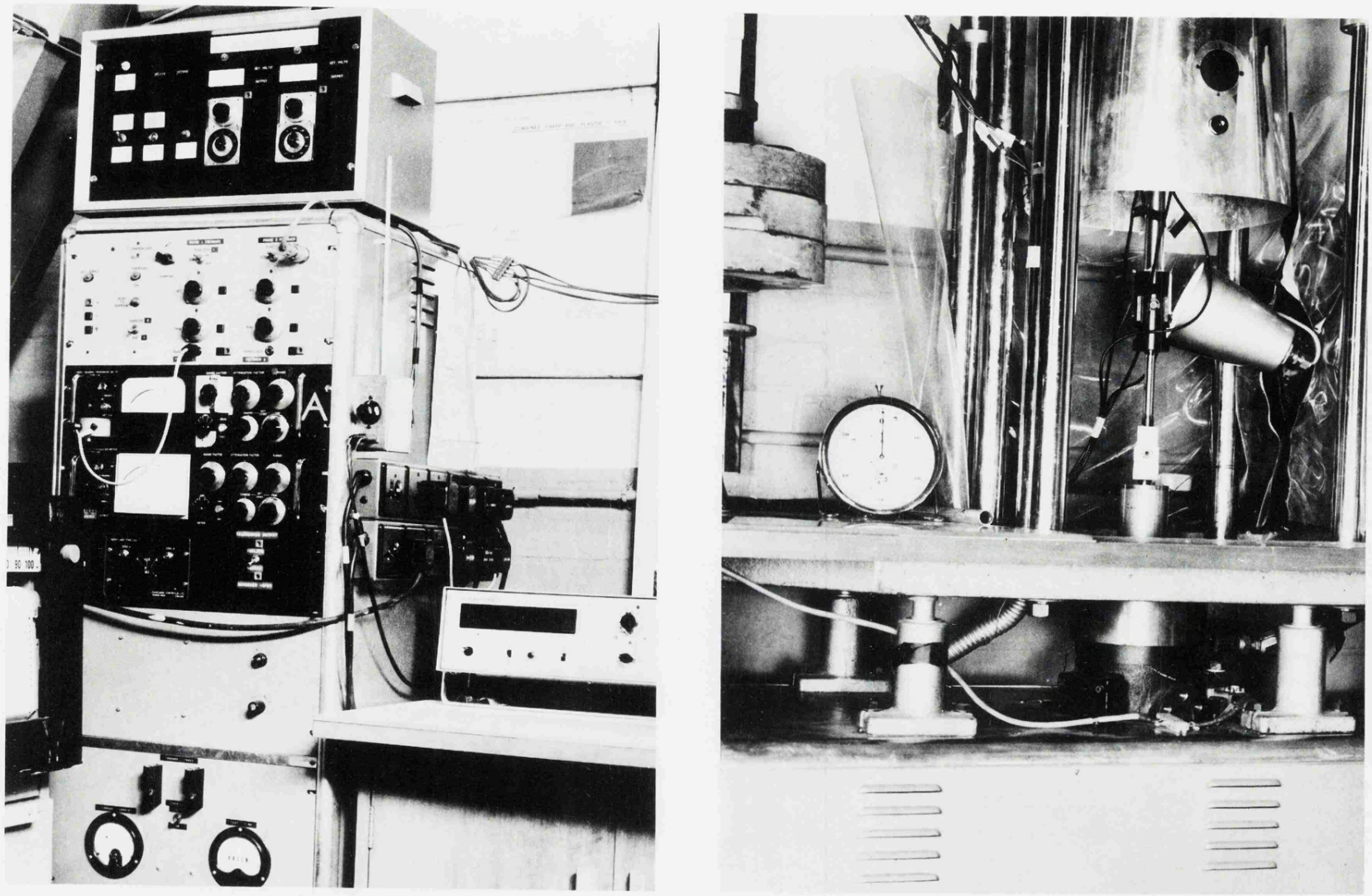

FIGURE 11 THE CREEP-PLASTICITY RIG

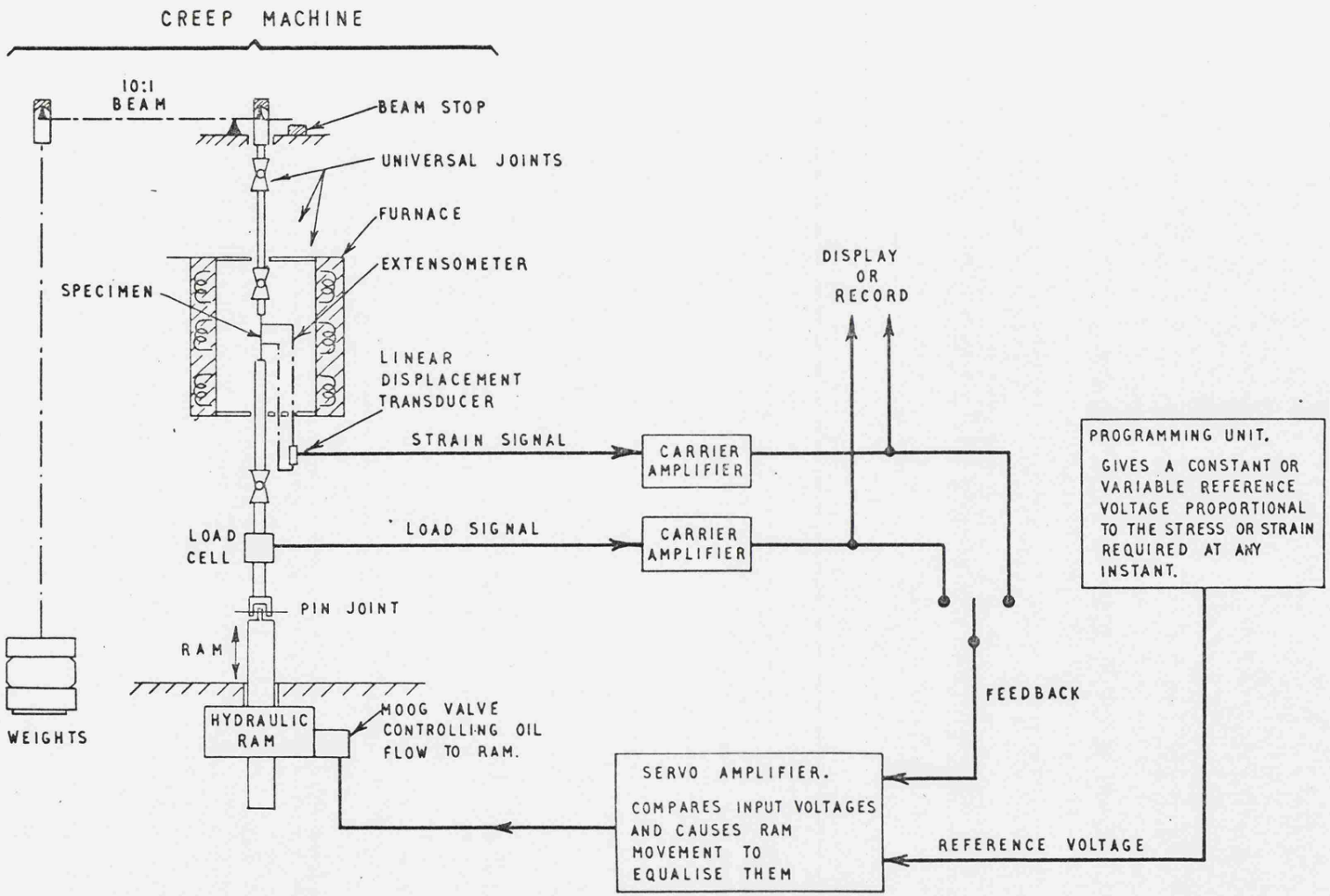

SCHEMATIC LAYOUT OF CREEP-PLASTICITY RIG.

FIGURE 12

Printout of specimen temperature is digitised on a data-logger with an additional digitised display if required.

The specimen holders and rods have three universal joints to minimise specimen bending so that there are two above the specimen and one below. The lower universal is supplemented by a pin joint in one plane.

Strain measurements are made using an extensometer which is certainly better than class B and as far as can be ascertained might be classed as 'A'. The difficulty is in ensuring that the certified NPL wedge comparator used for checking, is itself accurate to these limits. The strain measurements are known to be accurate to 10^{-5} inches and it is believed to 10^{-6} inches. The extensometer was developed by Walters[68] and is described in Appendix 3. Briefly, it utilises four displacement transducers, two of which measure strain and compensate for rocking, two compensate for temperature excursions which are not experienced by the specimen. These latter temperature changes are mainly due to general ambient changes and to draughts affecting the exposed parts of the extensometer. Controlling the room temperature to $\pm 1\frac{1}{2}^{o}C$ and adding a protective skirt to the furnace minimises these effects but does not eliminate them, hence the need for compensation. The extensometer is attached to the specimen by means of two split collets sitting on ridges integral with the specimen. Load is measured, when required, by a proof-ring type load cell in the specimen string. This instrument also incorporates a displacement transducer of the same type used in the extensometer.

Signals from the extensometer and load cell are usually plotted continuously by a single point Honeywell recorder but can be recorded or displayed digitally. A U.V. recorder is employed to record high

speed stress changes during pre-straining.

The carrier amplifiers which drive the transducers are infinitely adjustable in range and span permitting transducer measurements from 0.35×10^{-5} cm up to a total movement of 0.58 cm to be the full scale output. It is therefore possible to follow strain or stress changes at a magnification level which is convenient. If the output is put on a 30 cm wide 100 division chart it is apparent that theoretically it is possible to read strains to 2.5×10^{-7} which adequately covers the sensitivities required in the experiments described in this thesis.

The remainder of the rig is designed to permit either stress or strain programmes to be performed in tension. The heart of this portion of the rig is the hydraulic ram and its associated control equipment. As shown in the diagram, Figure 12, it is mounted in the base of the creep machine and coupled to the specimen stringer at the pin-joint. A Dowty MOOG valve controls the oil flow to the ram and causes it to move up or down proportionally to an input voltage. The sign of the voltage defines the direction of movement and the size of the voltage defines the magnitude. Ram speed may be controlled to some extent by the supply pressure but more usually by change of voltage to the MOOG valve. At high speed the ram movement must be measured in microseconds so that a wide range of stress/strain rates are available. The voltage input to the MOOG valve comes from a 'summing' amplifier which accepts a number of inputs, sums them arithmetically and presents the resultant as a control voltage to the valve. The input voltages to the MOOG amplifier are derived in the present rig from a number of sources,

(a) strain transducer output

(b) stress transducer output

(c) pre-strain unit

(d) rate control unit

(e) wave-form generator

(f) curve-following unit

Units (c) and (d) were both designed and manufactured at Berkeley Nuclear Laboratories, (e) and (f) are proprietary items manufactured by Servomex and Data Trak respectively. In the present work the last two items have not been used, they are for use in the continuing programme. Items (c) and (d) are fully described in Appendix 1. An example of the programming of a pre-strain test is given in Appendix 2 but the basic requirements are as follows.

The pre-strain is required to be applied rapidly, in less than one second, and the stress necessary to apply it is to be decayed smoothly to the creep value. All operations to be carried out at the test temperature. Slow pre-straining can be effected by utilising the Rate Control Unit or manually by using a hydraulic jack to lower the creep weights directly.

Before each test is commenced all of the equipment to be used is calibrated for the range required. Repeatability of individual tests was checked several times throughout the series and an excellent correlation was always found.

2.3 The Creep Specimen

Figure 13 shows the two types used. The threaded end type was discontinued at the end of the pre-strain tests because it was decided to carry out density measurements on future specimens. The dumbell end configuration reduces the untested weight to improve the accuracy and sensitivity of measurements.

The 2 in.(508 mm) by 0.226 in.(5.7 mm) diameter gauge length detail has not changed throughout the test programme.

All test pieces were rough machined and then heat treated thus

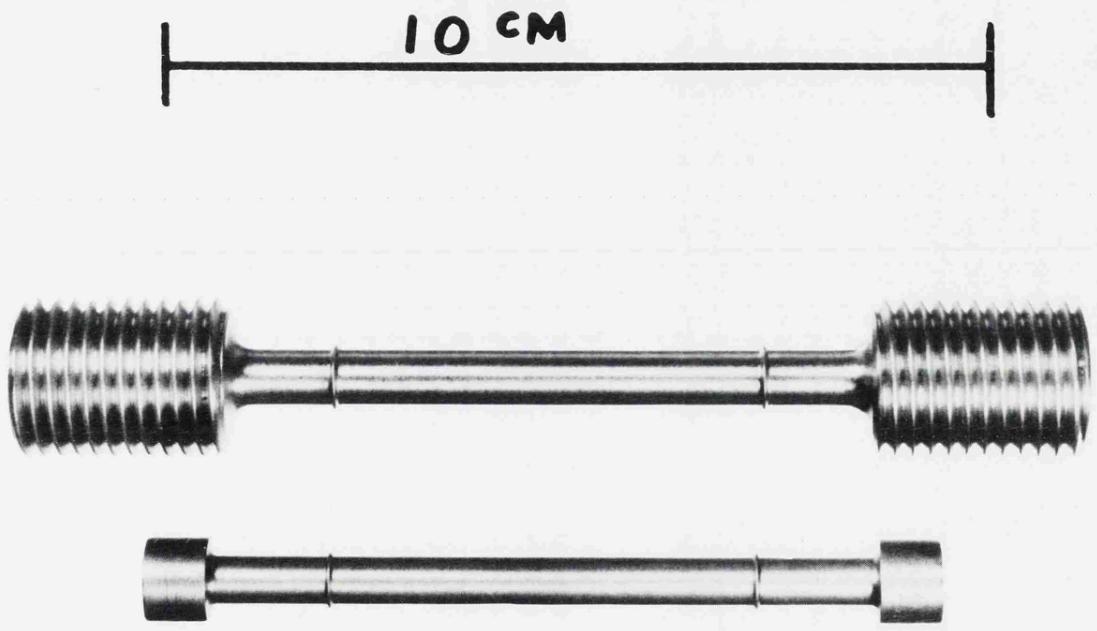

FIGURE 13 THE CREEP SPECIMENS

Austenitised 1000°C

Furnace cooled at 50°C/hour to 675°C

Held 70 hours

Air cooled

The intention was to minimise both work hardening and distortion. No evidence of either was subsequently observed.

3. EXPERIMENTAL RESULTS

3.1 Introductory Remarks. Discovery of a Loading Rate Effect

Very early in the test programme it was recognised that the material was sensitive to the rate at which the load was applied. This factor was deemed to be not only important to the C.E.G.B. materials behaviour work but worth examining as an unusual aspect of creep behaviour in an otherwise conventional steel.

Alterations were made to the programme to observe the effects of pre-strain rate as a separate piece of research to that of exploring the dependence of creep rate and time to failure etc. upon stress and loading rate in conventional creep tests.

The effect of pre-strain upon subsequent creep behaviour is therefore reported as two sets of results, (1) slow pre-strain and (2) rapid pre-strain.

Before presenting these results it is proposed to describe three tests made when the loading rate effect was first observed. The test which revealed the effect was intended to be a conventional creep test but the apparent creep rate was excessively high. Initial reaction was that either the creep conditions or the instrumentation was at fault but this was not found to be the case. Another possibility lay with the hydraulic jack which had been used for the first time to lower the weights. Previously a screw jack had been employed but this entailed jerky loading and inconsistencies in the pre-strain tests made up to this time may, it was thought, have been due to this.

The hydraulic jack was used to lower the weights smoothly and the hypothesis was made that in doing so the material experienced creep under a steadily increasing load which, at some stage, provided a critical amount of strain. This might trigger graingrowth or re-

crystallisation which would effectively provide dislocation 'free' material in which creep could be rapid.

Two tests were then made at 288 N/mm^2 (18.62 tsi) and 550°C. One was loaded by lowering the weights slowly in 50 seconds and the other loaded in one second. The slowly loaded test had a minimum creep rate which was three orders of magnitude greater than the rapidly loaded test. Failure occurred in the high creep rate test in about 10 hours and at the low creep rate in approximately 500 hours.

This was a dramatic departure from the expected behaviour and the results are shown in Figure 14. A log-log plot is essential because on linear axes the high creep rate test is so steep that it is impossible to detect primary, secondary or tertiary creep. The fact that the rate of change of creep rate goes through a minimum, indicating secondary creep, is demonstrated by the log-log plot.

One further question required an answer at this stage and that was whether a creep rate was stable once established. A slowly loaded specimen at 270 N/mm^2 (17.5 tsi) was unaffected by unloading and rapidly re-loading. The effect of various changes in conditions on a rapidly loaded test piece is shown in Figure 15. It is considered that a change in creep rate of only a factor of two demonstrates stability.

Having established that the loading rate effect was genuine the test programme was pursued on the lines indicated previously.

3.2 Pre-Strain Tests

In these tests the temperature was constant at 550°C and the stress at 270 N/mm^2 (17.6 tsi).

Pre-strain was applied at 550°C and the stress necessary to impose it was decayed smoothly to the test stress. An ultra-violet

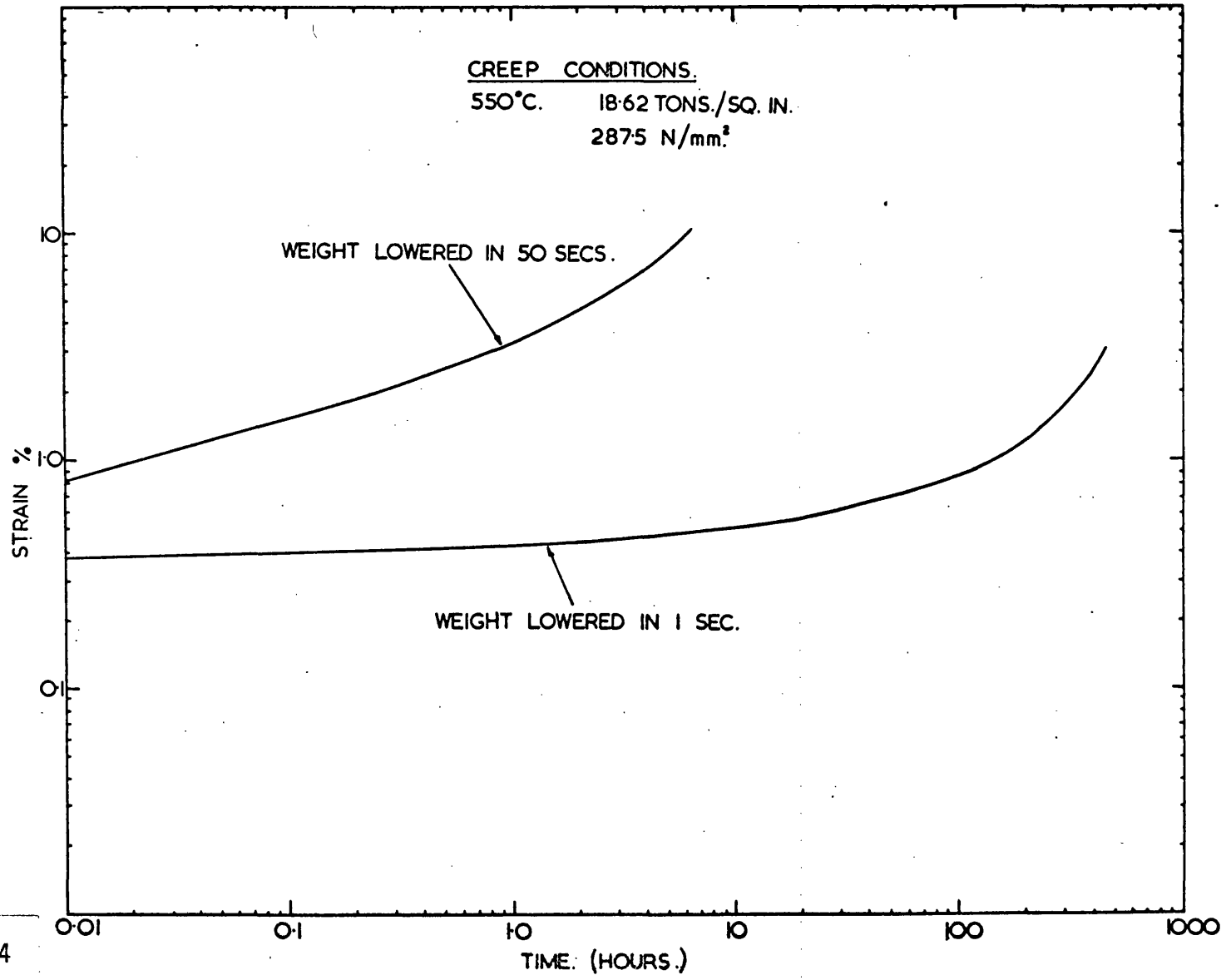
CREEP CONDITIONS.
550°C. 18·62 TONS./SQ. IN.
287·5 N/mm²
WEIGHT LOWERED IN 50 SECS.
WEIGHT LOWERED IN 1 SEC.
STRAIN %
1·0
0·1
0·01
0·1
1·0
10
100
1000
TIME. (HOURS.)

FIGURE 14

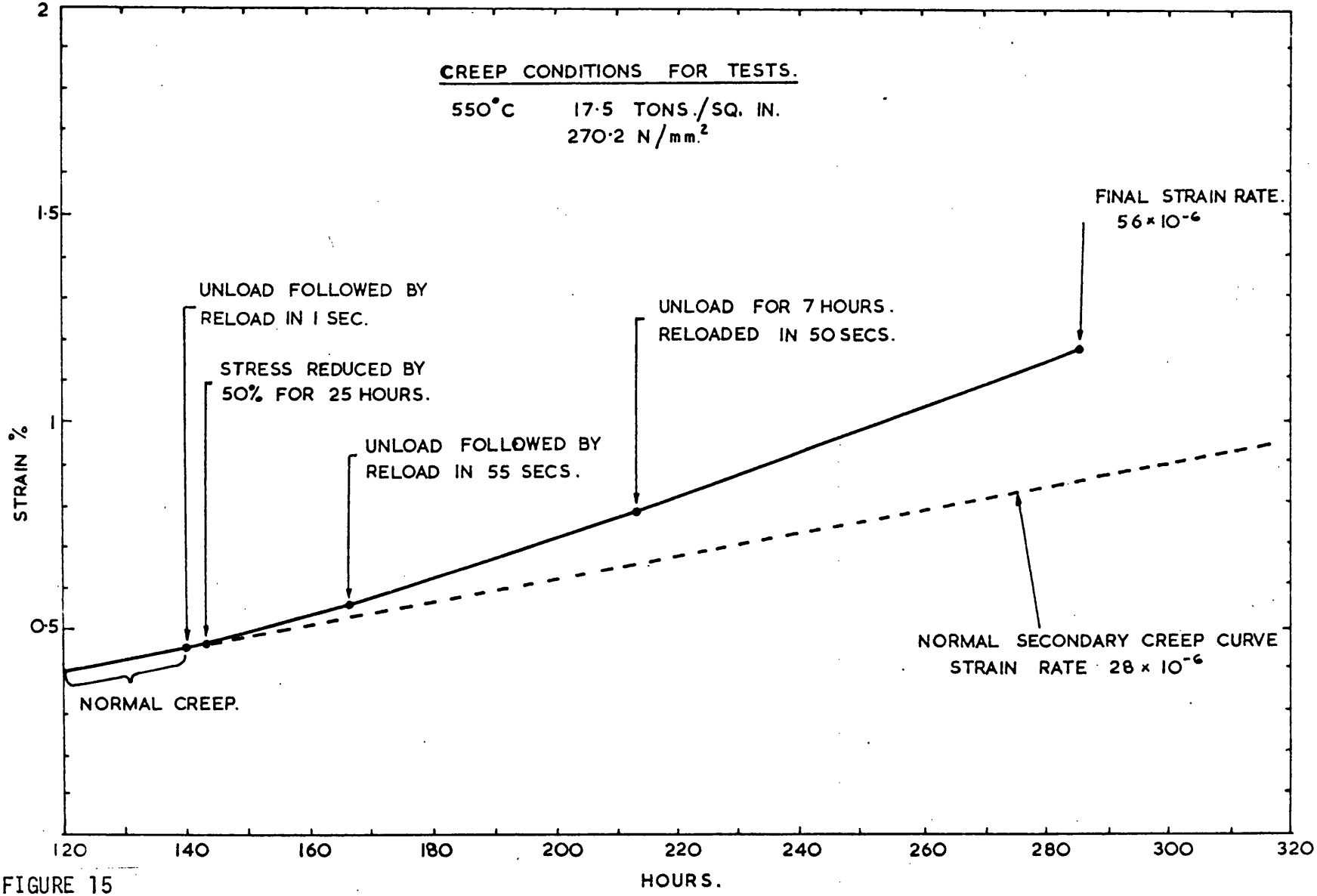
CREEP CONDITIONS FOR TESTS.
550°C 17·5 TONS./SQ. IN.
270·2 N/mm.²
FINAL STRAIN RATE.
56 × 10⁻⁶
UNLOAD FOLLOWED BY
RELOAD IN 1 SEC.
STRESS REDUCED BY
50% FOR 25 HOURS.
UNLOAD FOLLOWED BY
RELOAD IN 55 SECS.
UNLOAD FOR 7 HOURS.
RELOADED IN 50 SECS.
NORMAL SECONDARY CREEP CURVE
STRAIN RATE 28 × 10⁻⁶
NORMAL CREEP.
STRAIN %
HOURS.
2
1·5
1
0·5
120
140
160
180
200
220
240
260
280
300
320

FIGURE 15

(U.V.) recorder was used to monitor the stress-time pattern and a typical trace is reproduced in Figure 16. Pre-strain was applied at various rates but the results fell into two groups, those pre-strained in approximately 1 sec and those pre-strained in 55 secs or more. The results showed that within those broad divisions the specific rate of pre-straining was not important. As shown by Figure 17, comparable pre-strains of 0.9% and 0.88% were applied at quite different rates i.e. 0.98%min^{-1} and 0.17%min^{-1} respectively. The difference in creep rate was not only small but in the wrong sense to a minor extent.

As in the tests described in 3.1 it is impossible to discern the presence of primary, secondary or tertiary creep in the high creep rate tests. Since primary creep contributes approximately 0.6% strain there should be evidence of primary creep in the lower pre-strain tests. Therefore the results are also presented in log-log form in Figure 18 from which it will be seen that in each test there was a secondary and tertiary stage. Primary creep can be detected in the rapidly loaded pure creep and 0.65% pre-strain sample and is indicated in the slowly loaded 0.2% pre-strain test.

Table 3 compares various parameters for the pre-strained tests.

The results indicate that a slow load without pre-strain is by far the most severe form of pre-treatment. If the zero pre-strain, rapidly loaded test is taken as the datum then pre-strain improves the creep strength in slowly loaded specimens. Small pre-strains are damaging in rapidly loaded tests with a tendency towards normal lives as pre-strain increases. Equivalence of plastic and creep strain cannot therefore be assumed.

Even though there is a creep strength improvement in slowly loaded tests as pre-strain is increased the effect of slow pre-strain

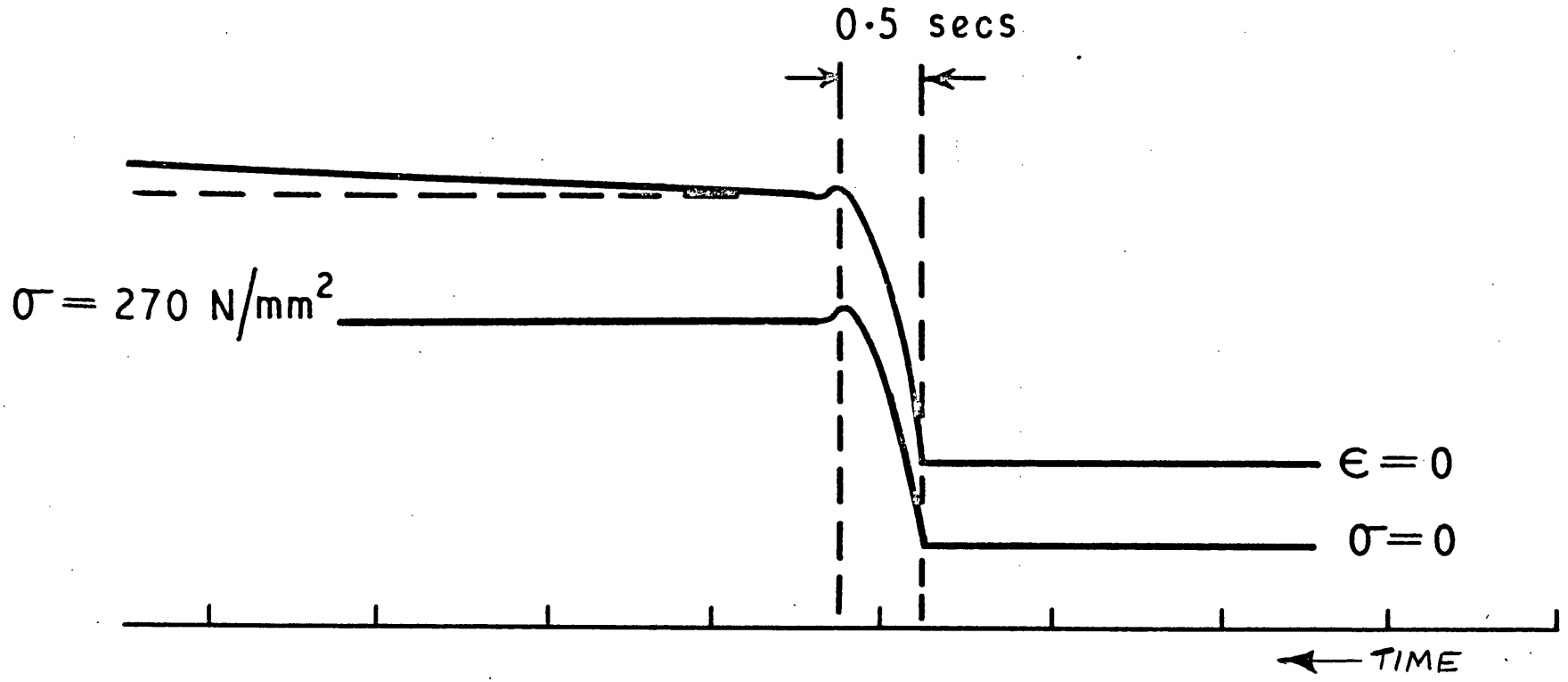

U.V. RECORDER TRACE FOR THE APPLICATION OF 0·2% ϵ_p

FIGURE 16

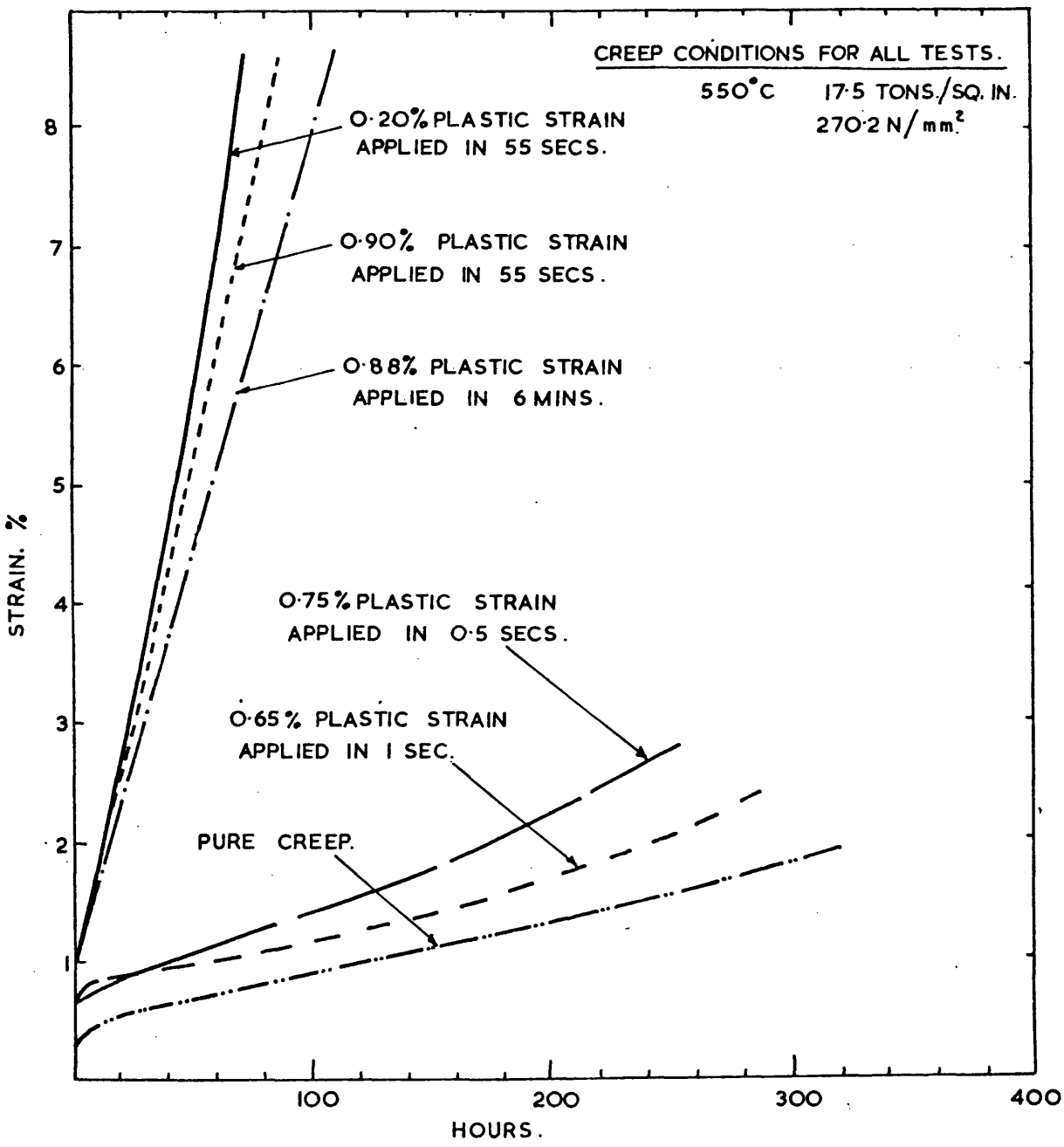
CREEP CONDITIONS FOR ALL TESTS.
550°C 17·5 TONS./SQ. IN.
270·2 N/mm²
0·20% PLASTIC STRAIN APPLIED IN 55 SECS.
0·90% PLASTIC STRAIN APPLIED IN 55 SECS.
0·88% PLASTIC STRAIN APPLIED IN 6 MINS.
0·75% PLASTIC STRAIN APPLIED IN 0·5 SECS.
0·65% PLASTIC STRAIN APPLIED IN 1 SEC.
PURE CREEP.
STRAIN. %
HOURS.
1
2
3
4
5
6
7
8
100
200
300
400

FIGURE 17

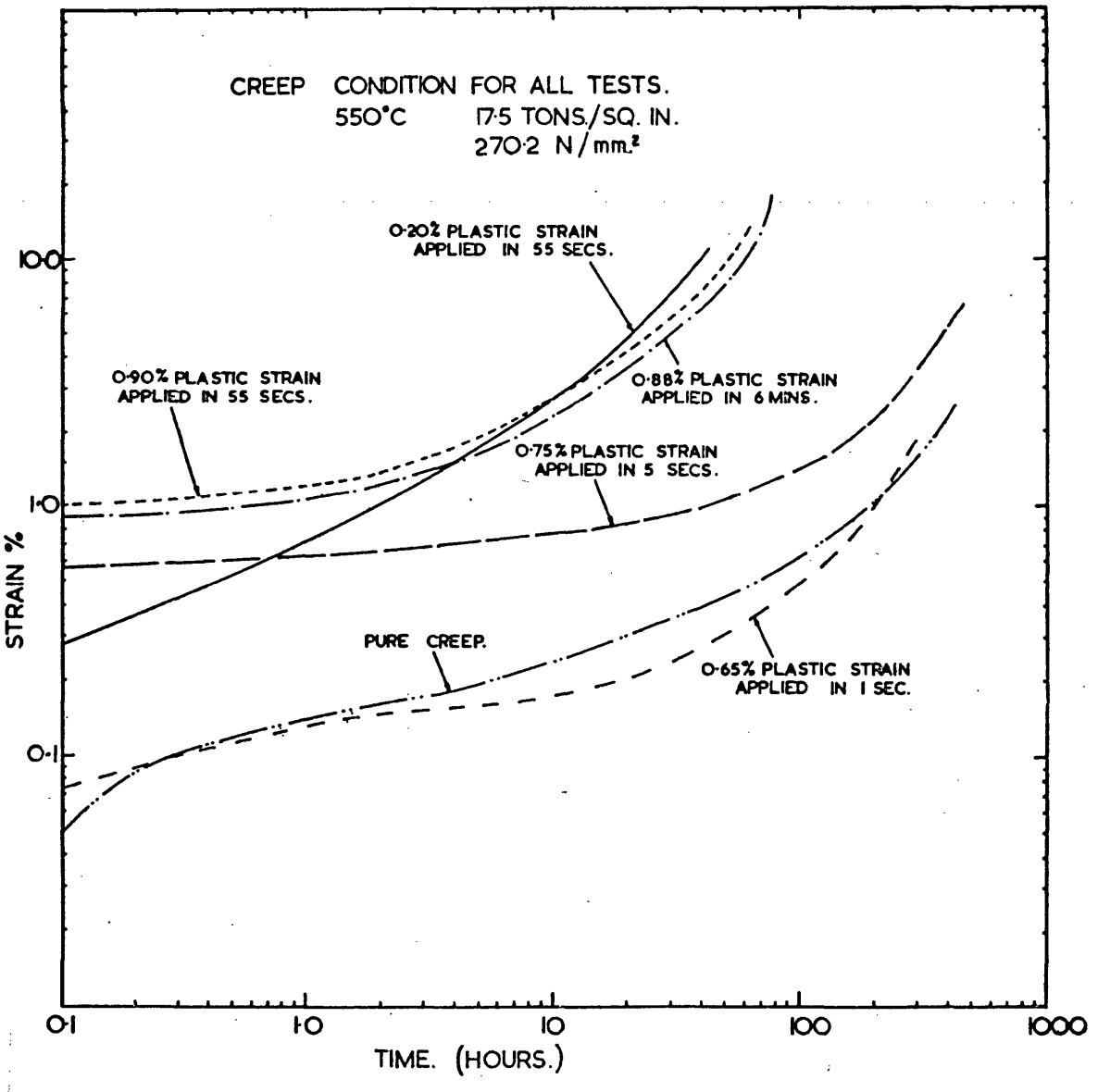
CREEP CONDITION FOR ALL TESTS.
550°C 17·5 TONS/SQ. IN.
270·2 N/mm.²
0·20% PLASTIC STRAIN APPLIED IN 55 SECS.
0·90% PLASTIC STRAIN APPLIED IN 55 SECS.
0·88% PLASTIC STRAIN APPLIED IN 6 MINS.
0·75% PLASTIC STRAIN APPLIED IN 5 SECS.
PURE CREEP.
0·65% PLASTIC STRAIN APPLIED IN 1 SEC.
STRAIN %
100
1·0
0·1
0·1
1·0
10
100
1000
TIME. (HOURS.)

FIGURE 18

TABLE 3

Rate of Loading	Pre-Strain %	$\dot{\varepsilon}_s$	t_t	t_f
Slow	0	2.4×10^{-2}	-	10
	0.2	1.9×10^{-3}	23	40
	0.75	1.95×10^{-3}	25	45
	0.88	1.4×10^{-3}	44	75
	0.9	1.2×10^{-3}	39	64
Rapid	0	3×10^{-5}	280	430+
	0.2	10×10^{-5}	125	270
	0.65	1×10^{-5}	230	280+
	0.75	6.8×10^{-5}	210	430

is still severe.

Figure 19 shows the general effect of pre-strain upon time to failure for both rates of loading.

In Figure 20 strain rate and the time to failure (and to tertiary creep rate) are plotted on log-log axes. The reason for choosing this plot is to see if the results fit the relationship

$$[t_f \times \dot{\varepsilon}_s^m] = K \qquad (10)$$

It will be seen that the slope of - 1 predicted from the relationship does not hold. The strain rate index is found to be 0.6 and the value of K, 1.2. A good correlation of the results with this slope is obtained. The times to tertiary t_f are included since this parameter is often quoted in the literature.

3.3 Creep Tests. The Effect of Slow or Rapid Loading

For this group of tests a new batch of test pieces was machined from the same billet. The heat treatment used was the same as before, viz.

Austenitise 1000°C

Furnace cool at 50°C per hour to 675°C

Hold for 70 hours

Air cool.

The test temperature was again 550°C but a range of stresses was used. The highest stress was 270 N/mm^2 (17.5 tsi) and the lowest 180 N/mm^2 (11.6 tsi).

The family of curves is given in the log-log ε vs. t plot, Figure 21. To aid comparison of the curves an arbitrary origin was defined at a strain of 0.0001 cm and a time of 0.01 hours. This artifice is justified not only on the grounds given but, as is well known, the nearer the true origin the harder it is to measure the

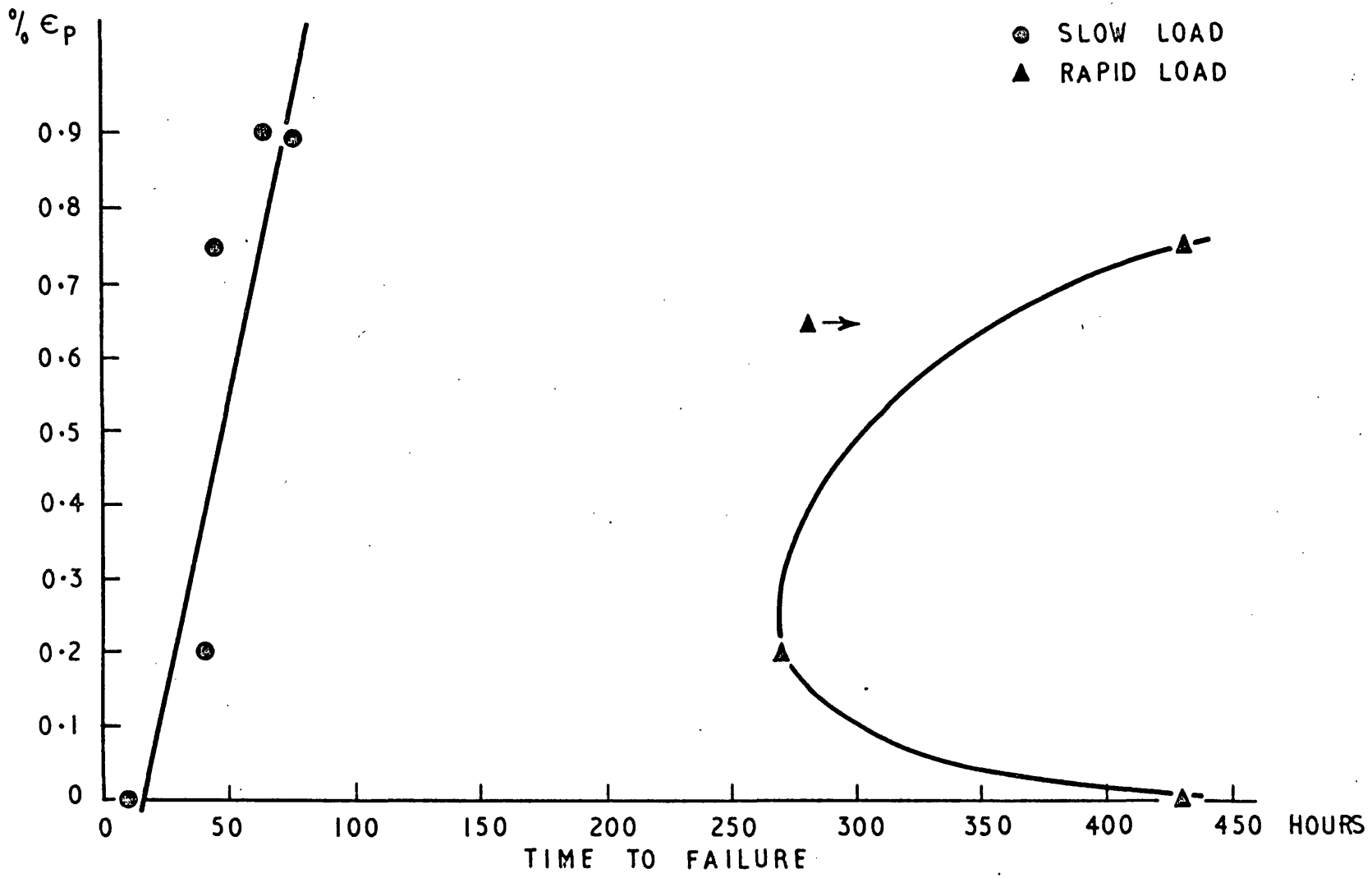

THE RELATIONSHIP BETWEEN PRE-STRAIN AND TIME TO FAILURE.

FIGURE 19

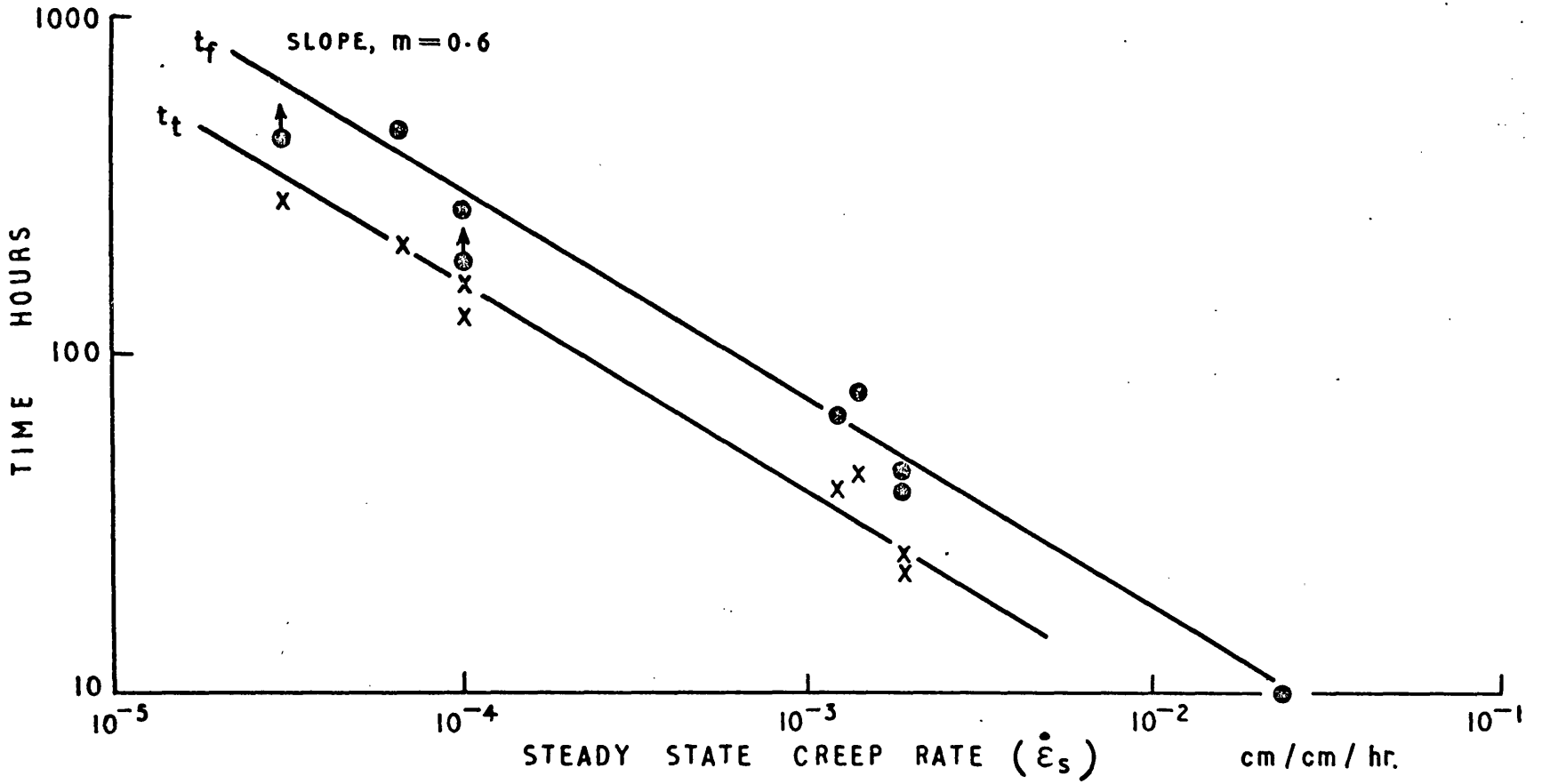

THE DEPENDENCE OF t_f AND t_t ON $\dot{\varepsilon}$.
COMBINATIONS OF SLOW AND RAPID LOADING AND PRE-STRAINS OF 0% TO 0·9% ARE INCLUDED.

FIGURE 20

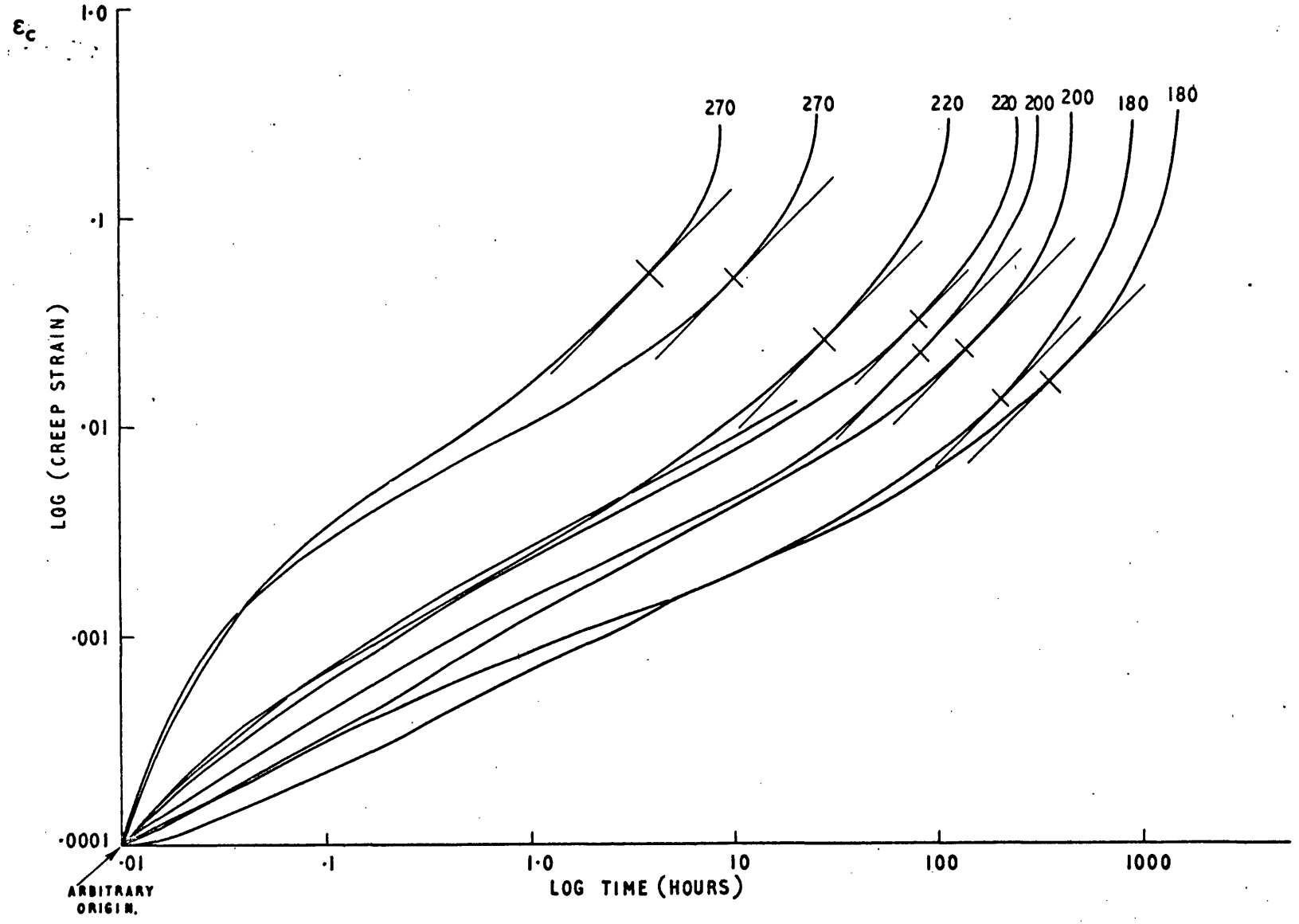

LOG (STRAIN) vs LOG (TIME) RELATIONSHIP FOR SLOWLY AND RAPIDLY LOADED SPECIMENS AT 550°C.

FIGURE 21

quanta involved. This in logarithmic plots, leads to a worsening of the accuracy rather than an improvement. Since, from the origin defined, the creep strain and time increments are exactly as measured the shape of the initial curve is altered. The purpose in using the single origin is to effect this alteration so that the form of the curves is truly comparable.

The numbers at the termination of each curve are the stresses in N/mm^2. Failure occurred in each case where the line terminates. All slowly loaded tests are the left hand ones of each pair at a given stress. Similarly the right hand result in each pair was rapidly loaded. A slope of 1 is shown tangential to each test and the point of contact is indicated by the short line cutting the curve.

The results have a good overall consistency and show two important features. Firstly, the remarkable uniformity of the strains at failure which are completely independent of the loading rate and stress. Secondly, the indicated relationship between strain at the tangents of unity and the stress.

As in 3.2, various parameters of the tests are given in tabular form in Table 4.

An initial analysis of the results may be made by plotting these parameters in various ways. The relationship between the minimum creep rate (or secondary creep rate) and the stress, already indicated by Figure 21 is given in Figure 22. As well as ($\dot{\varepsilon}_s$) the creep rate at 0.1%, 1.0% and 10% strain is plotted for comparison. The plot is of course a standard one to give the stress index and is represented by the equation

$$\dot{\varepsilon}_s = A.\sigma^n \qquad (11)$$

The points for the minimum creep rate of both slowly and rapidly loaded tests are well represented by the line given. A value of 12.0 is

TABLE 4

σ N/mm^2	Loading Rate	Loading Time	$\dot{\varepsilon}_s$	ε_f %	t_f (hours)
270	Slow	3m 5s	1.3×10^{-2}	27.9	8.5
270	Rapid	< 1s	4.5×10^{-3}	31.5	25
220	Slow	10m 15s	7.8×10^{-4}	30.5	112
220	Rapid	< 1s	3.2×10^{-4}	31.0	243
200	Slow	2m 40s	2.0×10^{-4}	31.3	306
200	Rapid	< 1s	1.4×10^{-4}	32.5	430
180	Slow	2m 12s	5.7×10^{-5}	29.0	870
180	Rapid	< 1s	4.0×10^{-5}	33.0	1439

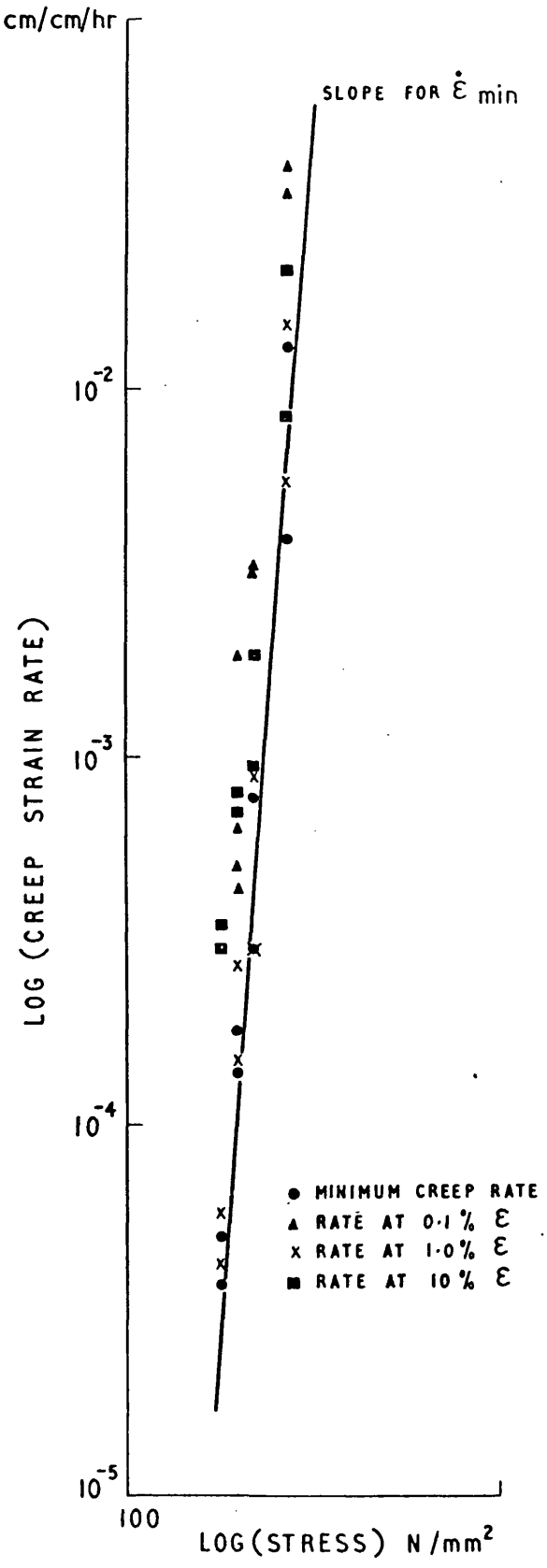

THE STRESS DEPENDENCE OF STRAIN RATE AT 550°C.

FIGURE 22

obtained for the stress index.

It can also be shown that the results fit the equation

$$t_t,\ t_f = \frac{K}{\dot{\varepsilon}_s^m} \qquad (12)$$

and in Figure 23 the plots are given for both slow and rapid loading at 'time to tertiary' and 'time to failure'. The correlation is good and a value of 0.85 is obtained for the strain rate index. Dependence of the time to tertiary and failure upon stress is demonstrated by Figure 24.

3.4 The Temperature Dependence of the Creep Rate

A series of tests at a stress of 220 N/mm^2 was made in the temperature range 500°C to 550°C.

The results are plotted on the $\log_{10} \dot{\varepsilon}_s$ vs. $1/T^oK$ graph given in Figure 25.

A value of ∿ 100 kcal/mol was obtained for the activation energy, Q, in the equation

$$\dot{\varepsilon}_s = A.e^{-\frac{Q}{RT}} \qquad (13)$$

3.5 Metallography

3.5.1 Optical metallography

A general examination showed a banded ferrite/pearlite structure, no doubt arising from the production of the 7.5 cm square, 1.2 m long billets. The pearlite was partially resolvable and the ferrite grains showed evidence of a homogeneous matrix carbide distribution with massive carbides at the grainboundaries. The ferrite grains varied in size from 10 μm to 60 μm in the 'as received' condition and were not equiaxed. Figure 10 shows the general form of the structure. Three heat treatment batches were used in these tests as stated in 2.1 and it was found necessary to control the heat treatment very carefully to obtain the same structure otherwise coarsening occurred. All three batches

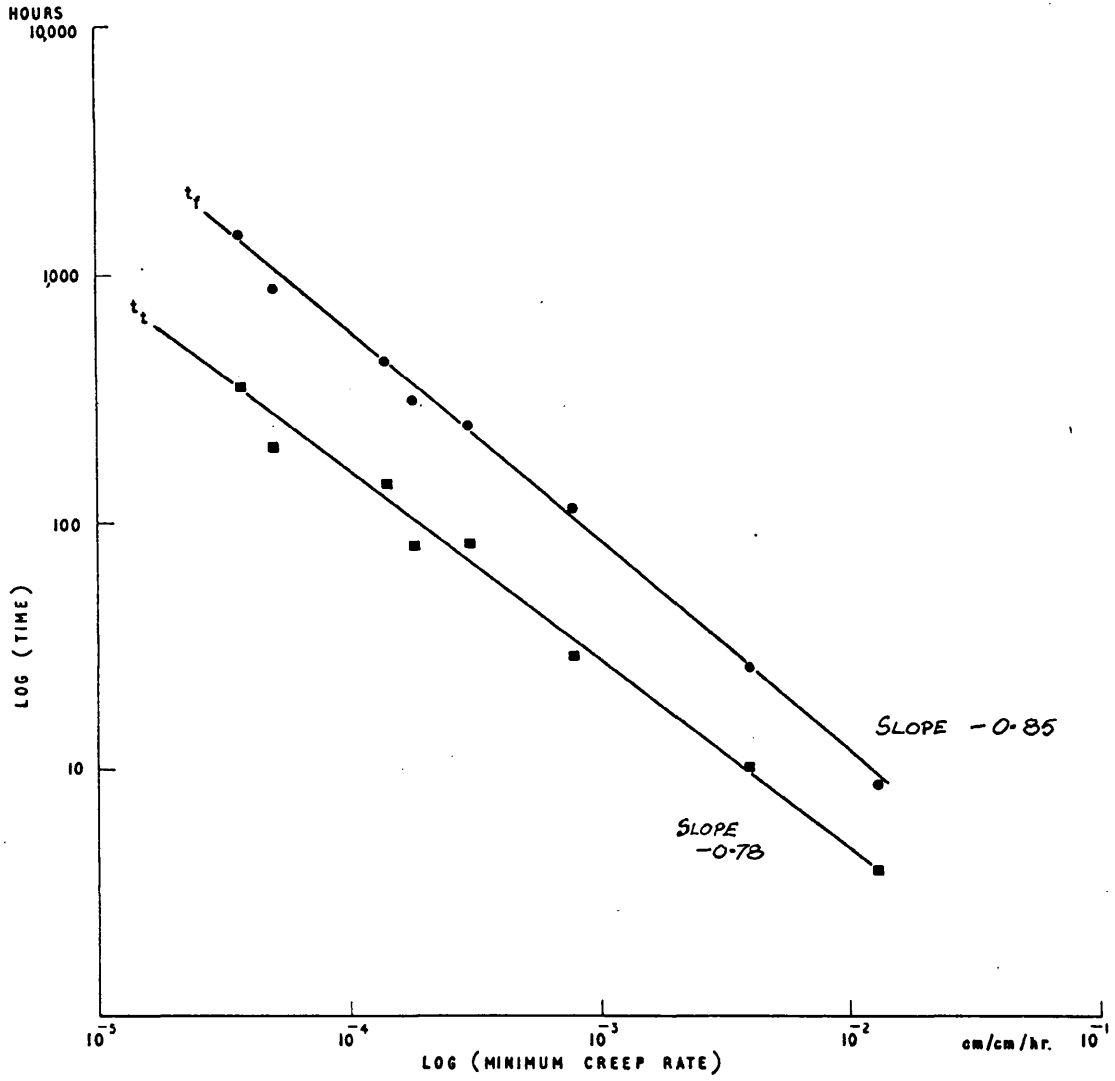

THE RELATIONSHIP BETWEEN MINIMUM CREEP RATE AND TIME TO ONSET OF TERTIARY (t_t) AND TIME TO FAILURE (t_f) FOR SLOWLY AND RAPIDLY LOADED SPECIMENS AT 550°C.

FIGURE 23

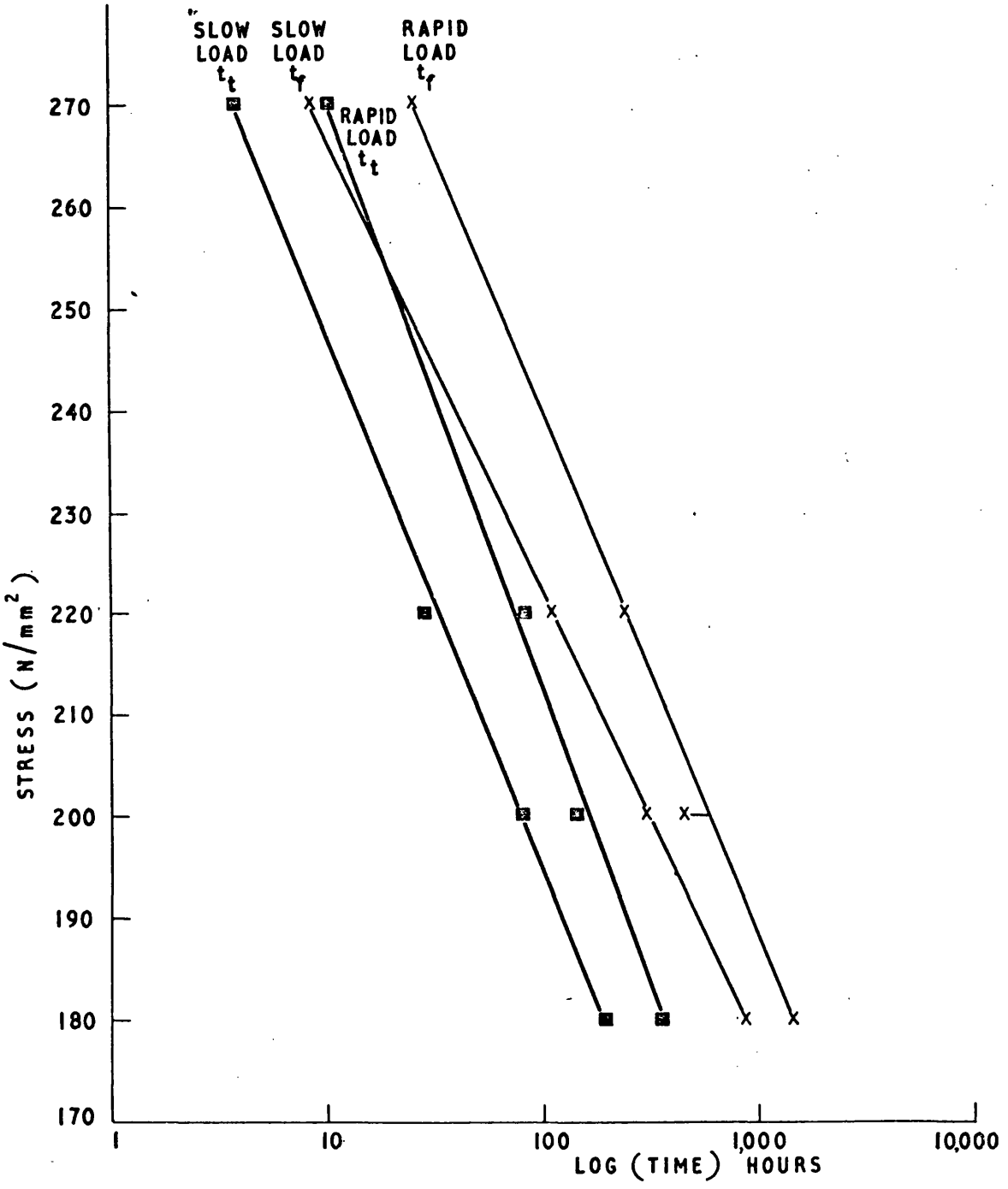

THE STRESS DEPENDENCE OF THE TIME TO ONSET OF TERTIARY CREEP (t_t) AND TIME TO FRACTURE (t_f) FOR SLOWLY AND RAPIDLY LOADED SPECIMENS AT 550°C.

FIGURE 24

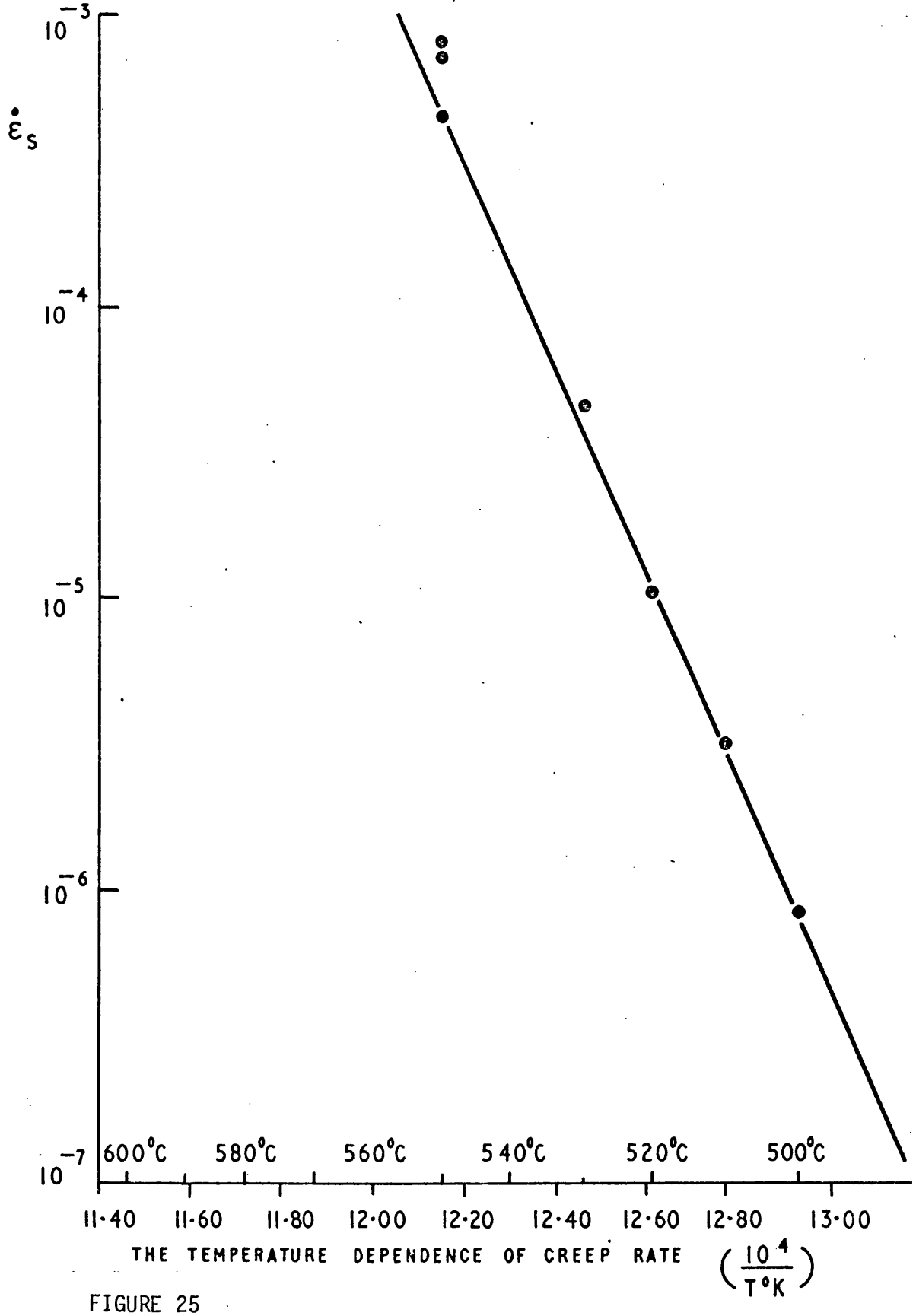
10^{-3}
$\dot{\varepsilon}_s$
10^{-4}
10^{-5}
10^{-6}
10^{-7}
600°C
580°C
560°C
540°C
520°C
500°C
11·40
11·60
11·80
12·00
12·20
12·40
12·60
12·80
13·00
THE TEMPERATURE DEPENDENCE OF CREEP RATE $\left(\frac{10^4}{T°K}\right)$

FIGURE 25

have the same basic structure. The fine ferrite grains appeared to be stable under all test conditions except the long test times, rapidly pre-strained tests and in the 'necked' portion of the failed test pieces. In the tests which ran for three or four hundred hours there was evidence of some graingrowth and the form became equiaxed. The diameter tended to a maximum of 200 μm where graingrowth occurred. The massive carbides at the boundaries would seem to be capable of stabilising the grainsize effectively in the short term.

3.5.2 Electron metallography - replica examination

If structures are ill defined under the light microscope it is logical to proceed to the examination of replicas in the electron microscope. The technique used is described in Appendix 5 and gives indirect carbon replicas shadowed with gold-palladium. The greatly improved resolution enabled the 'as received' grainsize to be confirmed, Figure 26, but showed that grainboundary migration certainly occurred in tests of short duration. Figure 27 shows the structure of a test piece which was slowly loaded and failed in 7.3 hours. In this figure, migration of a boundary is evident in the large original grain delineated by carbides. It is probable that of the three transverse boundaries visible, only the most distinct is a current one, the other two being arrest positions. Whether the arrests were due to heat treatment stages or occurred during creep is not known. The impedance of boundary movement by massive carbides is demonstrated by the kinked form associated with carbides.

Replicas of this type often extract a few particles and this affords an opportunity for identification. An example of this is given in Figure 28 which shows particles and the diffraction pattern obtained. These particles are reported by other workers as V_4C_3 platelets. The diffraction pattern in Figure 28 was found to belong to a cubic compound

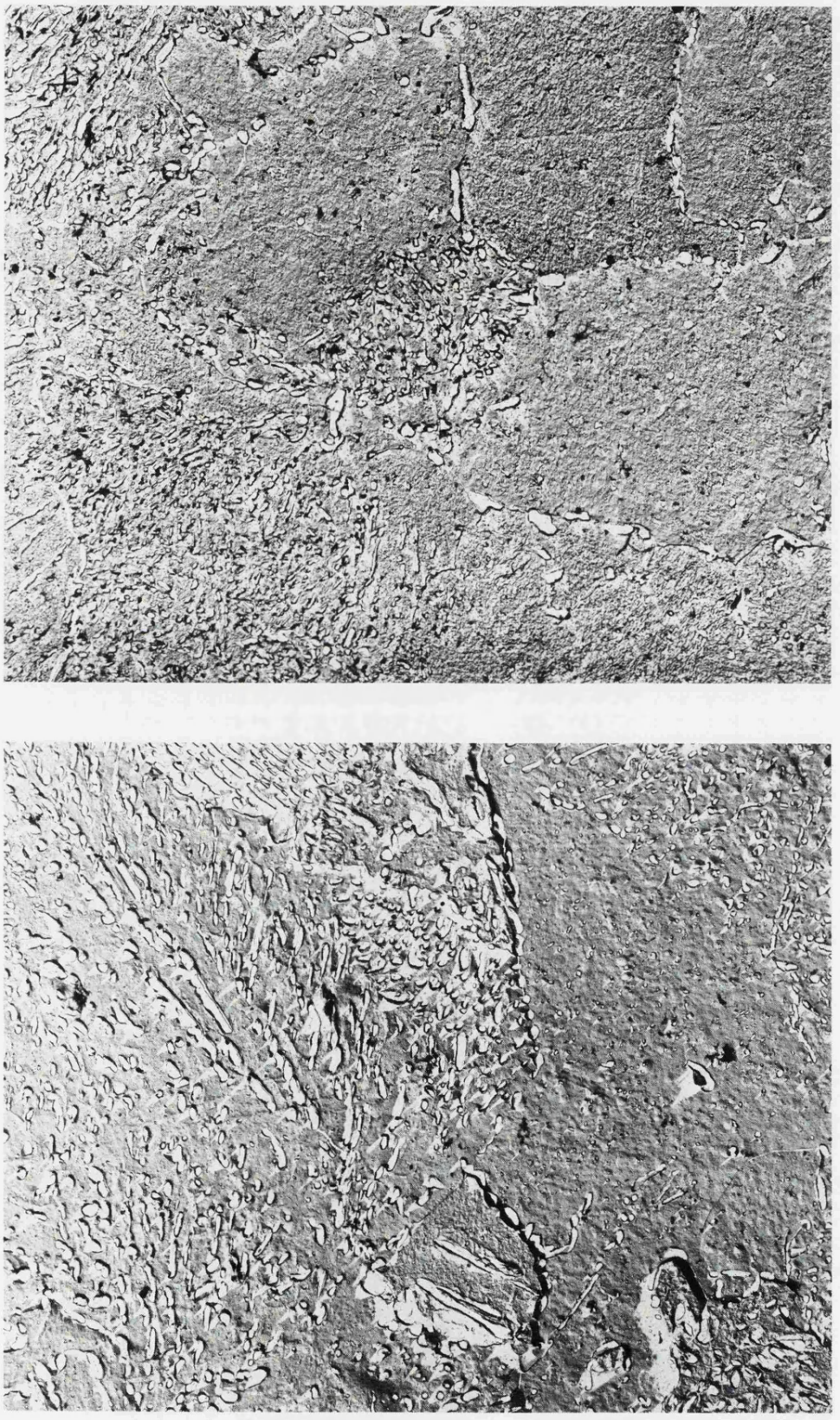

FIGURE 26 SHADOWED REPLICAS OF THE MICROSTRUCTURE PRIOR TO TEST. X 1,600
TOP BATCH 1, BOTTOM BATCH 2

FIGURE 27 SHADOWED REPLICA SHOWING GRAINBOUNDARY MIGRATION. X 1,600

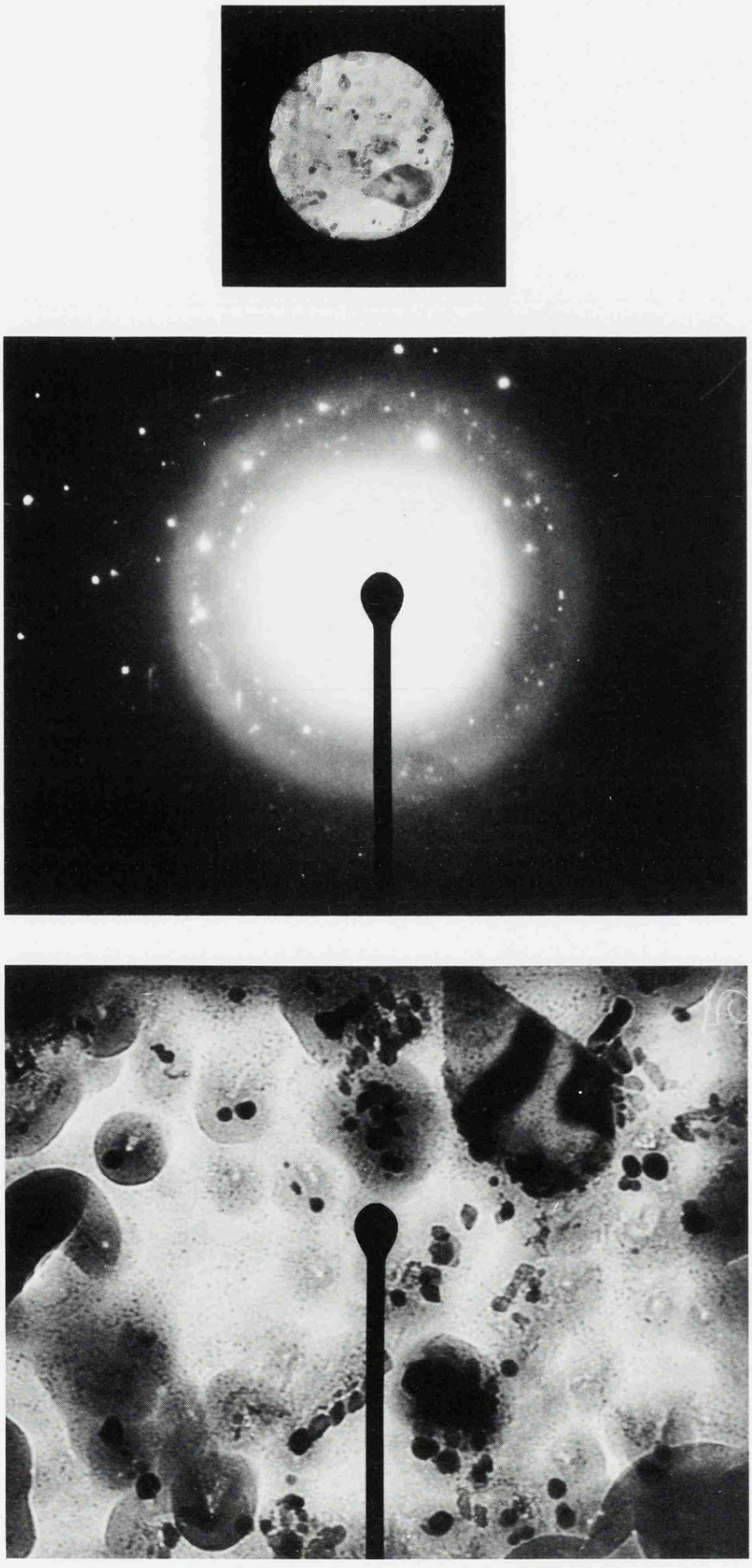

FIGURE 28 SELECTED AREA DIFFRACTION FROM THE SMALL AREA SHOWN. X 30,000
THE LOWER PHOTOMICROGRAPH SHOWS THIS AREA IN DETAIL. X 100,000
SHADOWED REPLICAS.

with a NaCl structure the 'a' parameter of which (cube edge) was approximately 4.14Å. An extract from Pearson (1967)[58] given in Table 5 shows that a wide range of VC_x values exist and phases δC, δ, δβ, βα and α exist in the cubic form. V_4C_3 approximates to the δ carbide with an 'a' value of 4.1285Å and the one given is also δ but nearer V_5C_4. The habit plane of the carbide is the (111). These carbides are also shown to be in platelet form by Figure 29 taken from a carbide extraction replica (see 3.5.3 for this topic). The platelets were partially transparent to electrons and exhibit Moiré fringes and possibly extended dislocations. Platelets are often found in lines and the two shown abutting here have an undoubted lattice coherence since the defects continue from one to the other. It is possible that partial coherency exists between the iron lattice and the platelets when they are very thin and small.

TABLE 5

VCx	Free C	Phases	a(cube edge in Å)
.939	.017	δC	4.1682
.933	.017	δC	4.1676
.923		δ	4.1686
.900		δ	4.1652
.876		δ	4.1644
.865		δ	4.1611
.797		δ	4.1425
.748		δ	4.1285
.704		δβ	4.1258
.701		δβ	4.1258

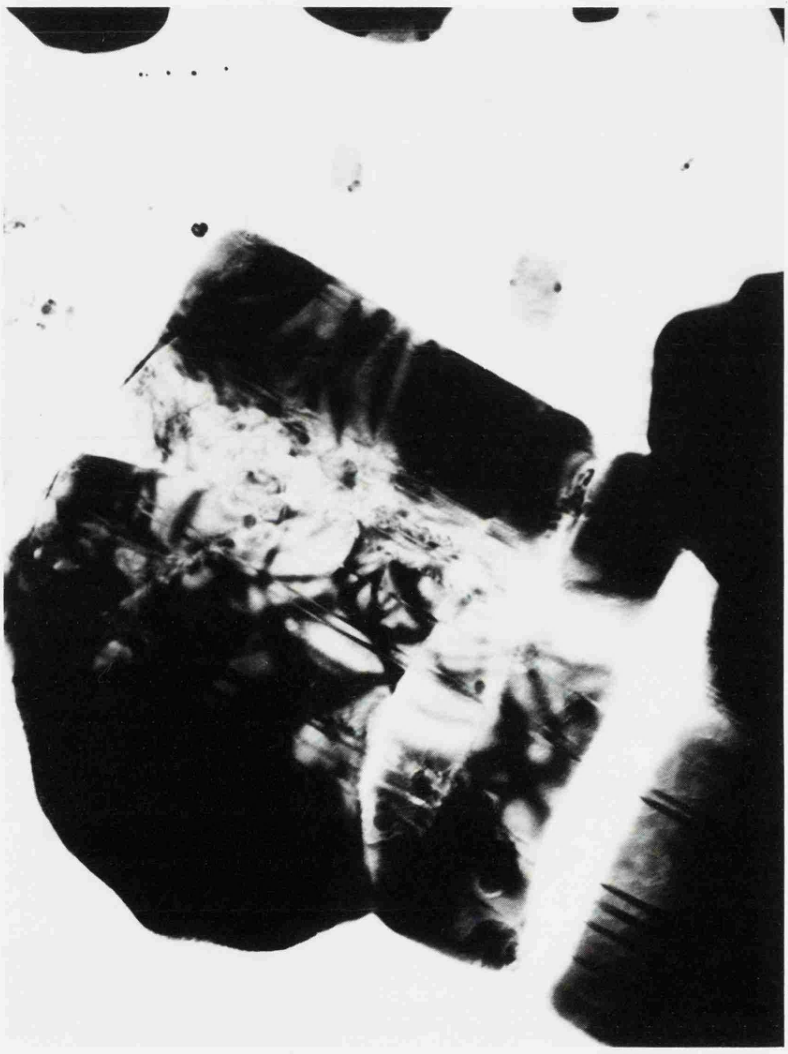

FIGURE 29 VANADIUM CARBIDE PLATELETS. EXTRACTION REPLICA. X 100,000

3.5.3 Electron metallography - extraction replicas

Since the dispersion of precipitates etc. is recognised to be of great importance as a strengthening mechanism the extraction technique was applied to the specimens. A description of the method is given in Appendix 5. A comparison has been made between the virgin material and both failed and partially tested specimens.

In general it may be said that the pearlite exhibited a range of forms and typical examples are given in Figure 30. Since creep in these structures will be limited they are of interest mainly because of the volume of pearlite and the effect on the surrounding matrix. The fine carbides, mainly VC_x and possibly M_2C are relatively unaffected by the pearlite masses whereas the more massive discrete matrix carbides often decrease in density adjacent to pearlite. Pearlite would therefore appear to denude the matrix of such elements as chromium but not vanadium or carbon.

The matrix carbides fell into two main groups, the profuse fine carbides of less than 300Å diameter and the much less numerous large carbides up to 1,500Å diameter. The untested material from Batches 1 and 2 used for the pre-strain and loading rate tests respectively, varied in the amount of carbide present in the matrix. Figure 31 shows the distribution and form at relatively low magnification. This fine precipitate would provide a reason for the longer creep lives attained in the pre-strained tests. Nonetheless the loading rate effect was present to a marked degree in both batches so that from this aspect there is little effect of prior spacing. The loading rate effect without pre-strain was examined using Batch 1 material for some tests and Batch 2 for the main test series. In Batch 1 the final carbide spacing had changed as shown by Figure 32. This figure includes replicas from test pieces 'frozen' after five minutes, little difference is

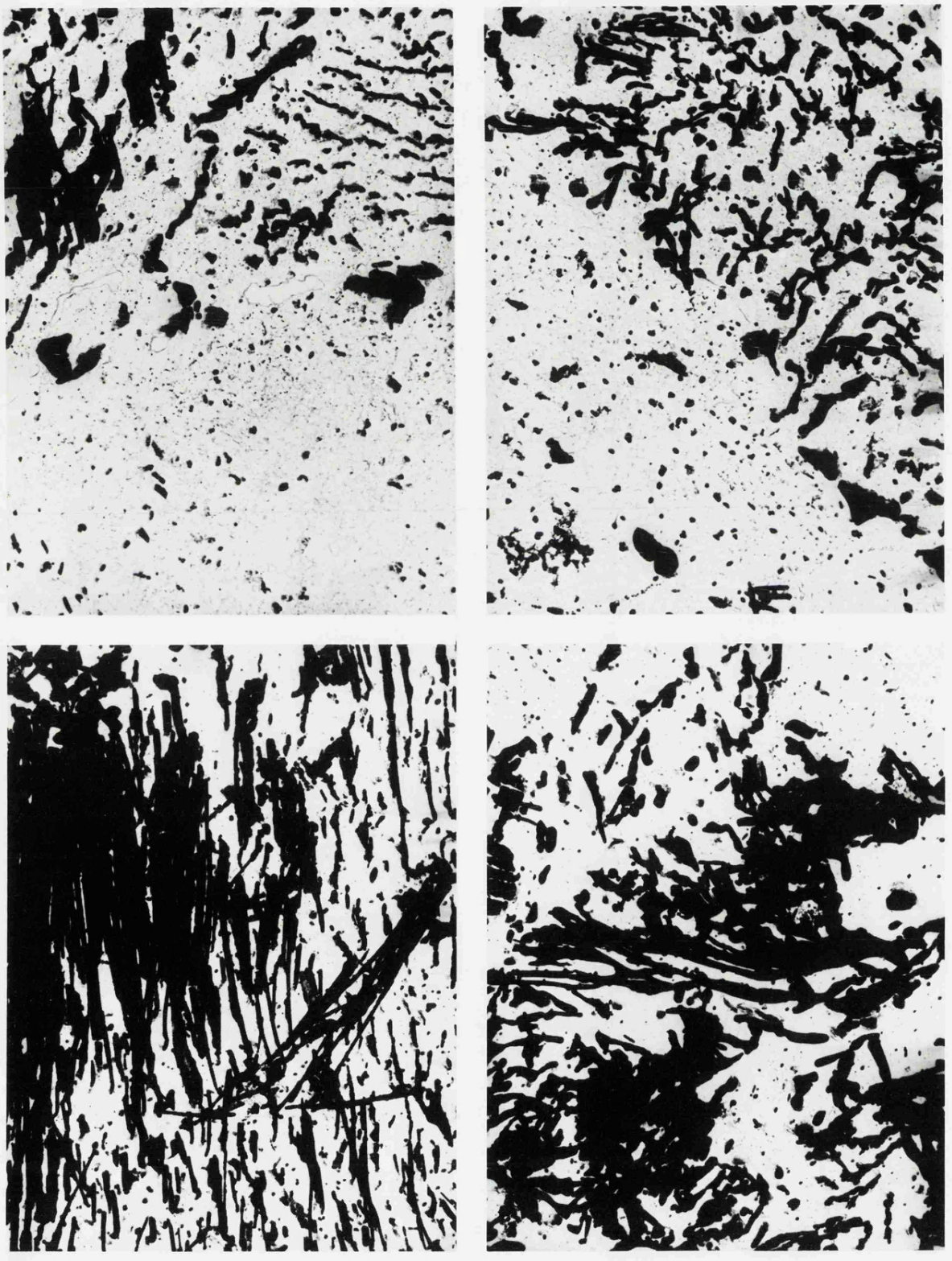

FIGURE 30 FORMS OF CARBIDES IN PEARLITE. EXTRACTION REPLICAS. X 5,600

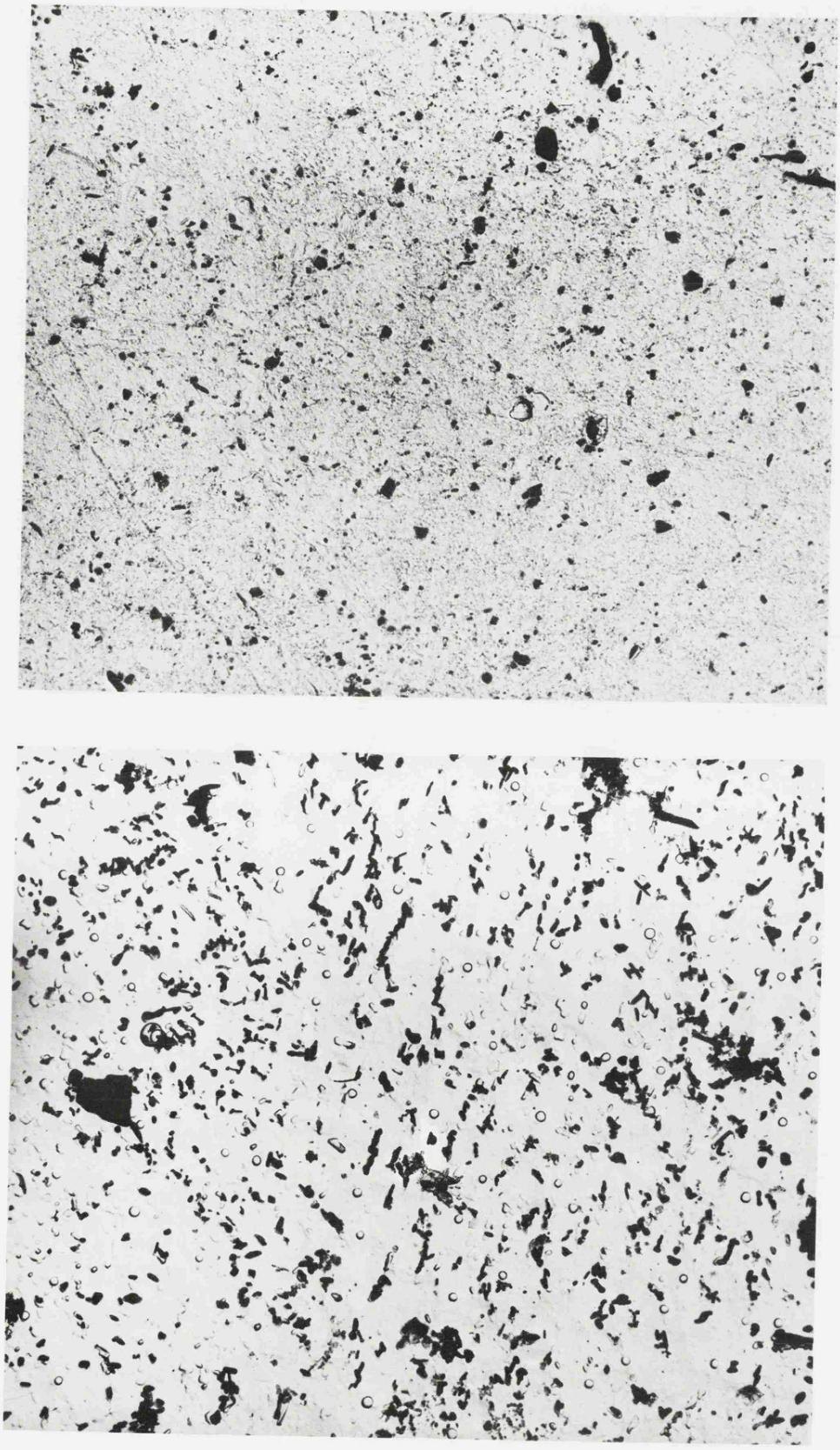

FIGURE 31 EXTRACTION REPLICAS OF THE STRUCTURE PRIOR TO TEST. X 5,600
TOP BATCH 1, BOTTOM BATCH 2.

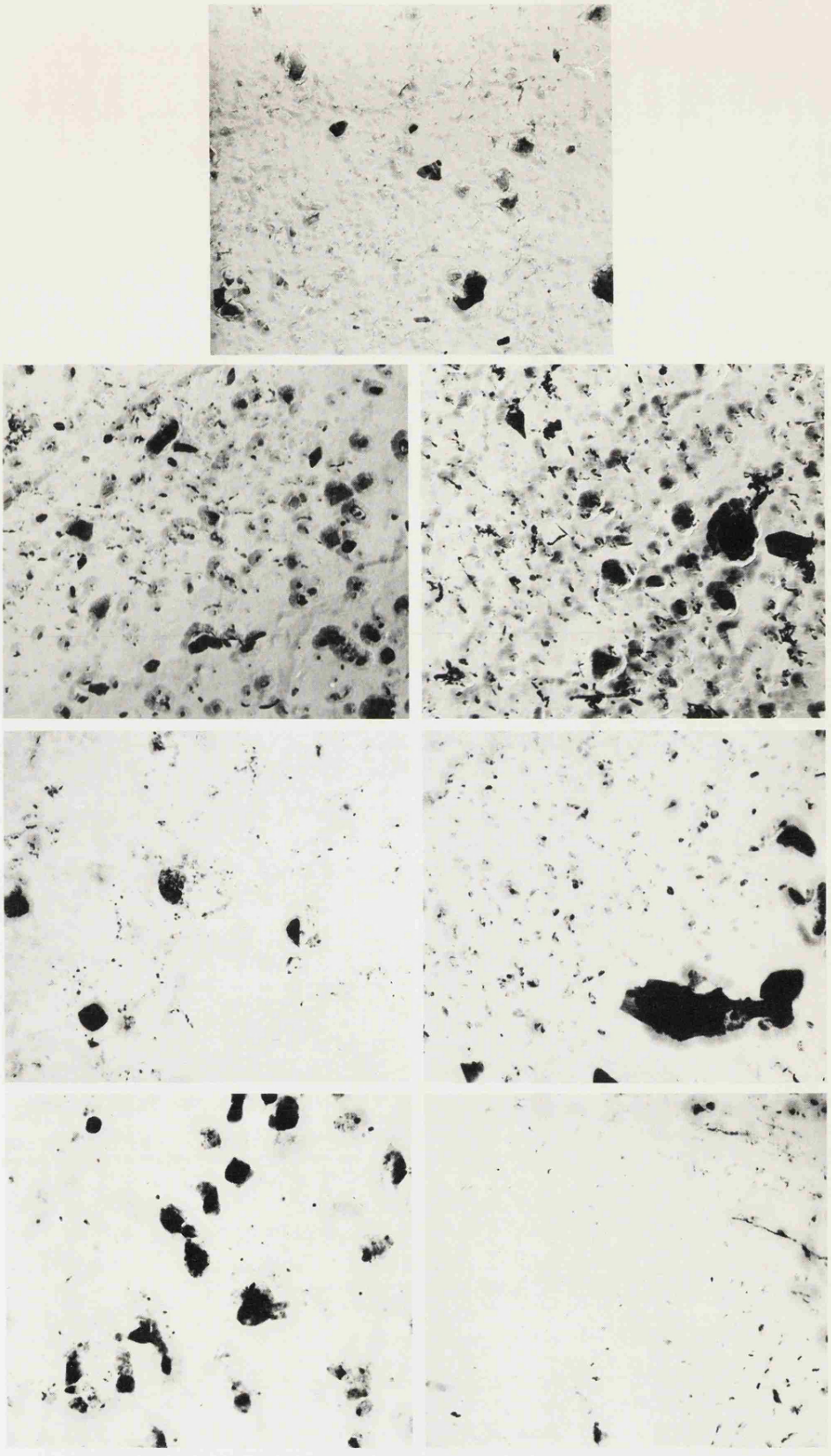

FIGURE 32 BATCH 1 CARBIDE DISTRIBUTION BEFORE, DURING AND AFTER TESTS.
EXTRACTION REPLICAS. X 33,000
TOP - BEFORE TEST.
2ND ROW - LEFT. RAPID LOAD AFTER 5 MINUTES TESTING.
RIGHT. SLOW LOAD AFTER 5 MINUTES TESTING.
3RD ROW - RAPID LOAD. FAILED TEST PIECE.
4TH ROW - SLOW LOAD. FAILED TEST PIECE.

observable between the virgin material and these test pieces. Insufficient loading rate work was performed on this batch to draw conclusions concerning the dependence of creep rate upon loading rate. However, the final fine carbide spacings (measured as 220Å for slow load, high creep rate and 200Å for the opposite condition) are in the right relationship with creep rate i.e. greater spacing, greater rate of creep. The comprehensive set of results from Batch 2 were much easier to analyse and gave more definitive answers to the question of creep rate dependence on particle spacing. Visual comparison of failed loading rate specimens from Batch 2 indicated that the fine carbide population decreased with both increasing creep rate and stress. At the same stress the slowly loaded test piece apparently contained fewer fine carbides than the rapidly loaded one, again consistent with the creep rate. The extremes are depicted in Figure 33 and once observed a corollary is particle spacing analysis. Section 3.6 covers the aspect of the work. It was performed because the spacing effect may have been present in Batch 1 but not obviously so. Comparison of the failed Batch 2 loading rate test piece carbide populations with the 'as received' structure revealed a paucity and inhomogeneity of fine carbide as shown by Figure 34.

Thus the fine carbide population of Batch 2 is a function of the test conditions. The creep rate is stable early in the test as described in 3.3 Therefore, if carbide spacing is important in this work the definitive spacing must be established early in the test. Analysis of the particle spacing and of relationships between spacing and other parameters is given in 3.6.

3.6 Particle Spacing Analysis of Extraction Replicas

Calculation of the mean spacing between particles is not a simple matter because few distributions are homogeneous and many contain

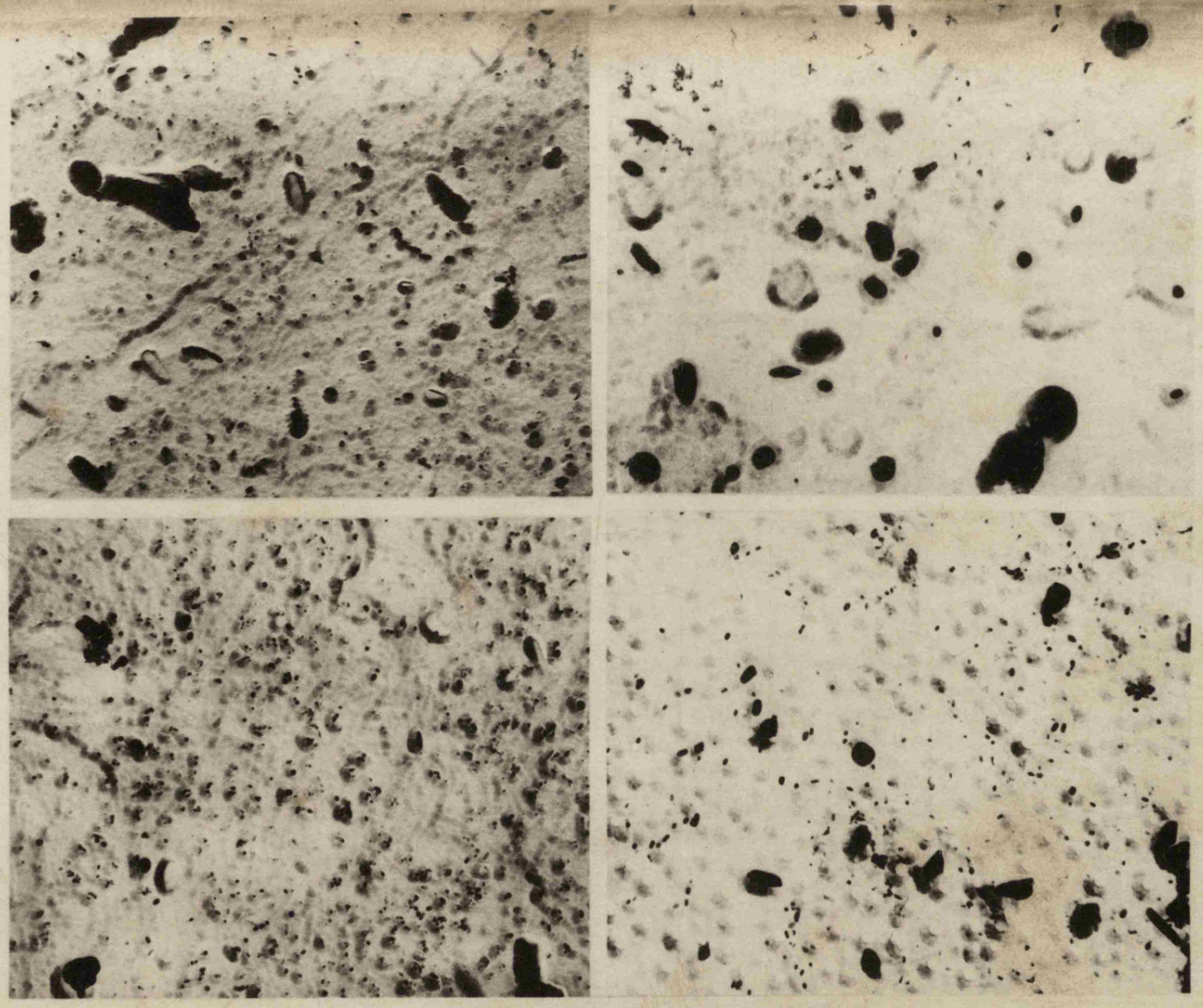

FIGURE 33 THE EXTREMES OF CARBIDE DISTRIBUTION IN FAILED, LOADING RATE TESTS. EXTRACTION REPLICAS. X 33,000
TOP LEFT - 270 N/mm^2, RAPID LOAD
TOP RIGHT - 270 N/mm^2, SLOW LOAD
BOTTOM LEFT - 180 N/mm^2, RAPID LOAD
BOTTOM RIGHT - 180 N/mm^2, SLOW LOAD

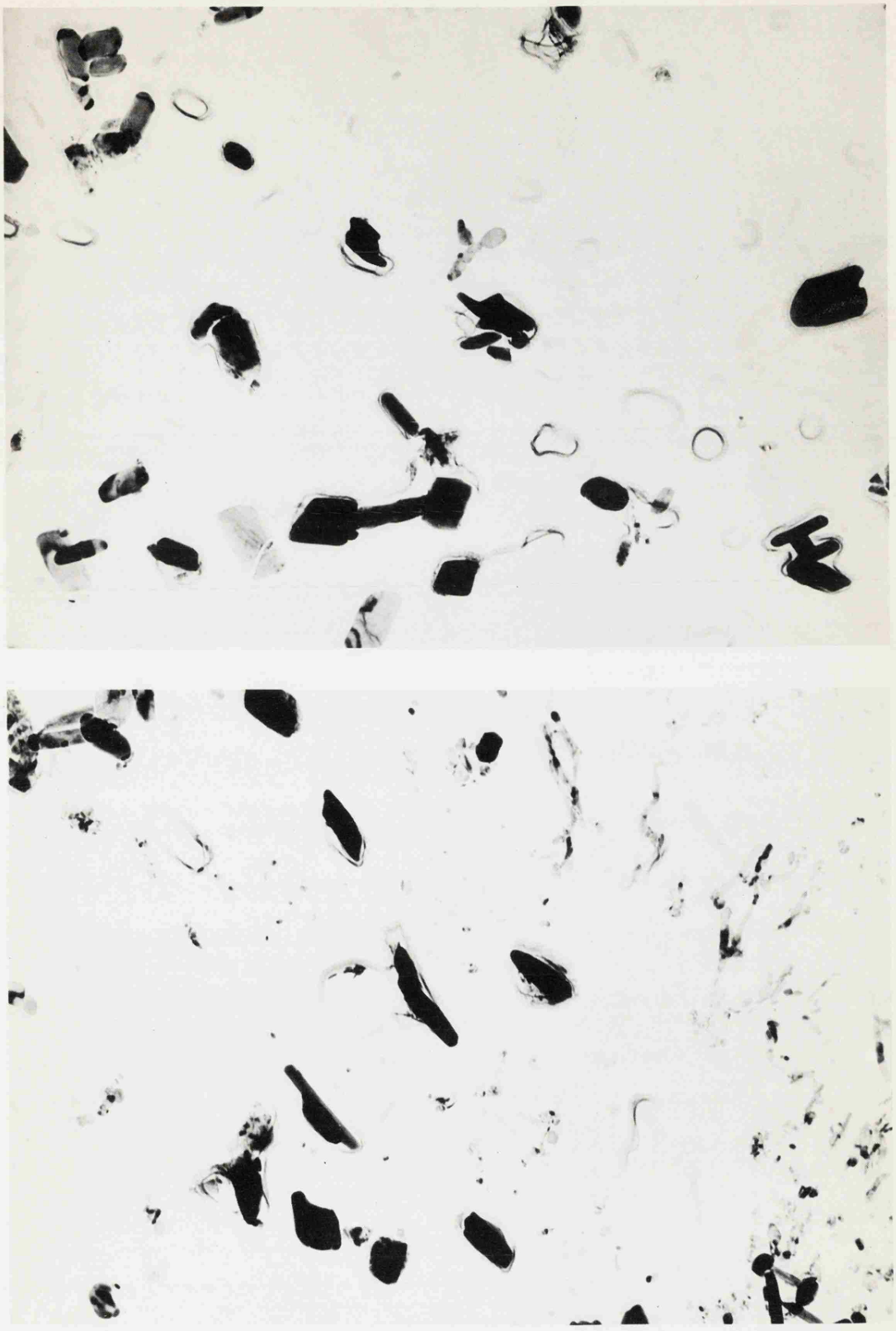

FIGURE 34 BATCH 2 CARBIDE DISTRIBUTION BEFORE TEST.
EXTRACTION REPLICAS. X 33,000

particles of varying size. The method of displaying particles for measurement is important since this can lead to misleading results. Ashby and Ebeling (1966)[2] and Prnka (1969)[60] consider the problems together with the methods of approaching them. Figure 35, taken from Ashby and Ebeling demonstrates the main problem associated with sampling, which is obtaining a planar sample. If all particles were known to be of one diameter and were large enough to be seen under the light microscope the distribution could easily be calculated from a polished planar sample. By ignoring all particle cross sections except those having the full diameter, a reasonable planar spacing could be derived. If the particles are sub-microscopic, extraction replicas are necessary and as Figure 35 demonstrates, the release of the carbon film by etching will leave all of the particles attached to the film. Thus particles have been removed from a volume and not a plane. The required result is the average centre to centre spacing between a particle and its nearest neighbour in a random, three dimensional array, when measured in the volume containing the array. The method used (Ashby and Ebeling) was to specify arbitrary particle size limits and further to divide the field into a convenient number of small fields. The number of particles in each size group is counted and tabulated. At the end of a count on a plate, film etc., the total in each column is obtained and the number of precipitates per unit area determined (n_s) for each size

$$n_s = \frac{\text{total precipitates x area of one field}}{\text{number of fields}}$$

The number per unit volume (n_v) is given by $n_s/\bar{d}$, where $\bar{d}$ is the mean diameter per column.

Interparticle spacings in a volume containing the array are given by

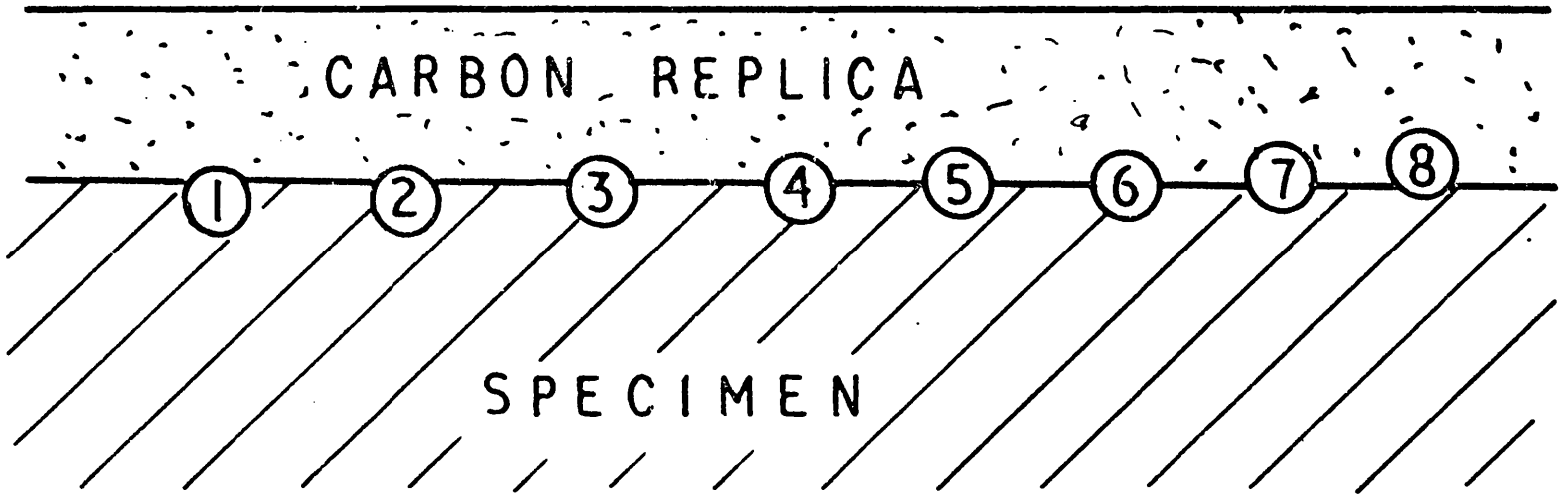

EIGHT PARTICLES, EMBEDDED TO DIFFERENT DEPTHS IN THE SURFACE OF THE SPECIMEN, BUT ALL TOUCHING OR INTERSECTING IT.

FIGURE 35

$$\bar{D}_v = 0.554 \left(\frac{1}{n_v^{-1}}\right)^{\frac{1}{3}} \qquad (14)$$

where $\bar{D}$ is the average centre to centre spacing.

The results obtained were treated to give two values of $\bar{D}_v$, one for particles whose diameter was less than 300Å and the other for particle diameters greater than 300Å. Those are presented in Table 6 together with the relevant test data. The reasons for separating the two sizes of particle are, firstly the small ones are believed to be mainly VC_x which precipitates during creep. Secondly there is no real gradation of sizes since the VC_x is relatively uniform in size whereas the remaining carbides vary from ∿ 300Å to 1,500Å in diameter.

TABLE 6

Stress N/mm^2	Loading rate	Creep rate ($\dot{\varepsilon}_s$)	Particle Spacing (λ) in Å	
			< 300Å dia.	> 300Å dia.
270	Rapid	4.5×10^{-3}	160	537
270	Slow	1.34×10^{-2}	242	737
220	Rapid	3.2×10^{-4}	125	508
220	Slow	7.8×10^{-4}	161	746
200	Rapid	1.4×10^{-4}	140	758
200	Slow	2.0×10^{-4}	176	597
180	Rapid	4.0×10^{-5}	133	918
180	Slow	5.7×10^{-5}	141	667

Figures 36 and 37 show the relationship of particle spacing with steady state creep rate and stress. A satisfactory set of plots was obtained. In order to test the results for possible creep rate

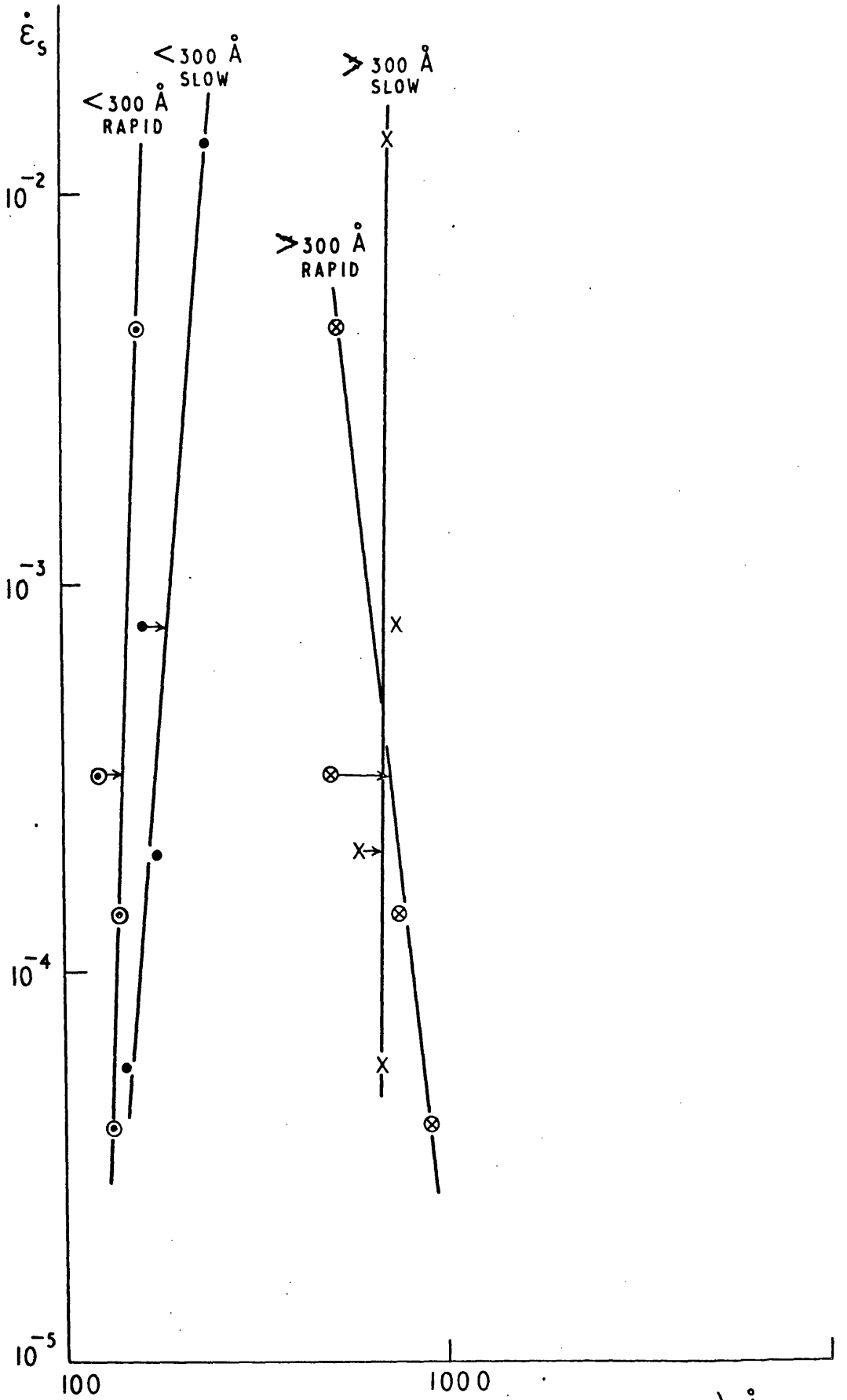
$\dot{\varepsilon}_s$
10^{-2}
10^{-3}
10^{-4}
10^{-5}
< 300 Å RAPID
< 300 Å SLOW
> 300 Å SLOW
> 300 Å RAPID
100
1000
THE STRAIN RATE RELATIONSHIP WITH PARTICLE SPACING λ Å

FIGURE 36

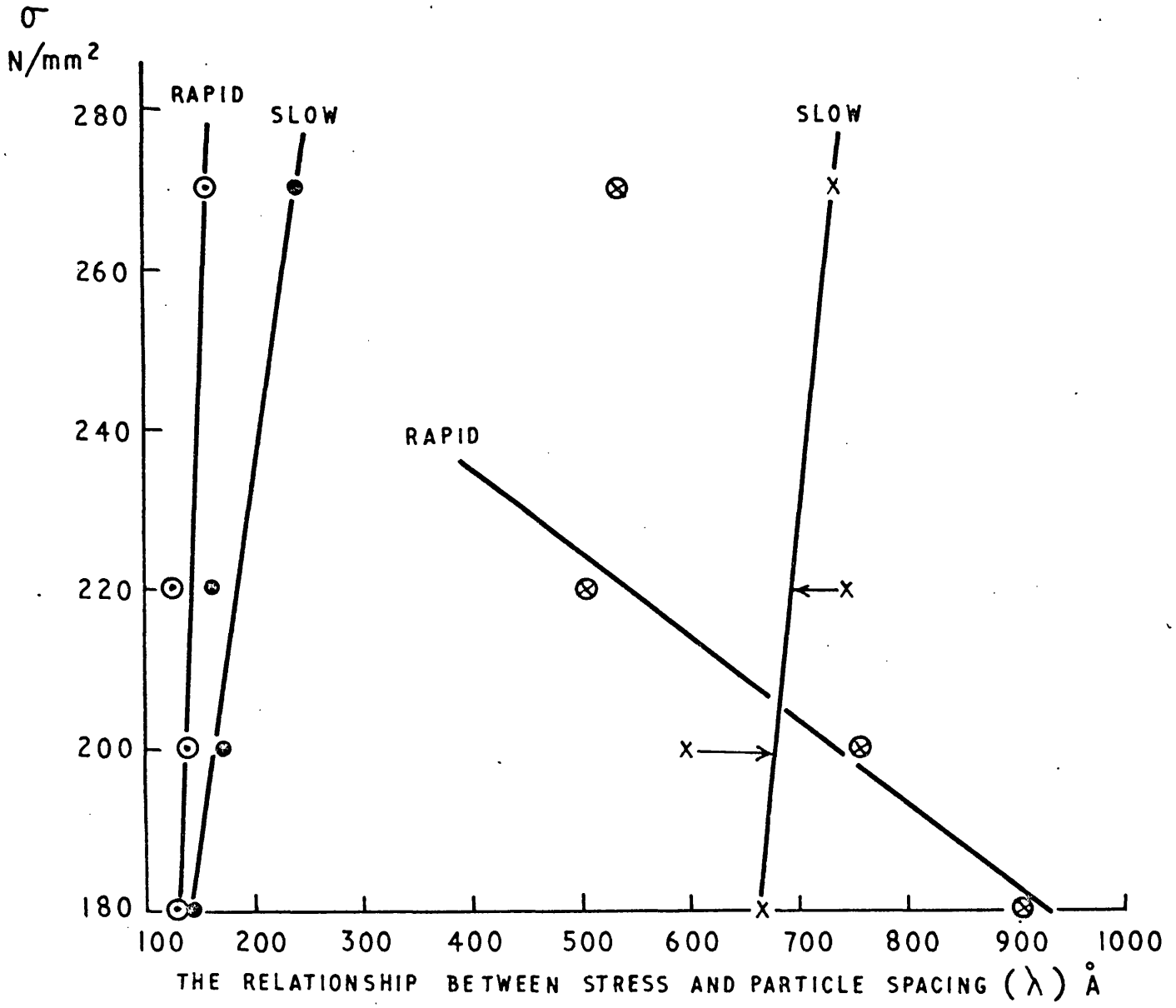
σ
N/mm²
RAPID
SLOW
SLOW
RAPID
280
260
240
220
200
180
100
200
300
400
500
600
700
800
900
1000
THE RELATIONSHIP BETWEEN STRESS AND PARTICLE SPACING (λ) Å

FIGURE 37

dependence on particle spacing the model of Ansell and Weertman (1959)[1] was used (see Appendix 5). Their equation for high stress creep was as follows

$$\dot{\varepsilon}_s = K \sigma^4 \lambda^2 \tag{15}$$

where λ is particle spacing.

This equation is normally used to show that, at constant stress

$$\dot{\varepsilon}_s \propto \lambda^2 \tag{16}$$

In these tests the stress was not constant and so the stress term must be used. The stress exponent determined in 3.3 had the value of 12. By re-arranging and re-stating equation (15) we obtain

$$\left(\frac{\dot{\varepsilon}}{\sigma^{12}}\right) = K \lambda^2 \tag{17}$$

by plotting log $(\dot{\varepsilon}/\sigma^{12})$ vs. log λ we can test for a creep rate dependence upon λ and obtain the exponent for λ. Figure 38 shows the results plotted in this form and it will be observed that a slope of 2.5 gives the best fit to both sizes of particles. If the creep rates at the different stresses and loading rates are dependent upon particle spacing then, by evaluating K for each test, for both fine and coarse particles, it should be possible to predict the creep rates from a mean value of K.

The values for K were calculated from the results using equation (18) and are given in Table 7.

$$K = \frac{\dot{\varepsilon}_s}{\sigma^{12} . \lambda^{2.5}} \tag{18}$$

From the mean values of K the creep rates for the tests were predicted using equation (18) and the results are presented in Table 8.

It is considered that the predicted results are in good agreement with the experimental values.

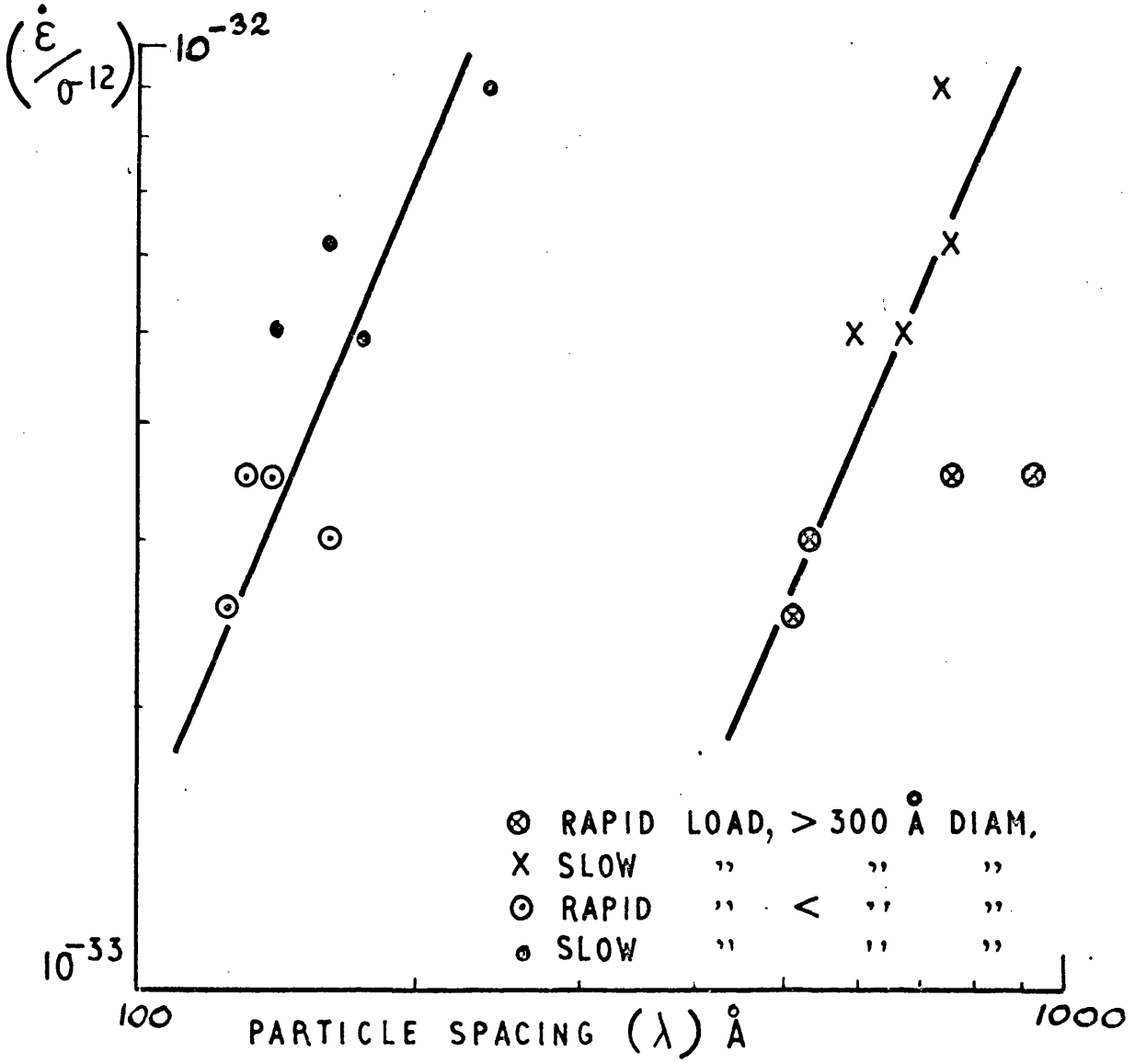
$\left(\frac{\dot{\varepsilon}}{\sigma^{12}}\right)$
10^{-32}
10^{-33}
⊗ RAPID LOAD, > 300 Å DIAM.
X SLOW " " " "
⊙ RAPID " < " " "
• SLOW " " " "
100
PARTICLE SPACING (λ) Å
1000

FIGURE 38

TABLE 7

σ N/mm^2	Loading Rate	$\dot{\varepsilon}_s$	Particles < 300Å dia.		Particles > 300Å dia.	
			λÅ	$Kx10^{-37}$	λÅ	$Kx10^{-39}$
270	Rapid	4.5×10^{-3}	160	9.2	537	4.5
270	Slow	1.3×10^{-2}	242	9.8	737	6.1
220	Rapid	3.2×10^{-4}	125	14.3	508	4.3
220	Slow	7.8×10^{-4}	161	18.6	746	4.0
200	Rapid	1.4×10^{-4}	140	14.6	758	2.2
200	Slow	2.0×10^{-4}	176	11.8	597	5.6
180	Rapid	4.0×10^{-5}	133	17.1	918	1.4
180	Slow	5.7×10^{-5}	141	21.0	667	4.3
Mean Value				14.6		4.0

TABLE 8

σ N/mm^2	Loading Rate	Experimental $\dot{\varepsilon}_s$	$\dot{\varepsilon}_s$ predicted from fine particles	$\dot{\varepsilon}_s$ predicted from coarse particles
270	Rapid	4.5×10^{-3}	7.1×10^{-3}	4.0×10^{-3}
270	Slow	1.3×10^{-2}	2.0×10^{-2}	8.9×10^{-3}
220	Rapid	3.2×10^{-4}	3.3×10^{-4}	3.0×10^{-4}
220	Slow	7.8×10^{-4}	6.1×10^{-4}	7.9×10^{-4}
200	Rapid	1.4×10^{-4}	1.4×10^{-4}	2.6×10^{-4}
200	Slow	2.0×10^{-4}	2.5×10^{-4}	1.4×10^{-4}
180	Rapid	4.0×10^{-5}	3.4×10^{-5}	1.2×10^{-4}
180	Slow	5.7×10^{-5}	4.0×10^{-5}	5.4×10^{-5}

3.7 Density Measurements

Measurements were made to try and detect changes from specimen to specimen in the amount of structural damage of the grainboundary cavity type.

The specimens examined were the loading rate series, using the method and apparatus described in Appendix 3.

Measurements were made prior to test and after failure. In order to make the final readings as sensitive as possible the ends of the specimens were removed together with about 0.1 in. either side of the fracture face. The latter was deemed necessary to prevent trapped air or foreign matter at the fracture face from affecting the readings. A density decrease was observed in all specimens of between approximately 1% and 3% but no trend with respect to other measured parameters was noted.

The results to four places of decimals are given in Table 9.

TABLE 9

σ	Loading Rate	$\frac{\Delta\rho}{\rho}$
270	Slow	0.0279
270	Rapid	0.0226
220	Slow	0.0213
220	Rapid	0.0135
200	Slow	0.0072
200	Rapid	0.0267
180	Slow	0.0235
180	Rapid	0.0226

3.8 Hardness Measurements

Hardness values were obtained from the failed loading rate specimens to test further the correlation of structure with the parameters stress, creep rate and particle spacing.

The values obtained are presented in Table 10 and were obtained on a Vickers machine using a 5 Kg load with a diamond indenter.

TABLE 10

Stress N/mm^2	Loading Rate	VPN	Mean VPN
270	Rapid	241, 249, 246	245
270	Slow	244, 254, 246	248
220	Rapid	227, 234, 232	231
220	Slow	232, 236, 241	236
200	Rapid	232, 234, 232	233
200	Slow	229, 232, 227	229
180	Rapid	221, 223, 227	224
180	Slow	223, 223, 225	224

These values are plotted against stress in Figure 39 and against ($\log \dot{\varepsilon}_s$) in Figure 40, both plots show a good correlation. Figure 41 shows that the relationship between particle spacing and hardness is similar to that between spacing and stress. The similarity is to be expected in view of the dependence of hardness upon the creep stress. However, only in the instance of the large carbides in rapidly loaded tests is the dependence in the expected sense with hardness increasing with decreasing spacing. The implication is that the degree of matrix strengthening by work hardening is the dominant factor.

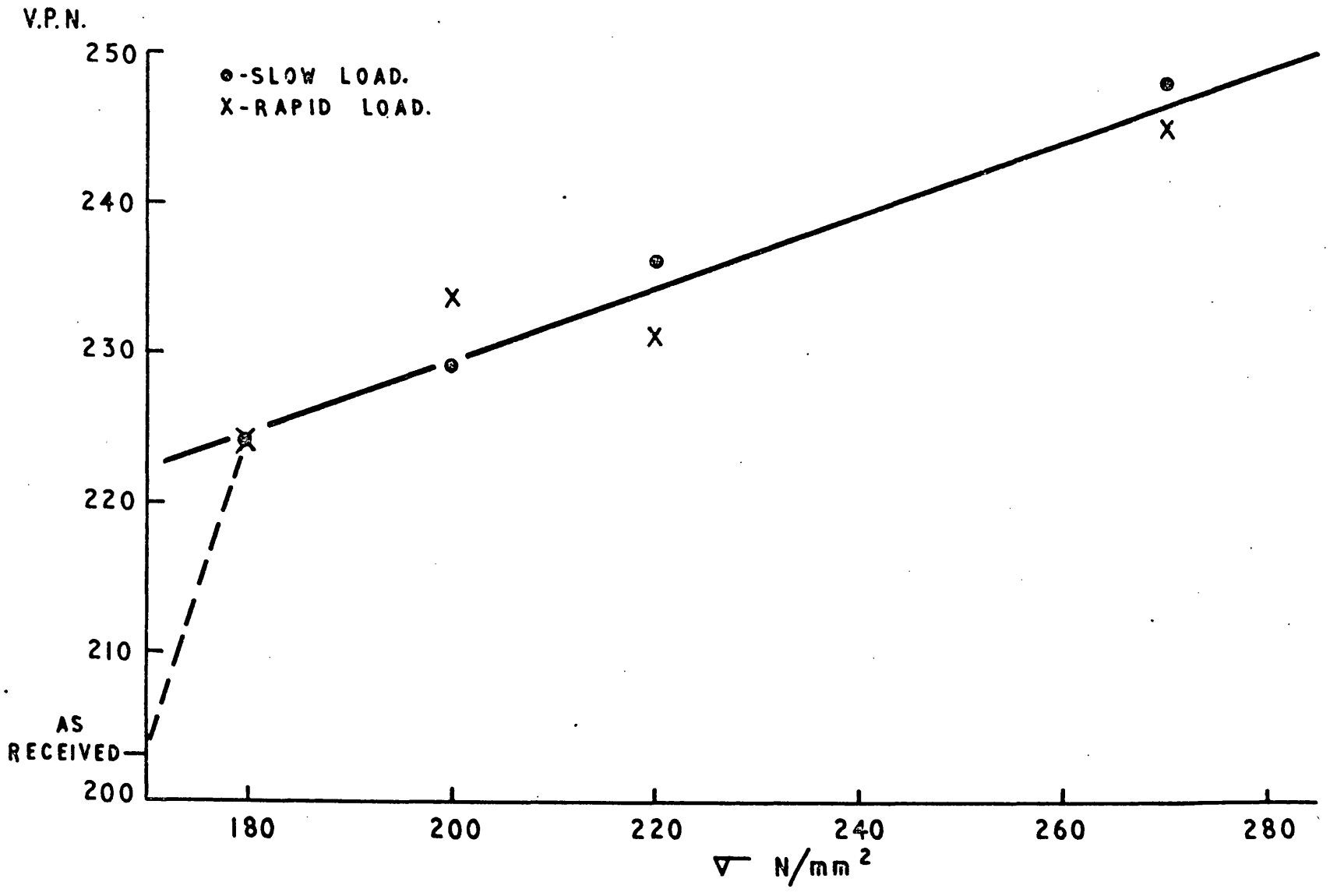
V.P.N.
250
240
230
220
210
AS
RECEIVED
200
⊙-SLOW LOAD.
X-RAPID LOAD.
180
200
220
240
260
280
∇ N/mm²

FIGURE 39

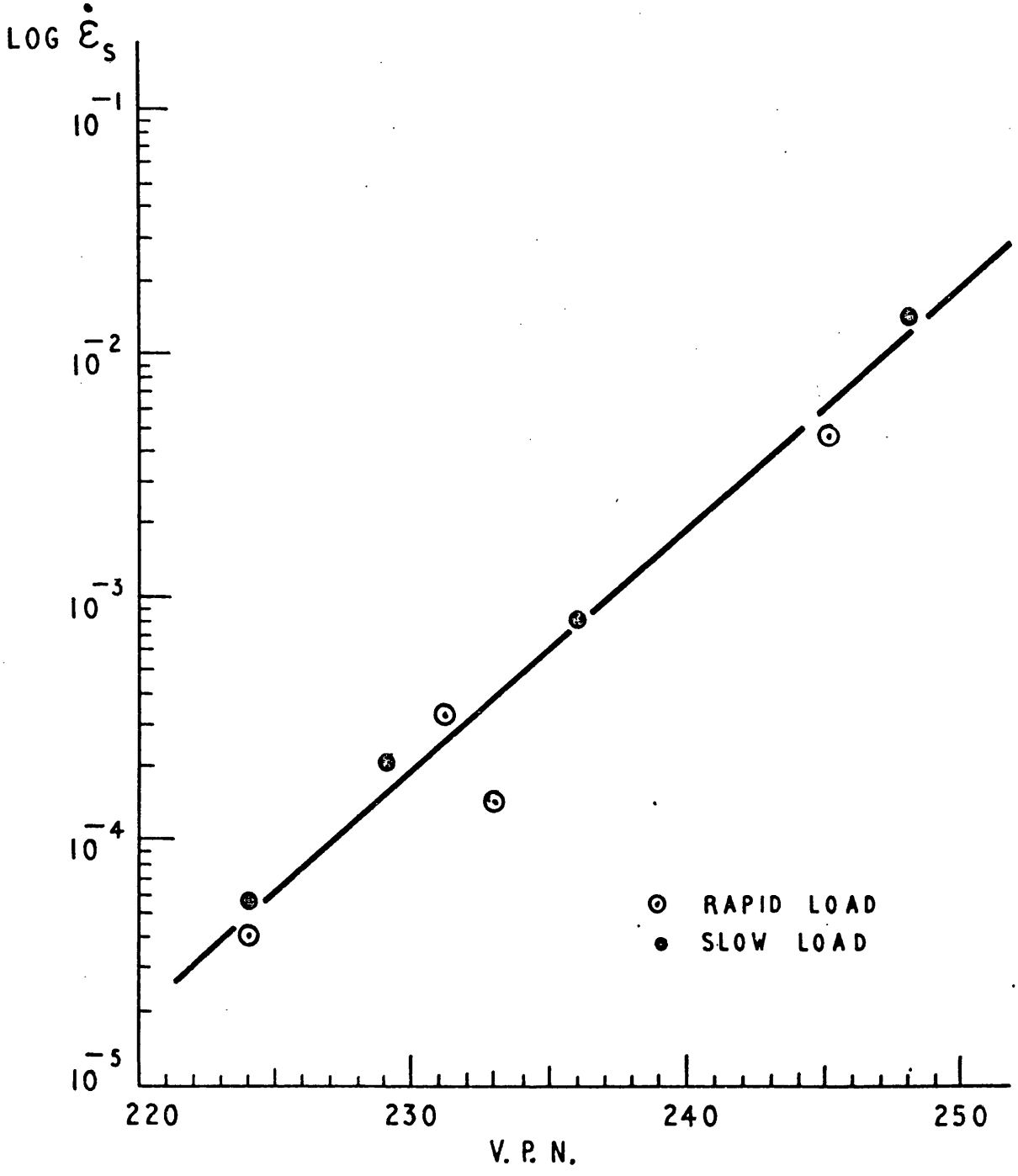
LOG $\dot{\varepsilon}_s$
10^{-1}
10^{-2}
10^{-3}
10^{-4}
10^{-5}
220
230
240
250
V. P. N.
RAPID LOAD
SLOW LOAD

FIGURE 40

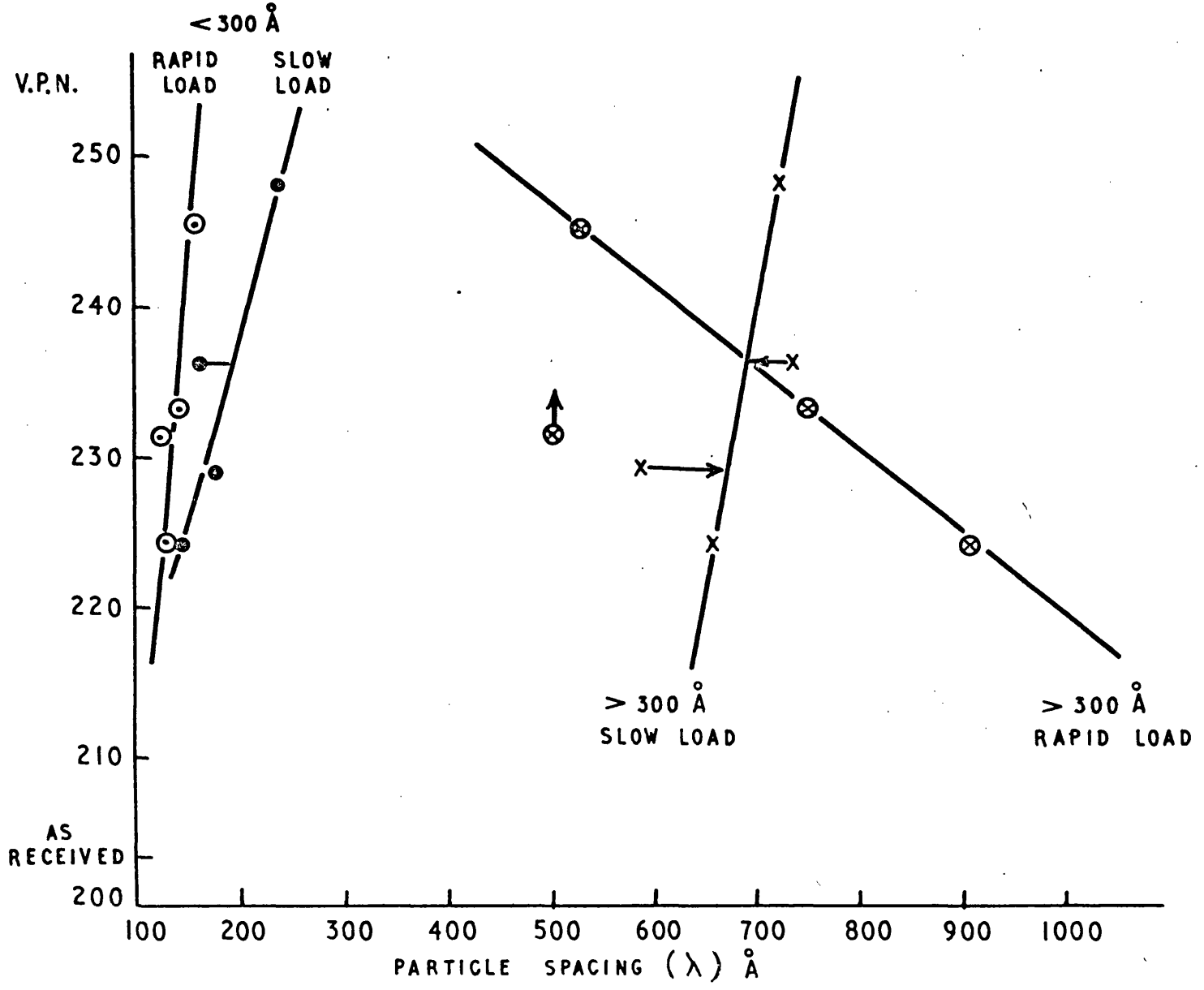
< 300 Å
RAPID LOAD
SLOW LOAD
V.P.N.
250
240
230
220
210
AS RECEIVED
200
100
200
300
400
500
600
700
800
900
1000
PARTICLE SPACING (λ) Å
> 300 Å SLOW LOAD
> 300 Å RAPID LOAD

FIGURE 41

4. DISCUSSION

The most interesting part of this research on 1Cr.Mo.V. steel is undoubtedly the unexpected variation in creep rate with loading rate. However, the origins of the work lie with the unknown response of this steel to pre-straining prior to creep. Originally this programme of research would have been amplified to establish the behaviour of such steels in more complex situations but the loading rate effect became the important topic.

The pre-strain effect is discussed separately from the loading rate effect because, although there may be an interaction, the two topics are not interdependent.

4.1 The Effect of Pre-Strain upon Creep Behaviour

In 1.5 the work in this field was reviewed, with emphasis upon pre-strain at elevated temperatures. Perhaps the impression given by this review is one of confusion, that no distinct trend emerges. The key to this confusion is the parameter f(s), the function of structure already mentioned in 1.4.1. Goldhoff (1962)[30] and 1967[31], stresses this with particular reference to 1Cr.Mo.V. steel. An important factor is whether the workhardening occasioned by pre-straining results in either an increase in internal stress, which requires recovery processes to relieve it, or an increase which triggers a further process such as re-crystallisation or graingrowth. If the former occurs then the likely process, once creep commences, is first a tendency towards a zero or negative creep rate while the mobile dislocation population attempts to attain a configuration in equilibrium with the stress. Creep will then proceed but at a rate which is lower than in a non pre-strained test and apparently from a point on the ε vs. t plot roughly equivalent to that defined by the pre-strain. The rate of creep will probably be somewhat lower than in a non pre-strained test

at the same total strain value, as Mitra and McLean (1967)[50] observed. They were conducting stress reduction creep tests and the creep rate after reducing the stress was lower than under constant load. As pointed out in 1.4.2, this is not surprising since recovery is a logarithmic process and at temperatures near the threshold of self-diffusion may never be complete in a practical sense. Recovery in the creep range will never be complete in the theoretical sense either but once the rate becomes asymptotic to zero its effect will not be detected.

If pre-strain triggers re-crystallisation or graingrowth then the situation will be entirely different. Both of these processes remove matrix defects and soften the material thus leading to a higher creep rate than normal. Hence the concern of Davies et al. (1961)[13] that re-crystallisation should not occur because in earlier tests a decrease in creep resistance had followed graingrowth caused by pre-straining.

On this basis alone, the equivalence of creep strain and plastic strain cannot be assumed as stress analysts would prefer. The particular material under consideration must be evaluated in the condition in which it is used.

The tests conducted for this research show that 1Cr.Mo.V. steel in the ferrite pearlite condition does not exhibit an equivalence of creep strain and plastic strain. Furthermore, the effect on slowly loaded material is to strengthen it, creep life tends to increase with increasing pre-strain. The improvement in life is not sufficient to overcome the adverse effect of slow loading, however. In rapidly loaded tests the trend is for small pre-strains to reduce life markedly but again the higher the pre-strain the greater is the improvement in life. The higher pre-strains give lives which begin to

approach the non strained value. Figure 23 shows these results, the rapidly loaded tests being fitted to a curve to indicate the trend.

Another effect of pre-strain is that proposed by Davies et al.[13][15][18], namely the suppression of the failure process. In 1.4.3 their concept of grainboundary ledge formation during loading and during primary creep, which subsequently become cavities by sliding, is described. Evans and Wilshire[20] have used pre-strain tests to attempt to prove that such ledges are the origins of the failure mechanism and that pre-strain suppresses ledge formation. If this is valid it may be part of the effect in the 1Cr.Mo.V. results and may account for the general increase in time to failure with increasing pre-strain (ignoring pure creep). Therefore it is proposed to examine the 1Cr.Mo.V. results with a view to assessing the role of pre-strain in modifying the failure mechanism. It will not account for the change in creep rate with pre-strain nor for the difference between the strengthened slow-load tests and the weakened rapid-load tests. There is however a possible flaw in Evans and Wilshire's method, they performed a series of tests at constant temperature, over a range of stresses but applied the same amount of pre-strain to each specimen. They plot these and a series of non pre-strained results on a $(t_f \times \dot{\varepsilon}_s)$ vs. stress plot and obtain the lines given in Figure 9. The product $(t_f \times \dot{\varepsilon}_s)$ is derived and explained in 1.4.3 From the plot it is apparent that the pre-strain results, open circles, are independent of stress. This is taken to show that ledge formation is responsible for the stress dependence of the product. However, the specimens were pre-strained 15% to eliminate primary creep. Application of a constant pre-strain, in excess of primary creep strain, to isothermal tests over a range of stresses should intrinsically modify the product $(t_f \times \dot{\varepsilon}_s)$ by a predictable amount. Consider the case of

several tests at different stresses, the severity of a constant value of pre-strain will be greatest at the lower stress as indicated by the hypothetical creep curves in Figure 42. Thus it is either fortuitous that the value of Evans and Wilshire's pre-strain produced a stress independent plot or it will work for any value of pre-strain, possibly qualified by the elimination of primary creep.

Figure 43 shows three curves of the type given in Figure 6, from which the product ($t_f \times \dot{\varepsilon}_s$) is derived. If a line is drawn for a constant value of pre-strain the following can be stated.

TABLE 11

σ	t_f	Original t_f reduced by
σ_1	$t_3 - t_1$	t_0, t_1
σ_2	$t_5 - t_2$	t_0, t_2
σ_3	$t_6 - t_4$	t_0, t_4

Now, using the results of Davies et al.[14], pre-strain in a comparable alloy to that used by Evans[20], reduces the steady state strain rate by approximately an order of magnitude. Furthermore, since the time to failure is linearly proportional to stress in the 1Cr.Mo.V. material (Figure 24), and considering Figure 43, it is apparent that the greatest reduction in (t_f) occurs with the lowest stress test. An equally probable interpretation of Evans and Wilshire's results is that a stress independent product is obtained by exhausting a quantum of the available ductility in a proportionally inverse relationship with stress, in isothermal tests. It is proposed that the effect of such a pre-strain is not to suppress 'ledge' formation but simply to reduce the available ductility by a predictable amount. The rapidly loaded, non pre-strained 1Cr.Mo.V. results given in Figure 21 can therefore

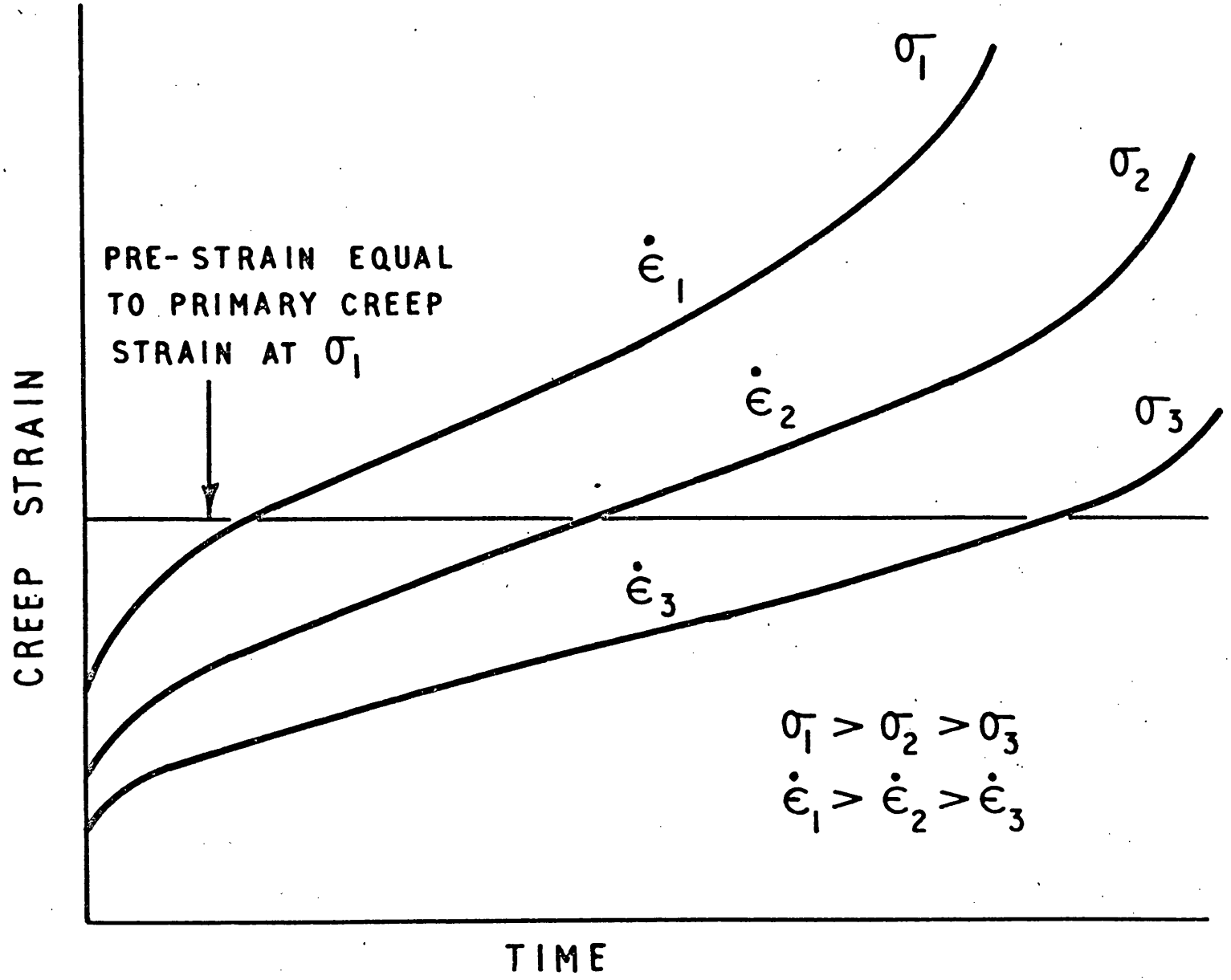
σ_1
σ_2
σ_3
PRE-STRAIN EQUAL TO PRIMARY CREEP STRAIN AT σ_1
$\dot{\epsilon}_1$
$\dot{\epsilon}_2$
$\dot{\epsilon}_3$
CREEP STRAIN
TIME
$\sigma_1 > \sigma_2 > \sigma_3$
$\dot{\epsilon}_1 > \dot{\epsilon}_2 > \dot{\epsilon}_3$

FIGURE 42

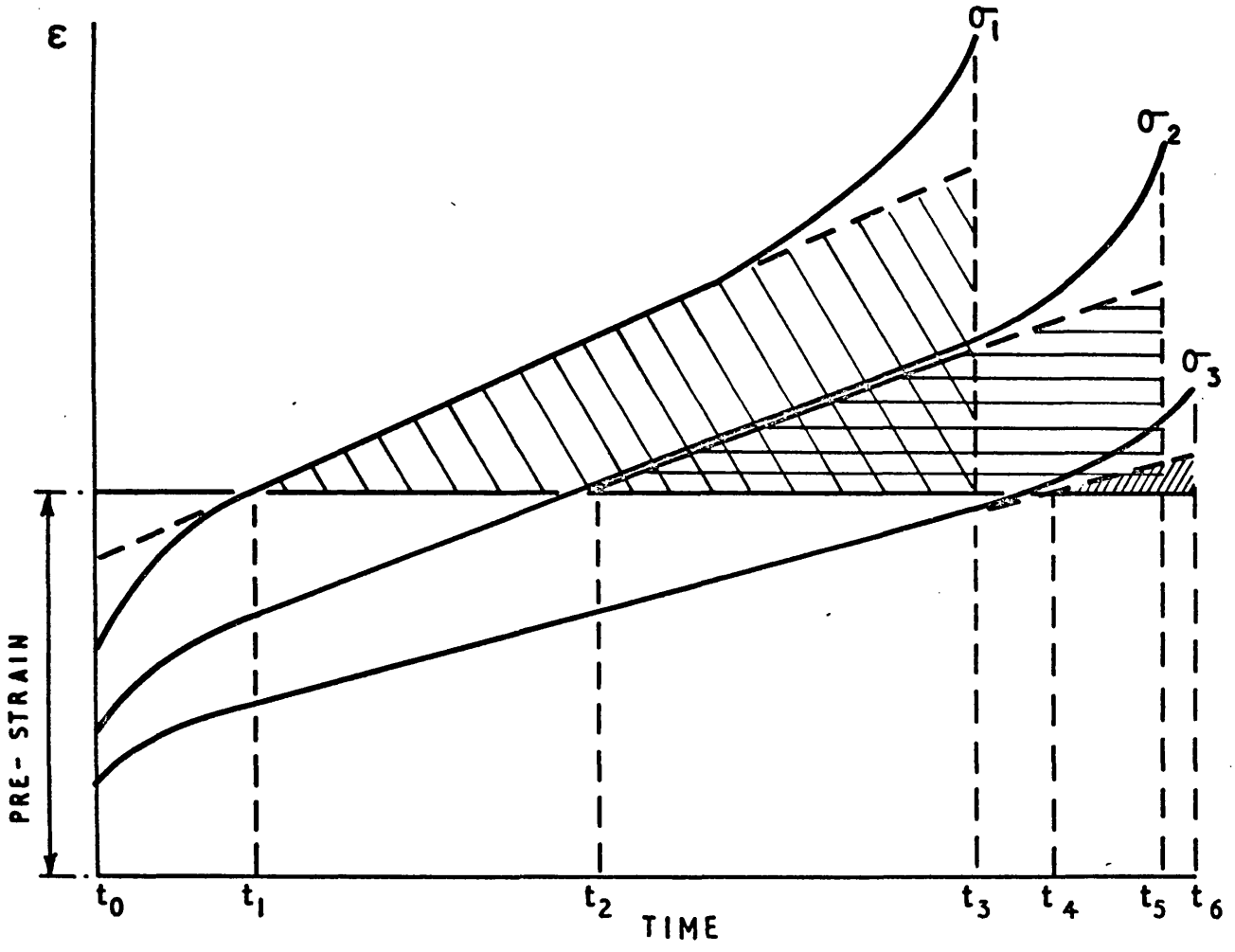

SCHEMATIC CREEP CURVES TO SHOW THE EFFECT OF CONSTANT PRE-STRAIN ON t_f AND HENCE THE PRODUCT $(t_f \times \dot{\varepsilon}_s)$. SEE TEXT.

FIGURE 43

be treated using an arbitrary plastic strain value with which to obtain values of (t_f) and ($\dot{\varepsilon}_s$) to produce a theoretical value of ($t_f \times \dot{\varepsilon}_s$). This can be plotted against stress to test the theory. If this is successful then predictions of the effect of pre-strain are then possible for materials which react to pre-strain in the same way as 1Cr.Mo.V. steels. This would mean that even though creep strain and plastic strain were not equivalent the actual reduction in life was predictable; not because the failure mechanism had been suppressed but because the product was no longer equal to a constant, thus

$$(t_f \times \dot{\varepsilon}_s) = K - f(\varepsilon_p) \qquad (19)$$

where $f(\varepsilon_p)$ is a function of pre-strain.

Therefore, using Figure 21 and a pre-strain value of 1.0%, values for (t_f) can be extracted and combined with the original strain rates, reduced by an order of magnitude, to obtain the products given in the following table.

TABLE 12

σ N/mm^2	New t_f (hrs)	New $\dot{\varepsilon}_s$	Product ($t_f \times \dot{\varepsilon}_s$)
270	24	4.5×10^{-4}	1.08×10^{-2}
220	165	4.4×10^{-5}	7.3×10^{-3}
200	380	1.4×10^{-5}	5.3×10^{-3}
180	1260	4.0×10^{-6}	5.1×10^{-3}

If the theoretically derived values of the product are plotted against stress, together with the non pre-strained values, the lines in Figure 44 are obtained. The plot through the predicted points is purposely drawn parallel to the stress axis even though this is not an exact 'best fit'. It is considered that the points fit such a line

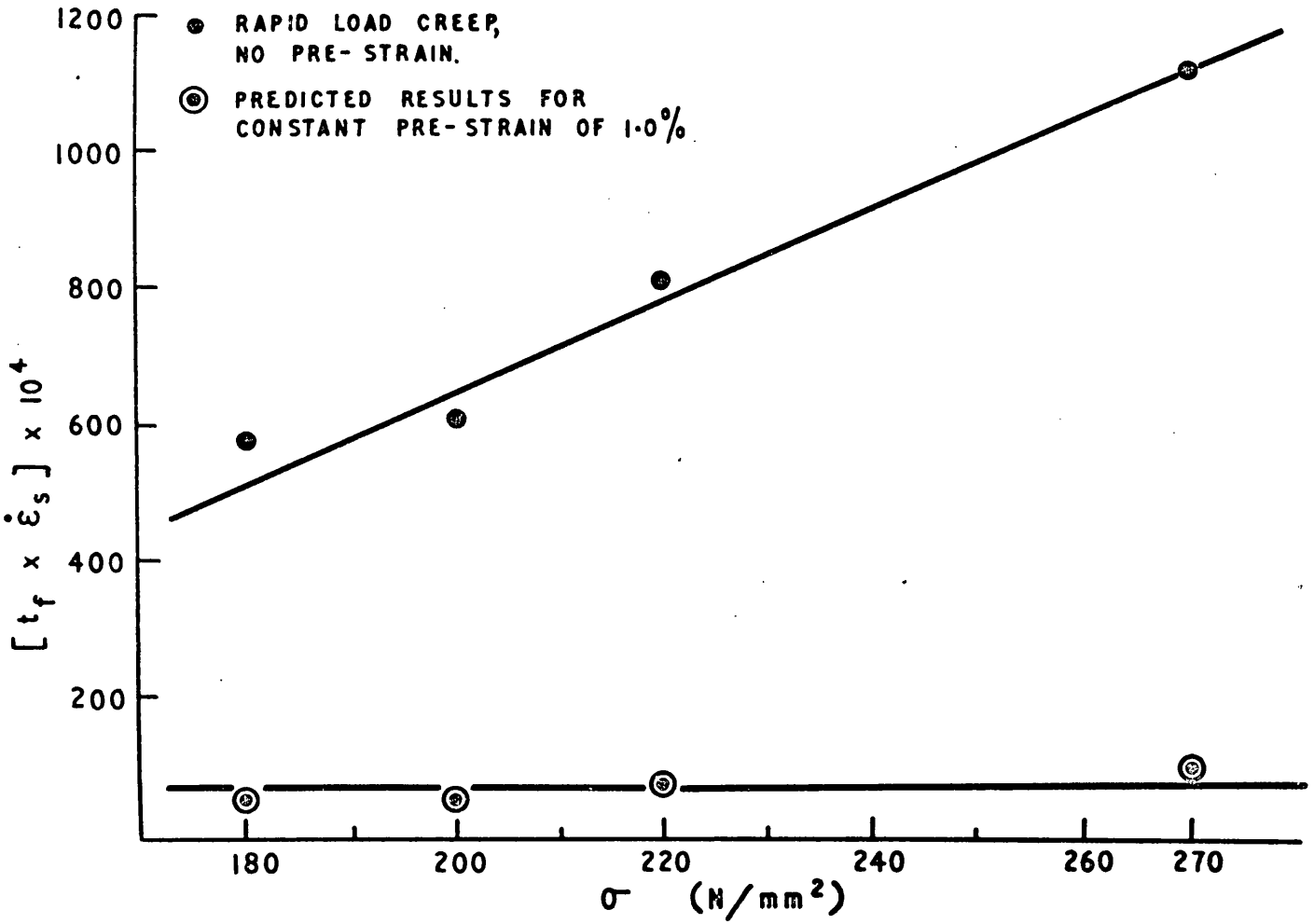

TEST OF THE THEORY THAT A CONSTANT PRE-STRAIN, IN EXCESS OF PRIMARY CREEP STRAIN, WILL YIELD A STRESS INDEPENDENT PRODUCT.

FIGURE 44

well enough to give excellent support for the theory. A test for this behaviour in an unknown material would therefore be a series of three or four isothermal tests at different stresses but constant pre-strain. If a stress independent product was then obtained a complete set of results could then be produced by pre-straining specimens to the upper and lower pre-strains of interest plus two or three intermediate values. These could be tested at constant stress, plotted on σ vs. $(t_f \times \dot{\varepsilon}_s)$ axes and lines through the points drawn parallel to the stress axis. Thus viable predictions could be made for any stress or pre-strain, within the limits set, after five or possibly seven tests. The indication that the theory works on an entirely different material to the dilute solid solution of Evans and Wilshire implies a wide application.

Finally, Figure 20 shows all of the pre-strain results plotted on (t) vs. $(\dot{\varepsilon}_s)$ axes to explore the dependence of (t_f) and (t_t) on creep rate. The points do not lie on a line with a slope of one as predicted by the equation

$$(t_f \times \dot{\varepsilon}_s) = K \qquad (20)$$

but indicate a strain rate exponent of 0.6 and a value for K of 1.2 for (t_f).

It may therefore be stated that the effect of pre-strain in rapidly loaded tests is most probably to promote the graingrowth observed in these specimens. In the slowly pre-strained specimens the effect may well be straightforward workhardening with a consequent increase in life due to sluggish recovery processes causing a lower creep rate.

Suppression of grainboundary ledge formation and therefore of the failure mechanism cannot be ruled out. The concept of cavities formed

in this manner is sound. However, the foregoing analysis does not support the view that pre-strain affects the process and even if it does occur there is no reason to believe that grainboundary sliding is confined to primary creep. Sliding may even be promoted in a pre-strained material particularly in the slowly loaded tests where longer lives ensue. What does emerge from the analysis of Evans and Wilshire's work is a method for testing materials by which the pre-strain response may be recognised and extrapolated.

4.2 The Dependence of Creep Rate upon Loading Rate

The existence of a marked loading rate effect is indisputable. Figures 17, 18 and 21 amply demonstrate this. The problem is to define the factor(s) responsible for such a phenomenon since this is a commonly used material and the effect has not been previously reported. The implication is, therefore, that the cause lies with the type of process which is sensitive to a critical change in energy. For example, graingrowth is such a process, which under the right conditions is sensitive to a critical amount of workhardening and may produce very large grains.

It would seem to be pertinent to see how well the data fit existing models and to modify these as necessary.

Consider first some factors which are not only important but can be regarded as unambiguous and relate to both loading rates.

4.2.1 Possible models for rate controlling factors

The temperature dependence of the creep rate yielded a value for Q of $\sim$ 100 kcal/mol in the equation

$$\dot{\varepsilon}_s = Ae^{-\frac{Q}{RT}} \qquad (21)$$

This is very high but the plot shown in Figure 25 shows a good fit to the experimental points. Myers et al. (1968)[55] obtained a

similar value of Q for creep in the same material so that the result is not unsupported.

In addition, the development of a matrix carbide dispersion was established. The spacing of the carbides is apparently too small for dislocations to bow between the particles according to Myers et al. (1968)[55]. The spacing which would permit dislocations to bow is given by

$$\lambda = \frac{Eb}{\sigma} \qquad (22)$$

and yields a value of $\sim 3{,}000\text{Å}$ for the lowest stress used in these tests which is at least an order of magnitude greater than the experimentally derived values for fine carbides.

Thus the rate controlling mechanism for creep in both slowly and rapidly loaded tests ought to be independent of particle spacing. The results indicate positively that a relationship exists between particle spacing and creep rate. Now, the particle spacing is defined by the creep test parameters in Batch 2 and modified by them in Batch 1. It might therefore be argued that since the spacing is controlled by the test it cannot reciprocally control the test. Nevertheless, the particles exist, in a fine dispersion, and may not be ignored. The choices are that they exist as plates on planes which are not, or need not be, used for slip and do not form pinning points for dislocations, or they do act as barriers; or dislocations can pass through them. Whichever is the correct interpretation the activation energy for the process is high. This rules out a creep mechanism in which self diffusion in the matrix is rate controlling since the value of Q has a maximum of $\sim$ 80 kcal/mol for iron and high iron content alloys. Generally the value is about 60 kcal/mol. However, some interesting facts emerge from a consideration of the activation energies for creep. Garafalo (1965)[21], in his Table 4.2, gives values

for Q which, in plain carbon steels rise from 61.2 kcal/mol at 0.05%C to 102.6 kcal/mol at 0.79%C. Thus as the pearlite content increases towards the 100% value at the eutectoid composition the activation energy increases, which is consistent with a decreasing mean free path for dislocations before meeting a cementite island. It is also consistent with diffusion controlled creep where either climb is a lengthy process due to the barrier height and hence climb distance, or to a severely reduced iron matrix volume plus the necessity to cut the massive carbides. Other dispersions have a high value for Q, such as the S.A.P. alloys where alumina is dispersed in aluminium, here the value of Q rises from the normal aluminium alloy value of 30 - 40 kcal/mol to values for S.A.P. of 37 to 300 kcal/mol depending on the dispersion. Ansell and Weertman (1959)[1] derived their model, used in this thesis, because the activation energy for creep in their S.A.P. alloy was 150 kcal/mol. They assume two things in developing their argument, one is that for a dispersion hardened alloy the rate controlling process is the climb of dislocations over second phase particles, the second assumption concerns the nature of the dislocation generation process in dispersion hardened matrices. Either Frank-Read sources are present in a three dimensional network or, if the particle spacing is small, short dislocation lines may exist between particles and these under stress, may act as sources. It is the latter process which may well be rate controlling in the present material and a slightly modified version of Ansell and Weertman's schematic drawing will explain the principle. Their original drawing is given in Figure 1, Appendix 5 and the modified version in Figure 45. Their model is perfectly feasible and it has found a wide use in explaining the creep rates obtained in dispersion hardened materials. A resumé of their proposals is given in Appendix 5. It fits the results of the tests described in this

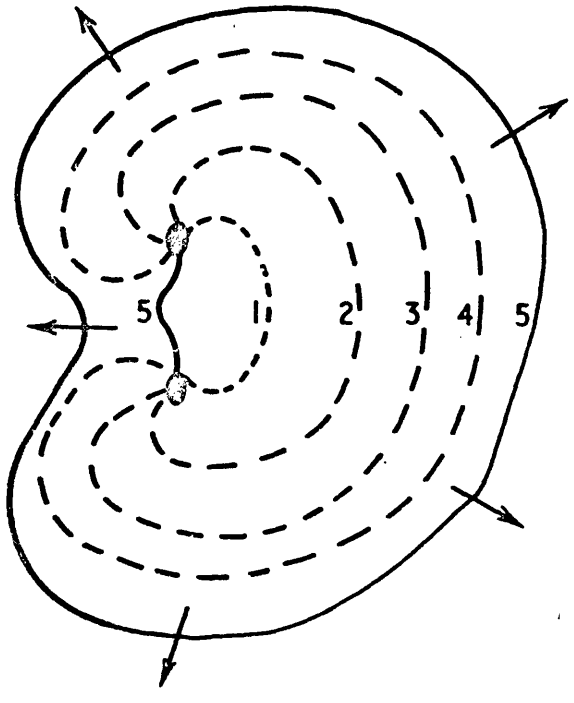

(a)

A SHORT LENGTH OF DISLOCATION LINE TERMINATING AT TWO PARTICLES MAY ACT IN A SIMILAR MANNER TO A FRANK- READ SOURCE.

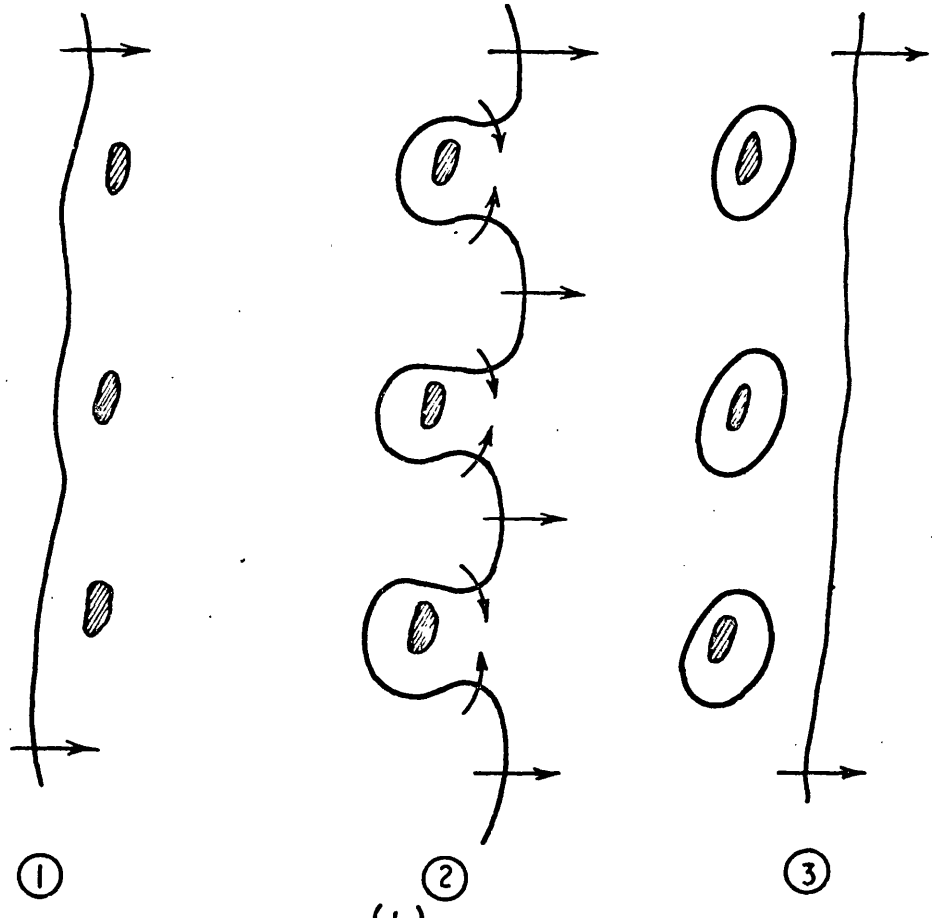

(b)

DISLOCATIONS FROM A SOURCE PRODUCING PINCHED OFF LOOPS AROUND PARTICLES.

FIGURE 45

thesis and must, if accepted, cast doubt upon the accuracy of the $\sigma = Eb/\lambda$ expression. Probably this expression is an over simplification of the relationship between the parameters used and should be qualified by use of a correction factor. Correction factors are somewhat ubiquitous but are often necessary in situations, such as this, where a complex factor is present such as f(s), the function of structure.

The high creep rates attained in the 1Cr.Mo.V. are accounted for in the model by a stress exponent of 12 compared to 4 in Ansell and Weertman's case.

Thus it is possible that the rate controlling mechanism in the creep of any dispersion hardened material is, at high particle spacings, that for self diffusion. As the particle spacing decreases an increasing number of dislocations are forced between particles leaving loops which have to climb over the particles before further loops can form. The rate controlling mechanism for climb under these conditions is not, from experimental evidence, the rate of arrival of vacancies but climb distance and the frequency with which the local energy attains a value high enough to promote climb.

A further possibility is that dislocations, pinned by precipitates and obeying the concept that bowing between particles is restricted according to $\sigma = Eb/\lambda$, may climb over the barriers by becoming Bardeen-Herring sources (Bardeen and Herring 1952)[3]. Such a source is created by an edge dislocation pinned at some spacing L. Assuming that slip cannot occur in the glide plane it is possible for the line to bow in the climb plane and act as a source producing either an increased half plane or a decreased half plane. The first case arises when there is less than the equilibrium concentration of vacancies and more are created by removing atoms from adjacent planes to form the extending half plane. The second case arises when there

is an excess of vacancies and the loop formed by the source will draw on these to remove a plane of atoms. The criterion for operation of this source, according to Bardeen and Herring, is that the applied stress, σ, satisfies the equation

$$\sigma \geq \frac{Gb}{L} \qquad (23)$$

where G is the shear modulus, b is Burgers vector and L the length of pinned dislocation. A mechanism such as this can operate at the lowest stresses employed in these tests. The source is schematically represented by Figure 46 and should operate as in the second case using the vacancy excess assumed to exist at the particle/matrix interface by Ansell and Weertman (1959)[1]. Gibbs and Harris (1969)[26] point out that in order to be a defect source/sink an interface cannot be coherent and should preferably be incoherent. Semi-coherent interfaces can act as sources/sinks if there is a local increase in elastic strain energy. The diffusion rate of vacancies at particle/matrix interfaces is reported (Gibbs and Harris) to be several orders of magnitude greater than in the lattice and this must enhance such a mechanism. Support for a process involving Bardeen-Herring sources also comes from the high stress index value obtained for these tests.

Consider now the solute drag model proposed initially by Russell et al. (1968)[62] and used by Myers et al. (1968)[55] in their analysis of the creep behaviour of 1Cr.Mo.V. steel. They assumed that dislocations had to climb over particles because the stress was not high enough to bow particle-pinned dislocations sufficiently for them to act as sources. It was shown that simple climb based on the diffusion of vacancies was not rate controlling because the activation energy was too high at 95 kcal/mol. Their solute drag model was based on vanadium-carbon pairs diffusing to dislocations and pinning them.

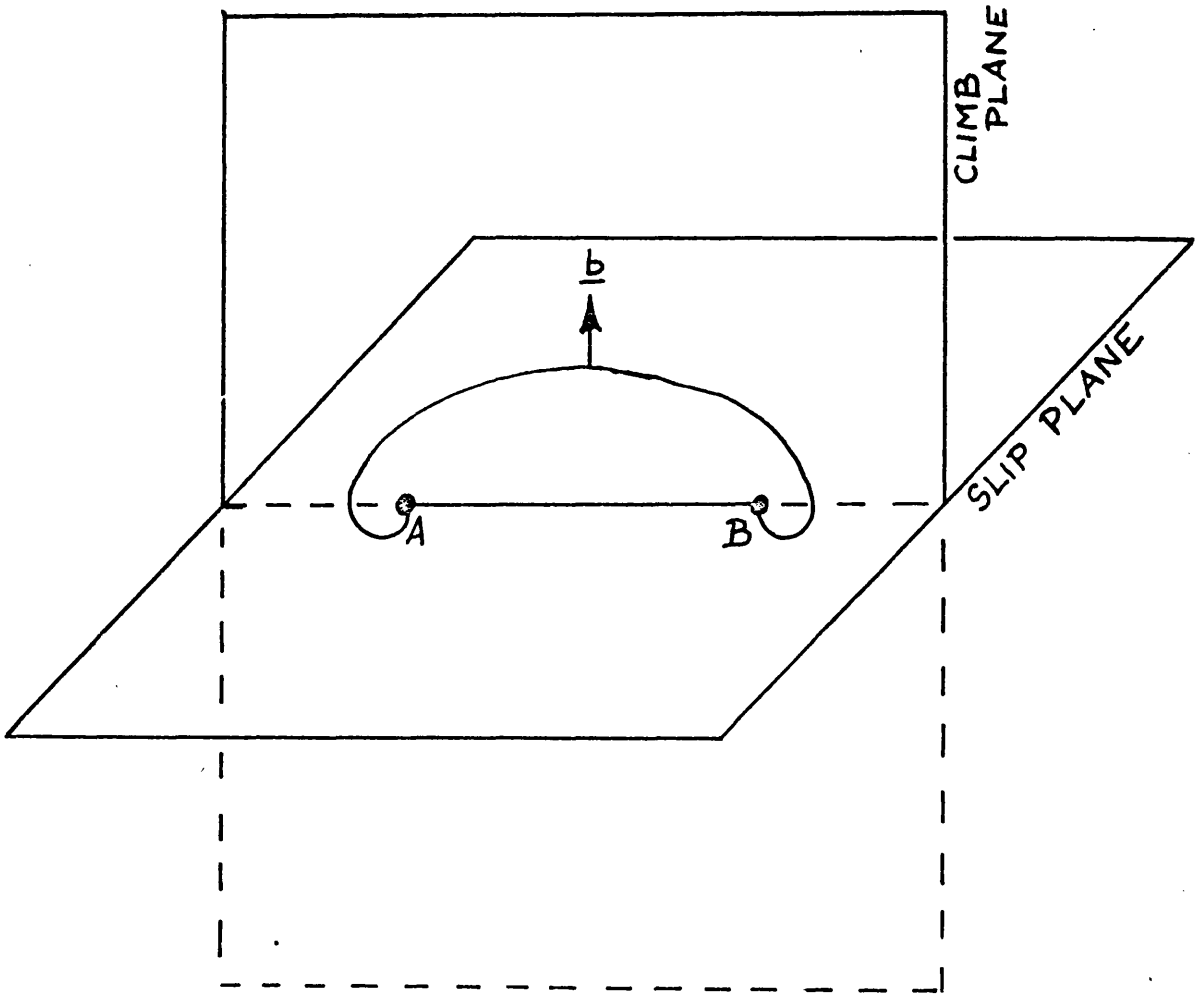

REPRESENTATION OF A

BARDEEN-HERRING SOURCE.

FIGURE 46

A similar approach has been made by Goldhoff and Beattie (1965)[32] in which they assess the possibility of Mo_2C precipitation on dislocations. They observed such precipitates in forged 1Cr.Mo.V. steels and so compared the diffusion velocity of molybdenum with the dislocation velocity and concluded that the process was possible at their lower strain rates.

In the tests presented here there was copious vanadium carbide. If vanadium in solution, in equilibrium with these precipitates, can diffuse to dislocations then a solute drag effect can at least contribute to the creep rate controlling process and may even by the rate controlling factor.

The average dislocation velocity may be obtained from

$$V_D = \frac{\dot{\varepsilon}}{\rho_D . b} \qquad (24)$$

where ρ is the dislocation density, b the Burgers vector and V_D the dislocation velocity. Using Myers value for ρ_D in this material and the highest value of $\dot{\varepsilon}$ observed in these tests a velocity of $\sim 5 \times 10^{-6}$ cm.sec^{-1} is obtained. A similar calculation for the lowest observed strain rate yields a velocity of $\sim 1 \times 10^{-8}$ cm.sec^{-1}.

The lattice diffusion velocity V_L for vanadium may be obtained from

$$V_L = \frac{F}{\rho_V} \qquad (25)$$

where F is the flux and ρ_V the density of vanadium in the matrix adjacent to the precipitates.

Now F is usually expressed as

$$F = - D \left(\frac{\Delta C}{\Delta x}\right) \qquad (26)$$

where - D is the diffusion constant, ΔC is the concentration in solution and Δx the distance over which diffusion is being considered.

So, using equations (25) and (26) we may write that

$$V_L = \frac{F}{\rho_V} \approx \frac{F}{\Delta C} \approx \frac{-D}{\Delta x} \qquad (27)$$

D is derived from the conventional equation

$$D = Ae^{-\frac{Q}{RT}} \qquad (28)$$

in which A has a value of 0.10 for vanadium in α iron, Q is 61.5 kcal/mol for α iron, T is 823°K and R is the gas constant. Evaluating the equation yields a value of 4.65×10^{-14} $cm^2.sec^{-1}$ for D.

Δx may be assigned the value most favourable to a solute drag model, i.e. that for the semi-spacing of the highest density of vanadium carbide, this gives a magnitude of $\sim 7 \times 10^{-7}$ cm.

The derived diffusion velocity from $\frac{-D}{\Delta x}$ is therefore $\sim 7 \times 10^{-9}$ $cm.sec^{-1}$.

Comparing the value obtained for V_L of 7×10^{-9} $cm.sec^{-1}$ with the limiting values for V_D, which are 5×10^{-6} $cm.sec^{-1}$ and 1×10^{-8} $cm.sec^{-1}$, it is possible that vanadium may exert a drag at the lowest strain rates but not in the majority of tests.

A further model which is of interest is that proposed by Coble (1963)[10] for grainboundary diffusion controlled creep in polycrystalline materials. The process is essentially one of mass transfer via grainboundaries. Creep is thought to occur due to the fact that the vacancy flow will tend to be from grainboundaries which are normal to the stress axis to those parallel to the axis. This results in an effective transfer of atoms in the reverse direction so that grains grow in length in the tensile direction and their transverse cross section reduces proportionately.

Since it is known that lattice diffusion (D_L) is less rapid than grainboundary diffusion (D_B) it follows that any process dependent upon diffusion would be enhanced if D_B were rate controlling. In the

case of creep this will obviously apply but the more common structures have a high ratio of matrix volume to boundary volume and although D_B will make a contribution to the deformation process it will be insignificant. Only when the grainboundary volume attains significant proportions and D_L is limited does D_B become important or, in some instances, rate controlling. For D_B to be the dominant factor in deformation, the role of D_L must be small and hence the processes dependent upon it insignificant. Thus, except in a very thin layer of lattice adjacent to the boundary, recovery will be comparatively sluggish and recovery creep will not dominate. This is the opposite end of the scale from the high temperature process of Herring-Nabarro creep and, as Gibbs (1964)[23] points out, at 'low' temperatures (< 0.6 Tm) and for sufficiently small grains, D_B becomes rate controlling.

Since these conditions are met by the parameters in the tests described in this work it is pertinent to apply Coble's model. A spherical grain is assumed since this analog can be compared with Nabarro's (1948)[56] model for lattice diffusion. An applied stress across such a grain, say from pole to pole, will disturb the equilibrium concentration of vacancies and cause a flow from the poles to the equator. As a source/sink for vacancies the grainboundary is excellent and Coble finds the diffusion flux to be insensitive to the uniformity of the source and sink. The expression obtained by Coble is

$$\dot{\varepsilon} = \frac{150.\sigma.D_B.W.\Omega}{\pi.\bar{G}^3.k.T} \qquad (29)$$

where W is grainboundary width, Ω is the volume of a vacancy and $\bar{G}$ is the average grainsize. The other symbols have the usual meaning. Since, in practice, $(D_B.W)$ is obtained as a single figure it is not

proposed to estimate the value of W but to employ a value for the product. Using a test result at 550°C, 270 N/mm^2 and the appropriate creep rate the expression may be treated to yield a mean grain size for comparison with the results obtained on the 1Cr.Mo.V. material. Using the value of $(1.5 \times 10^{-6}.e^{-44,000/RT})$ for $(D_B.W)$, 8.25×10^{-24} cm^3 for Ω and 3×10^{-5} cm/cm/sec for ε, equation (29) may be re-arranged and evaluated

$$\bar{G} = \frac{150.\sigma.(D_B.W).\Omega}{\pi.\dot{\varepsilon}.k.T} \qquad (30)$$

yielding a result

$$\bar{G} \simeq 50\ \mu m \qquad (31)$$

Therefore, if Coble's model is accepted and from the literature it is, there should be a contribution at least from D_B to the creep rate since this order of grainsize fits the observed values for the 'as received' material and for much of the failed material.

Considering the discussion on rate controlling factors, the models of Ansell and Weertman, Bardeen and Herring plus that of Coble are all capable of being fitted to a general model for the creep rates observed in these tests.

The proposed general model is that the creep rate is primarily dependent upon both particle size and spacing and obeys a modified Ansell and Weertman equation of the form

$$\dot{\varepsilon}_s = \frac{2.\pi.\sigma^{12}.\lambda^{2.5}.D}{h.\mu^3.k.T} \qquad (32)$$

In simplified form the expression becomes

$$\dot{\varepsilon}_s = K.\sigma^{12}.\lambda^{2.5} \qquad (33)$$

The high activation energy of $\sim$ 100 kcal/mol is assumed to be due to the climb distance for dislocations to move past particles and to the mechanism (possibly Bardeen-Herring type) by which climb is achieved.

It has been demonstrated that a stress dependent mechanism such as the operation of Bardeen-Herring sources is possible and that the creep rates may be accounted for on this basis.

The contribution of grain boundary diffusion creep to the creep rate is difficult to assess and it must therefore be included in the constant of equation (33).

Having established a model for the overall rate of creep a hypothesis must be formed to account for the loading rate phenomenon.

4.2.2 The effects of loading rate

The effect of a slow or rapid load was readily apparent at an early stage of each test, particularly in Batch 1 where the material was extremely sensitive to loading rate. So much so that within a few minutes it was possible to judge the creep rate and be certain that the test would fall into a particular category of behaviour. Therefore the structural modification necessary to produce the differing creep behaviour must be effected early in the test.

The structural feature which showed the greatest response to loading rate was of course the carbide population and distribution. Creep rate and spacing certainly show a relationship and it is contended that creep rate is dependent upon a carbide spacing which is defined early in the test.

For such a contention to be viable the carbide must be precipitated rapidly in both a pre-strain rate and stress dependent manner. One difficulty is to explain why vanadium carbide has not formed during the heat treatment since it is thermodynamically stable below about 1,730°C. However other workers, Jusko and Gut (1966)[41], Goldhoff and Beattie (1965)[32], have reported precipitation during creep as stated in 1.4.2 and there is no doubt that precipitation occurred in the tests reported here.

A possible explanation of the suppression of vanadium carbide formation is that under the conditions imposed the lattice strain energy associated with nucleation is too high, Gibbs (1970)[25]. The postulate is that this local lattice strain energy is suitably lowered to permit nucleation to occur. Such a state would exist if an excess of vacancies was created.

For such a model to apply in this case it must account for the different carbide spacings in rapidly and slowly loaded tests.

It is proposed that the conditions created during loading at the different rates give the conditions necessary for nucleation. Furthermore, since it is observed that the 'instantaneous' strain imposed during loading is of the same order of magnitude in both cases it is reasonable to assume that the vacancies created during this deformation are numerically of the same order also. However, there is obviously a critical vacancy increase necessary to lower the threshold nucleation energy and if the rate of vacancy generation is too low then either no nucleation will occur or it will be reduced. Such a reduction would decrease the number of nucleation sites. This is consistent with a slowly loaded test in which the rate of deformation and therefore the rate of vacancy generation is lower and the number of sites fewer. In the rapidly loaded test the vacancies would be created very quickly, establishing the conditions for simultaneous nucleation at a large number of sites.

4.3 Fracture Ductility

The failure strain of all Batch 2 specimens has been remarked upon as being nominally constant. This stress and carbide spacing independence is consistent with a uniform matrix which deforms in a temperature dependent manner. The high stress dependence of the creep rate does not detract from such a hypothesis since this is linked with

the creep rate controlling factor, carbide spacing. Ductility with such a uniformity as that observed here, strongly implies that the material should be considered as a ductile matrix in which deformation rate but not quantity, is determined by a superimposed dispersion of second phase particles. The two parameters behave in a complementary manner only.

5. CONCLUSIONS

The fourfold objectives set out in 1.2 have been achieved for 1Cr.Mo.V. steel in the ferrite-pearlite condition.

It must be concluded that the equivalence of creep strain and plastic or pre-strain cannot be assumed; the material under consideration should be tested under conditions which are as nearly as possible those obtained in service. A method has been derived to enable viable predictions to be made of the effect of pre-strain on subsequent creep behaviour.

The creep rate of this material is dependent upon the spacing of vanadium carbide precipitates and the climb of dislocations around them. A model is proposed which fits the data obtained experimentally.

Vanadium carbide spacing is dependent upon the initial strain rate if vanadium remains in solution until this stage.

1Cr.Mo.V. steel in the condition used for these tests is strengthened by pre-strain in the slowly pre-strained case but neither high or low rates of pre-strain achieve the creep resistance of rapidly loaded, non pre-strained material.

Over the range of stresses employed the material exhibits a nominally constant strain to failure due to an independence of ductility upon second phase particles.

ACKNOWLEDGEMENTS

The author would like to express his appreciation to the following:

The Staff of the School of Materials Science, Bath University of Technology; in particular Professor C.R. Tottle and Mr. P.C. Thornton.

The Management and the author's colleagues at the Berkeley Nuclear Laboratories of the Central Electricity Generating Board; especially Mr. B.J.L. Darlaston, Dr. P. Marshall and Miss S. Tucker.

Mr. K. Jerram of Berkeley Laboratories to whose designs the rig programming units were successfully made.

REFERENCES

(1) Ansell, G.S. and Weertman, J., Trans. Met. Soc. A.I.M.E., 1959, 215, 838.

(2) Ashby, M.F. and Ebeling, R., Trans. Met. Soc. A.I.M.E., 1966, 236, 1396.

(3) Bardeen, J. and Herring, C., 'Imperfections in nearly perfect crystals', J. Wiley & Sons, New York, 1952, Ed. Shockley.

(4) Barr, W., Plastow, B. and Winnett, W.B., Metallurgia, 1967, 75, (447), 9.

(5) Barr, W., Plastow, B. and Winnett, W.B., C.E.G.B. Midlands Region Report 82/1964.

(6) Bates, H.G.A. and Ridal, K.A., Joint Int. Conf. Creep, 1963, Paper 72.

(7) Boettner, R.C. and Robertson, W.D., Trans. Met. Soc. A.I.M.E., 1961, 221, 613.

(8) Bowring, P., Davies, P.W. and Wilshire, B., Met. Sci. J., 1968, 2, 168.

(9) Buchi, G.J.P., Page, J.H.R. and Sidey, M.P., J.I.S.I., 1965, 203(3), 291.

(10) Coble, R.L., J. Appl. Phys., 1963, 34(6), 1679.

(11) Davies, P.W., Dennison, J.P. and Evans, R.W., J.I.M., 1964, 92, 409.

(12) Davies, P.W. and Dutton, R., Acta. Met., 1966, 14, 1138.

(13) Davies, P.W., Richards, J.D. and Wilshire, B., J.I.M., 1962, 90(11), 431.

(14) Davies, P.W., Richards, J.D. and Wilshire, B., Metallurgia, 1963 (Dec.), 259.

(15) Davies, P.W. and Williams, K.R., Met. Sci. J., 1969, 3, 48.

(16) Davies, P.W. and Williams, K.R., Met. Sci. J., 1969, 3, 220.

(17) Davies, P.W. and Wilshire, B., Phil. Mag., 1965, 11, 189.

(18) Davies, P.W. and Wilshire, B., Met. Sci. J., 1968, 2, 168.

(19) Dennison, J.P., Llewellyn, R.J. and Wilshire, B., J.I.M., 1967, 95, 115.

(20) Evans, W.J. and Wilshire, B., J.I.M., 1967, 95(12), 382.

(21) Garafalo, F., 'Fundamentals of creep and creep-rupture in metals', 1965, Macmillan Series in Materials Science.

(22) Garafalo, F., Whitmore, R.W., Domis, W.F. and Von Gemmingen, F., 1961, Trans. A.I.M.E., 221, 310.

(23) Gibbs, G.B., C.E.G.B. Report RD/B/N300, 1964.

(24) Gibbs, G.B., Mat. Sci. and Eng., 1968, 2(5), 269.

(25) Gibbs, G.B., 1970, Private communication.

(26) Gibbs, G.B. and Harris, J.E., 'Interfaces Conference', Melbourne, 1969, Butterworths.

(27) Gindin, I.A., Starodubov, Ya.D. and Zakharov, V.I., Fiz. Met. Metalloved, 1966, 22(2), 254.

(28) Gittins, A., Met. Sci. J., 1967, 1, 214.

(29) Gittins, A. and Williams, M.D., Met. Sci. J., 1969, 3, 226.

(30) Goldhoff, R.M., Materials Res., 1962, 1(1), 26.

(31) Goldhoff, R.M., 1967, Private communication.

(32) Goldhoff, R.M. and Beattie, M.J.(Jr), Trans. Met. Soc. A.I.M.E., 1965, 233, 1743.

(33) Ham, R.K., Proc. Int. Conf. Thermal and High Strain Fatigue, Institute of Metals, London, 1967.

(34) Hirschorn, J.S. and Ansell, G.S., Acta. Met., 1965, 13, 572.

(35) Hodgson, B.J.R., C.E.G.B. Report No. RD/B/N698, 1967.

(36) Hodgson, B.J.R., C.E.G.B. Report No. RD/B/N1139, 1968.

(37) Hodgson, B.J.R., Met. Sci. J., 1968, 2, 235.

(38) Hodgson, B.J.R., Nature, 223, 392, 1969.

(39) Hull, D. and Rimmer, D.B., Phil. Mag., 1959, 4, 673.

(40) Ishida, Y. and McLean, D., Met. Sci. J., 1967, 1, 171.

(41) Jusko, J. and Gut, K., Schweiz. Arch., 1966, 32, 16.

(42) Kocks, V.F., Acta. Met., 1966, 14, 1629.

(43) Kozyrskiy, G.Ya. and Donenko, V.A., Fiz. Met. Metalloved, 1966, 22(1), 108.

(44) Langdon, T.G., Scripta. Met., 1968, 2(1), 17.

(45) Lister, E. and Harvey, R.P., BISRA Report MG/Q/153/67, 1967.

(46) McLean, D., Reports Prog. Phys., 1966, 29, 1.

(47) McLean, D., 'EMEN' J. Manchester Univ. Met. Soc., 1968, pp8-17.

(48) McMahon, C.J., Mat. Sci. and Eng., 1968/9, 3, 304.

(49) Marshall, P., 1970, Private communication.

(50) Mitra, S.K. and McLean, D., Met. Sci. J., 1967, 1, 192.

(51) Monkman, F.C. and Grant, N.J., Proc. Am. Soc. Test Mat., 1956, 56, 593.

(52) Mukherjee, T., Stumpf, W.B., Sellars, C.M. and Tegart, W.J.McG., J.I.S.I., 1969, 207(5), 621.

(53) Murphy, M.C. and Branch, G.D., J.I.S.I., 1969, 207, (10), 1347.

(54) Myers, J., 1968, Private communication.

(55) Myers, J., Willoughby, G. and Ham, R.K., Met. Sci. J., 1968, 2, 209.

(56) Nabarro, F.R.N., 1948, Report of a Conference on the strength of solids, The Physical Society, London.

(57) Norton, J.F. and Strong, A., J.I.S.I., 1969, 207(2), 193.

(58) Pearson, W.B., 'A handbook of lattice spacings and structures of metals and alloys', Pergammon, 1967, 2, 1393.

(59) Price, C.E., Scripta. Met., 1968, 2(1), 47.

(60) Prnka, T. and Foldyna, G., Arch Eisenk., 1969, 40, 499 (BISI Transl. 7635).

(61) Ratcliffe, R.T. and Greenwood, G.W., Phil. Mag., 1965, 12, 49.

(62) Russell, B., Ham, R.K., Silcock, J.M. and Willoughby, G., Met. Sci. J., 1968, 2, 201.

(63) Sherby, O.D., Goldberg, A. and Dorn, J.E., Trans. A.S.M., 1954, 46, 681.

(64) Sidey, D. and Wilshire, B., Met. Sci. J., 1969, 3, 56.

(65) Speight, M.V. and Harris, J.E., Met. Sci. J., 1967, 1, 83.

(66) Thölen, A. and Hyman, M., Jerkontorets Am., 1968, 152(9), 459.

(67) Voorhees, H.R., Freeman, J.W. and Herzog, J.A., J. Basic Eng., 1962, 84, 207.

(68) Walters, D.J., C.E.G.B. Report No. RD/B/N1469, 1970.

(69) Westmacott, K.H., Fountain, C.W. and Stirton, R.J., Acta. Met., 1966, 14, 1628.

(70) Williams, J.A., C.E.G.B. Report RD/L/N134/68, 1968.

(71) Williams, J.A. and Lindley, T.C., Zeitschrift für Metallkunde, 1969, 60(12), 957.

(72) Woodford, D.A., Mat. Sci. Eng., 1969, 4, (2/3), 146.

(73) Woodford, D.A., Met. Sci. J., 1969, 3, 50.

(74) Woodford, D.A., Met. Sci. J., 1969, 3, 234.

APPENDIX 1

Creep Rig - Programming Unit

The creep rig was described in 2.2 and mention was made of the programming unit. The schematic drawing is repeated in Figure 1 (Appendix 1). Briefly, the specimen may either be deformed in creep or strained by means of the hydraulic ram. This is controlled by a voltage derived from the servo, or summing, amplifier which adds input voltages arithmetically. Therefore if all signals from the specimen (load or strain) are of positive sign and control voltages of negative sign the ram will respond to the sign and magnitude of the resultant. It will move towards compression for a positive voltage and towards tension for a negative one. Thus if the specimen signals are zero and a negative control voltage is applied the ram will descend and produce a positive signal from the specimen transducers. This will arithmetically reduce the control signal until either zero voltage is reached (ram stationary) or a further negative voltage is applied from an external source.

Control voltages are supplied by one or other of the units whose circuits appear in Figure 2 (Appendix 1), shown separated by a dashed line. Control voltages are between 0 v and 1 v with a measured accuracy of 0.01 mV above 0.25 mV and 0.0025 mV at lower values.

The upper part of the circuit is the pre-strain unit.

Essentially it is used as follows for pre-straining:-

1. Load and strain signals are fed into the appropriate jack plug sockets (shown at the top of the drawing).
2. Phase 1 volts, 'set' and 'trim', potentiometers are adjusted to give the voltage proportional to the pre-strain required.
3. Phase 2 volts, 'set' and 'trim', potentiometers are adjusted to give the voltage proportional to the final creep load.

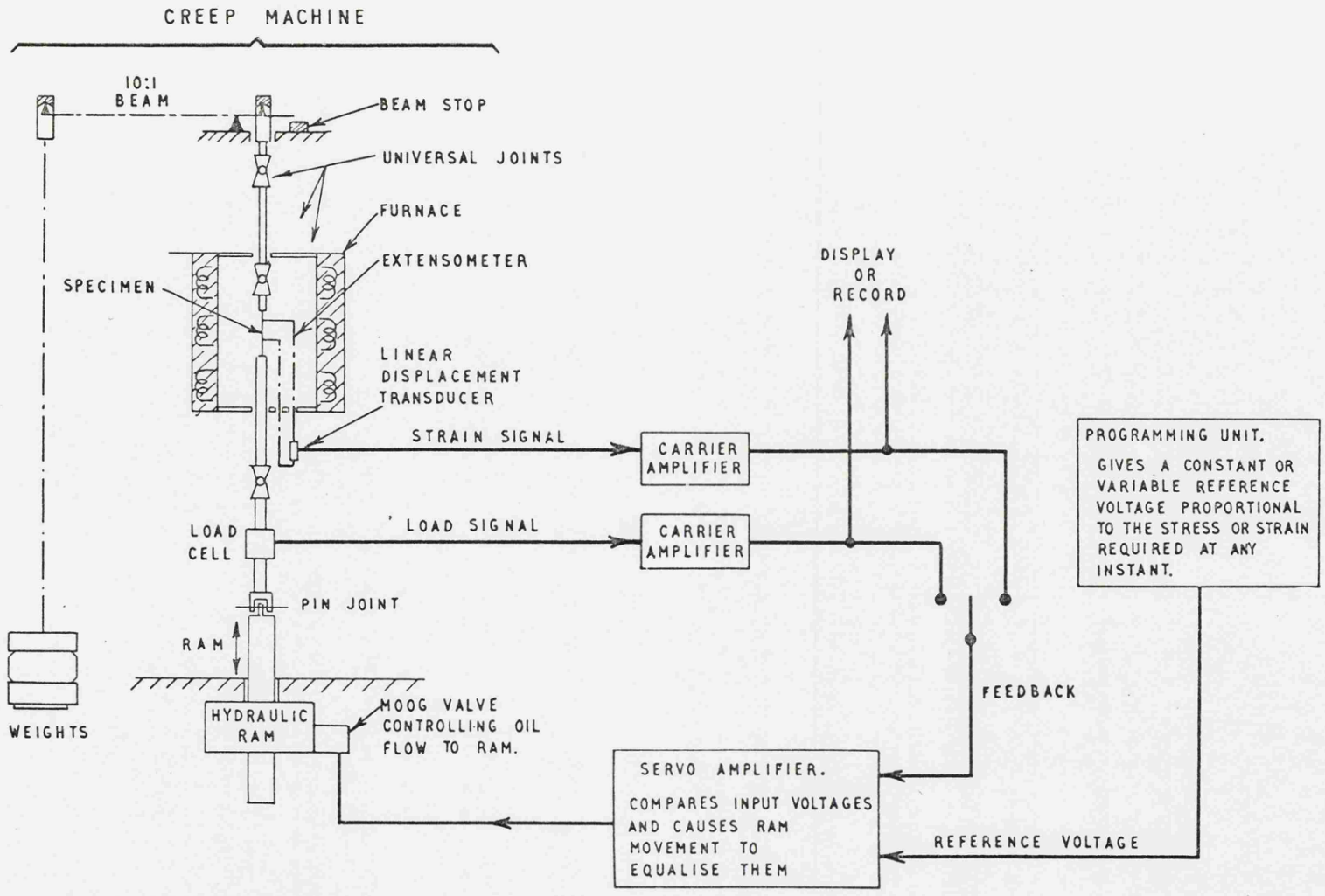

SCHEMATIC LAYOUT OF CREEP-PLASTICITY RIG.

FIGURE 1 (APPENDIX 1)

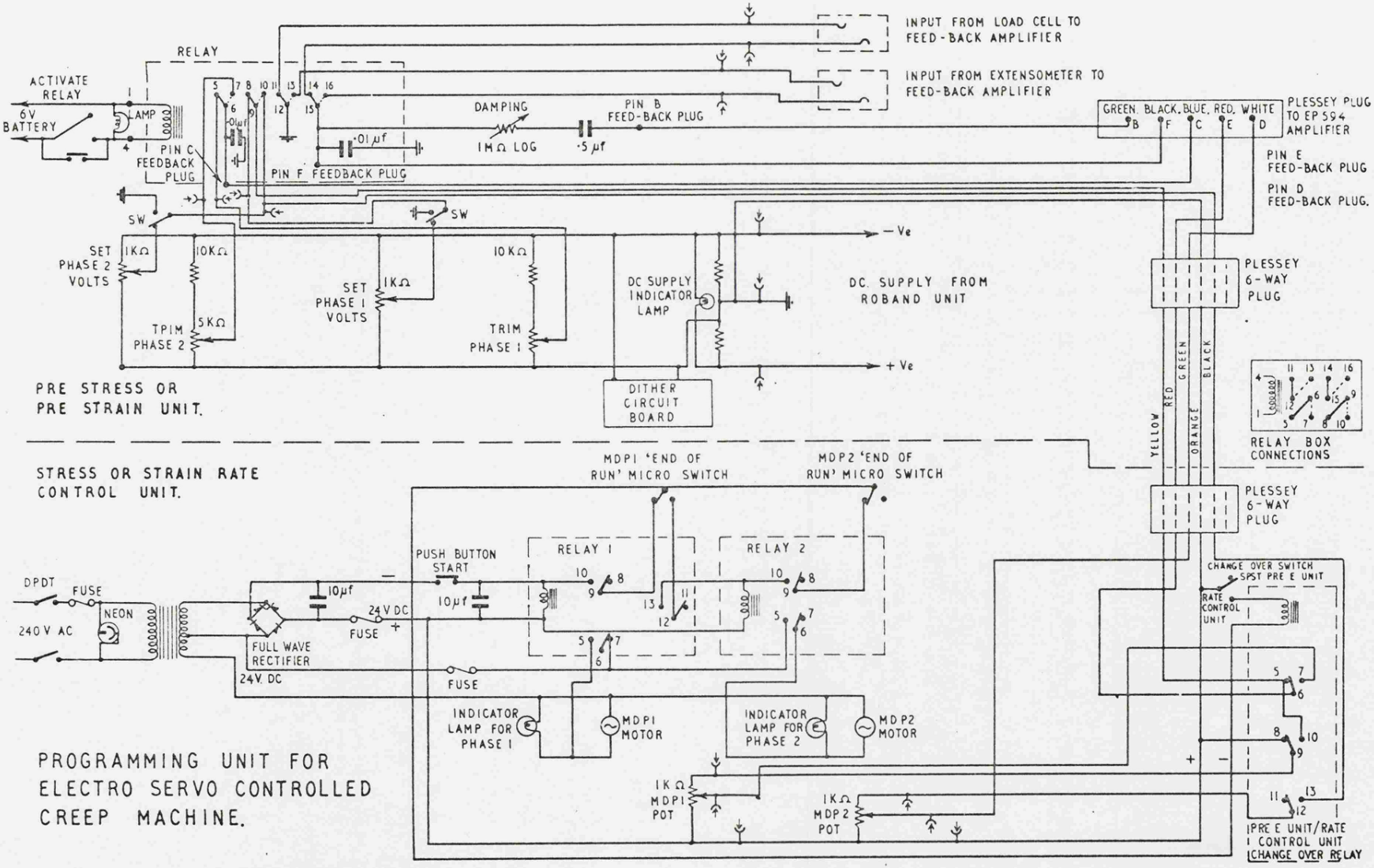

FIGURE 2 (APPENDIX 1)

4. The carrier amplifiers for both load and strain transducers are set to the correct range and attenuation. Full scale deflection on these is one volt but by adjustment this can be made proportional to any value of load or strain.

5. Activating the relay connects the Phase 1 voltage and the extensometer voltage to the summing (feed back) amplifier causing the ram to move until zero voltage is applied to it. At this time the relay is de-activated which disconnects the previous inputs and connects the Phase 2 voltage and the load transducer to the summing amplifier. The load necessary to cause the pre-strain is now decayed to the creep load. Weights can now be added to the 'pan' on the beam of the creep machine and as each is added the load cell voltage will change causing the ram to decrease its pull. When the last weight is in position the ram ceases to apply tension and it may be switched off. The rate of application of the strain or the load under these conditions is always rapid and occurs in less than 1 second. If a controlled rate is required e.g. for slow pre-straining or for long term straining at a specific rate the Rate Control unit is used.

This employs motorised potentiometers which, by selecting the appropriate range on the extensometer amplifier, can apply strain rates down to 10^{-6} cm/cm/hr. The required control voltage is applied across the potentiometers. This is then driven at a predetermined speed to change the output voltage at a controlled rate. At the end of its run a second potentiometer can be coupled automatically. Thus extended runs at a given strain rate can be made or the rate can be changed when the second potentiometer becomes operative.

A changeover relay permits combinations of the pre-strain and rate functions to be performed. A limitation is the ability of the ram valve to discriminate between background 'noise' and a slowly changing

signal voltage. This is partially overcome by use of a 'dither' circuit to apply a rapidly changing signal which the ram cannot follow thus swamping noise. Further improvement is achieved by the use of carefully matched transducers, temperature compensation and reduction of drift in the carrier amplifiers for the transducers.

APPENDIX 2

Extensometer

Figure 1 (Appendix 2) shows the general view of a complete extensometer. The extensometer is attached to the specimen by collets gripping ridges machined at the end of the gauge length. Yoke pieces at top and bottom carry the actuating rods, two to each yoke, which operate the displacement transducers. The rods from the top yoke incorporate a piece of the test material, equal in length to the gauge length, this removes differential expansion errors. The upper rods pass through tubes attached to the lower yoke pieces and actuate the strain transducers.

Also attached to the lower yoke piece are a pair of tubes containing fixed rods which actuate a second pair of transducers. This second pair only show a change in reading if there is a change in temperature below the gauge length. Such changes, due to ambient excursions etc., have been shown to affect the overall accuracy on sensitive ranges.

The transducers are connected electrically, first as a pair of strain and temperature ones in an opposite sense to cancel temperature variations. Secondly the output of a strain/temperature pair is fed into a unit which adds the inputs and divides by a factor of two. This latter function is to compensate for rocking of the yoke pieces.

This combination has been shown to be remarkably stable enabling strains of 10^{-6} inches to be monitored over long periods.

An essential requirement is that the transducers are carefully matched. Provided that matching is good and that the transducers are set properly so that the electrical and mechanical zeros are co-ordinated, tests may be carried out without good ambient temperature control. A full description of the equipment and the tests upon it is given by Walters (1970)[68].

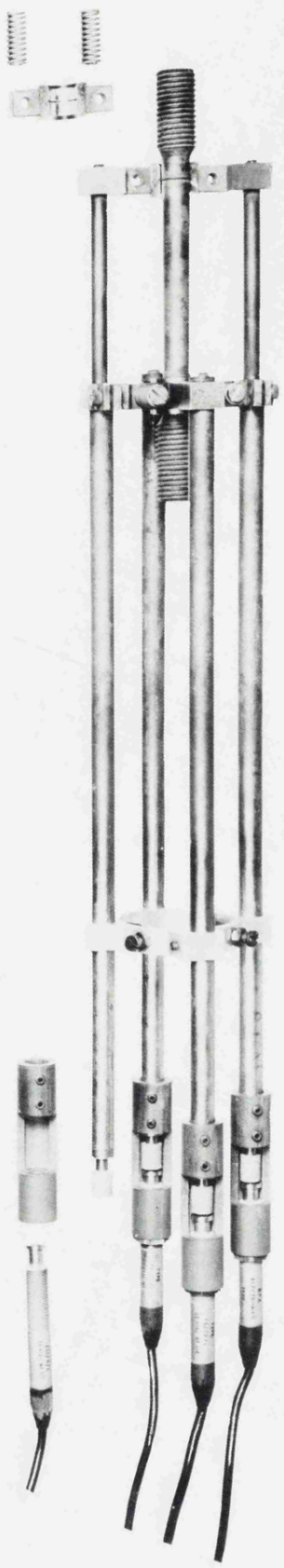

FIGURE 1 (APPENDIX 2) THE EXTENSOMETER USED IN THE TESTS (WALTERS)

APPENDIX 3

Density Measurement Techniques

Philosophy

The technique selected is that developed by Ratcliffe (1956) and is a differential method utilising Archimedes principle. In this method the test specimen is compared with a dummy which is preferably of similar material and in this particular case was an untested specimen. The masses of these may however be different. These are weighed in air and in liquid before testing and as often as required during the test. The density change is then given by

$$\frac{\Delta\rho}{\rho} = \frac{W(w - w_L)}{w(W - W_L)} - \frac{W_F(w_F - w_{FL})}{w_F(W_F - W_{FL})}$$

where W and W_L are the initial weight of the specimen in air and liquid respectively, and w and w_L are the initial weight of the dummy in air and liquid. Final weighings are identified by the subscript F.

Since the density of the liquid and of air are not included in the calculation, changes in these may be ignored. However it was considered prudent to eliminate such changes as much as possible using simple methods and so air currents were excluded even though the room was held nominally to $\pm 2^{o}C$. Heat sinks were immersed in the liquid and equilibrating times of at least an hour were used once the specimen was placed in the chamber. Pairs of weighings were then concluded as quickly as possible. Other factors which would affect accuracy were the amount of the suspension immersed and the effect of surface tension.

Apparatus

Figure 1 (Appendix 3) gives a general view of the equipment used. A Stanton CL5D single pan balance capable of weighing to 1×10^{-5} gms was adapted for under pan weighing. As shown, it is enclosed in a perspex box, with hand holes, supported on a brick and concrete plinth

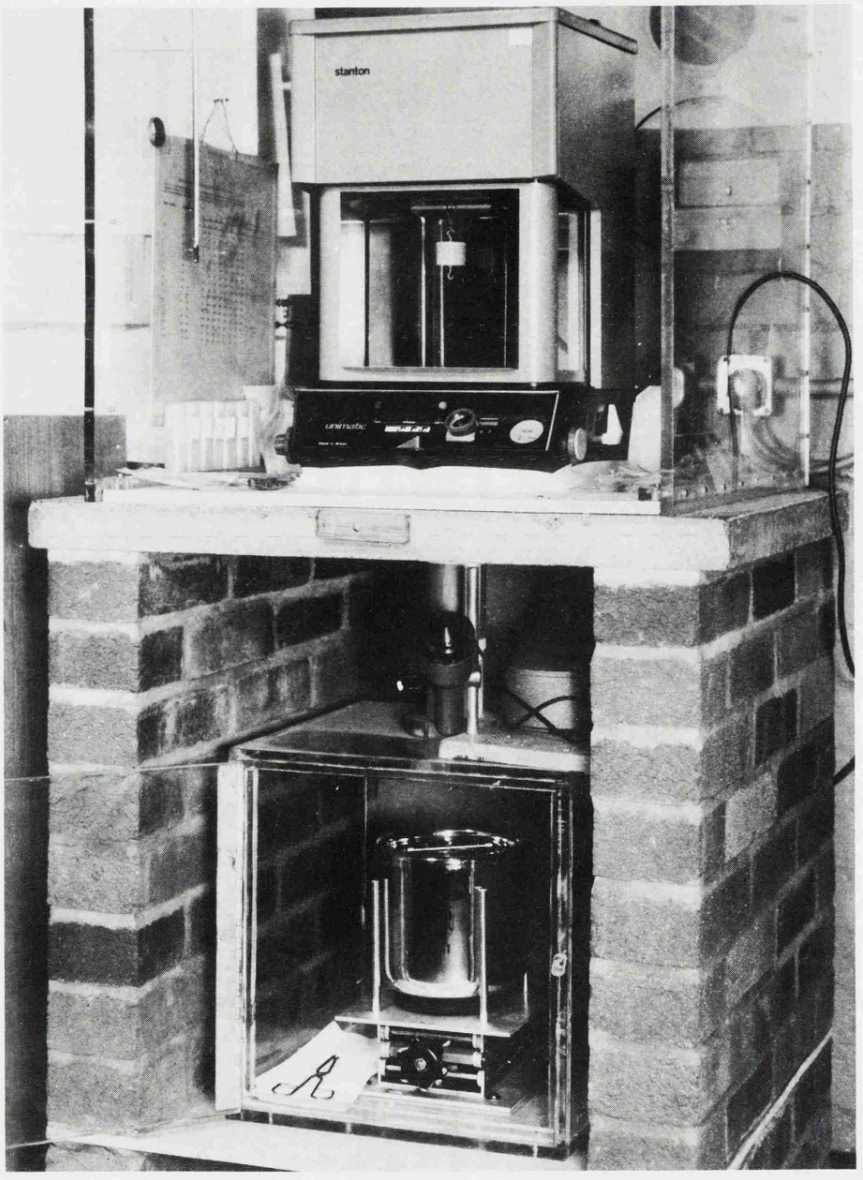

FIGURE 1 APPENDIX 3 THE DENSITY MEASUREMENT APPARATUS

standing on anti-vibration pads. A second platform supports the liquid container which contains diethyl pthalate. This liquid is employed because of its low surface tension, low volatility and good stability. The container is a highly evacuated custom built thermos bowl mounted on a Labjack for raising and lowering. Within the bowl copper blocks provide a heat sink as a precuation against rapid temperature changes. A $\frac{1}{2}$ in. thick perspex box encloses the bowl and jack and is connected by a 'chimney' to the balance chamber above. From the balance a 70 μm tungsten wire leads to a hook above the thermos bowl. A cradle, made largely of the same 70 μm wire is suspended from the hook. The only parts of the suspension subject to surface tension in practice are two strands of 70 μm wire. In order to ensure that the same volume of suspension is immersed in the liquid a vertical pointer made of the 70 μm wire is fixed below the hooks but above the cradle. With the liquid surface illuminated the bowl is raised until the pointer just attracts a meniscus, this plus the single suspension strain are the points affected by surface tension, Figure 2 (Appendix 3).

These precautions against experimental error are also supplemented by ensuring that the specimens are oxide free and that both they and the dummy are ultrasonically cleaned and dried in alcohol prior to weighing.

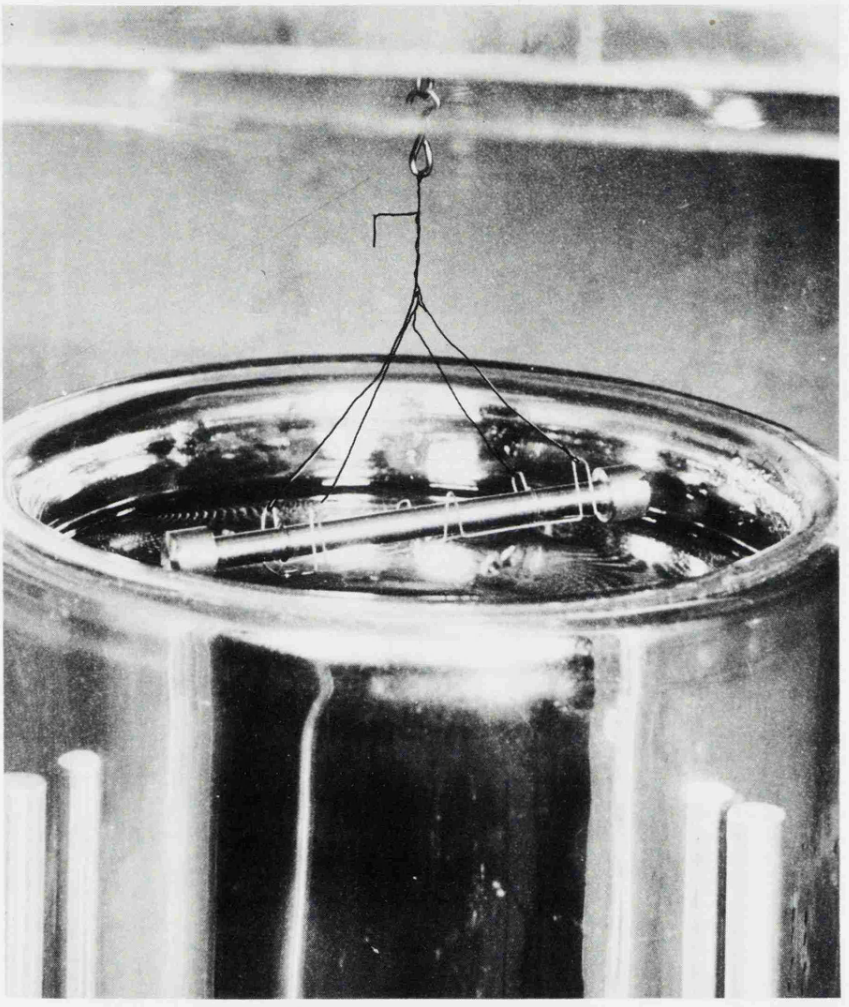

FIGURE 2 APPENDIX 3 DETAIL OF THE SUSPENSION FOR DENSITY MEASUREMENT

APPENDIX 4

Metallographic Techniques

Optical Metallography

Specimens were polished down to 600 mesh grit on water lubricated silicon carbide paper.

Final polishing was effected on diamond impregnated laps using 6 μm to 0.25 μm diamond paste.

Ultrasonic cleaning was used between each operation.

Etching was carried out electrolytically using 5% hydrochloric acid in Analar methanol at 5 v. This has been found to delineate the structure without attacking the carbides.

Replicas for Electron Metallography

A general method of preparing replicas is to polish and etch the surface. Then immerse a piece of Bexfilm in acetone until soft, this is then laid on the surface and left for 15 minutes. After this time the film may be removed and sellotaped face up on a microscope slide. Carbon is deposited and the replica shadowed using gold-palladium.

The replica may then be cut into small pieces which are placed on grids, on filter paper in a shallow dish. The paper is folded at one side to raise it slightly into an inclined plane. Acetone is poured into the dish and allowed to soak up to the grids which are not immersed but kept moist. When the plastic has apparently disappeared and the grids can be lifted without sticking they should be placed on a clean paper in fresh acetone to complete the removal of plastic. A final immersion in acetone may be necessary.

This method is very useful if (a) limited replicas are available, (b) particularly if it is desired to examine a specific portion. If the latter is the case the replica can be examined and cut under a microscope.

Extraction Replicas for Electron Metallography

The surface is polished and etched for 2 seconds. Carbon is then deposited on the surface for 2 seconds under a vacuum of about 1 - 2 x 10^{-4} torr with as little vibration as possible and using a carbon point which has been filed down to about 1.5 mm diameter over a length of at least 0.5 cm. A strong film results which holds particles of less than 100Å diameter and certainly up to about 5,000Å very well indeed.

The carbon film is then scored with a scalpel blade into small squares. The specimen is then immersed in the etchant again and re-etched until pieces of film are detached. These pieces are transferred to clean Analar methanol and may be picked up on grids or, if they are rolled up, straightened in distilled water.

Examination of the extraction replicas necessitated a technique which would permit the size to be determined accurately if possible. In this case the magnification is thought to be within 3 or 4% of that stated but all photographs were taken under the same conditions in the microscope to provide at least a good comparative study. Magnification in electron microscopes is extremely difficult to measure accurately and even methods such as the placing of polystyrene balls on the specimen is suspect.

APPENDIX 5

Ansell and Weertman's Model for Creep of a Dispersion - Hardened Material

This model was proposed to explain the dependence of creep rate upon particle spacing in an aluminium alloy hardened with a fine dispersion of alumina (Ansell and Weertman 1959)[1].

In the model the rate controlling process is the climb of dislocations over particles in the matrix. They assume a three dimensional network of dislocations providing sources, this would seem viable since deformation and a generation mechanism for dislocations must exist. They consider creep at low, high and very high stresses with the dividing line between low and high stresses defined by the fact that at low stresses dislocations cannot be forced past particles. The low stress analysis is valid in cases where

$$\frac{\mu b}{L} < \sigma < \frac{\mu b}{\lambda}$$

where μ is shear modulus, b Burgers vector, L length of a Frank-Read source and λ particle spacing. In the tests described in this thesis the high stress analysis is the correct one. Figure 1 (Appendix 5) gives a schematic representation of the high stress process. Dislocations are forced past particles and in doing so leave pinched off loops around them. The creep rate is defined by the rate at which these loops climb and are eventually annihilated. This process is in turn dependent upon the vacancy flux. In Ansell and Weertman's model it is assumed that the matrix-particle interface can be a source or sink for vacancies and that a flow will occur between dislocations and the interface.

The rate of annihilation of loops is estimated as follows. Loops climb because of the interaction between the piled-up loops, the

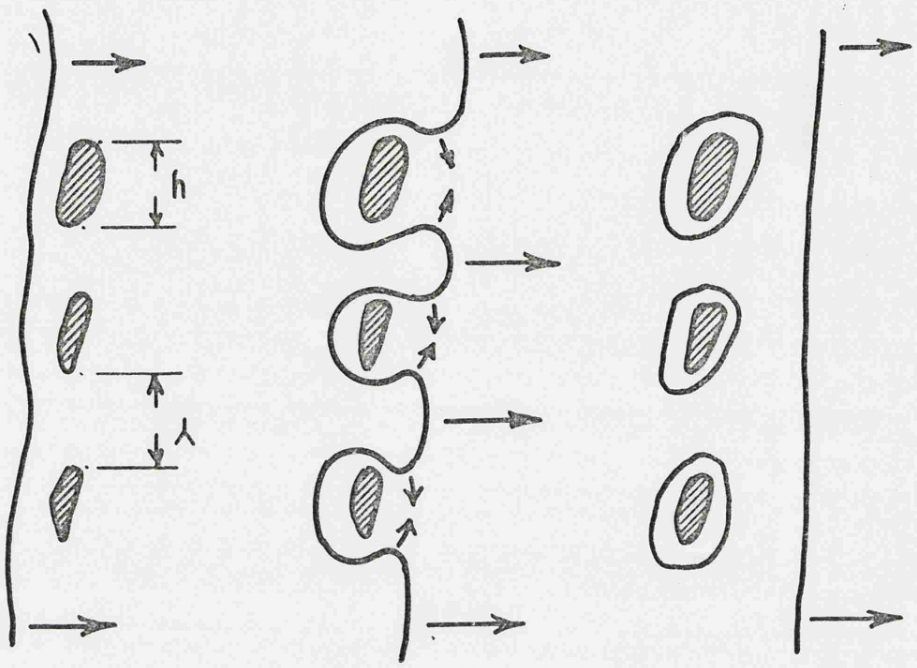

(a)

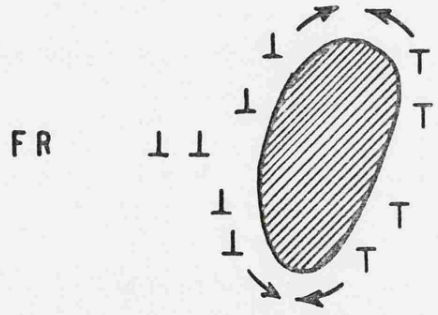

(b)

CREEP PROCESSES AT HIGH STRESS;
(a) PINCHING OFF OF DISLOCATION LOOPS;
(b) CLIMB OF DISLOCATION AROUND PARTICLE.

FIGURE 1 APPENDIX 5

dislocation line and the particle. If n loops are piled-up in the distance λ then the value of n is given by

$$n \approx \frac{2.\sigma.\lambda}{b.\mu} \tag{1}$$

The distance a loop must climb (Λ) before another loop is pinched off is approximately

$$\Lambda \approx \frac{\mu.b}{n.\sigma} \approx \frac{\mu^2.b^2}{2.\sigma^2.\lambda} \tag{2}$$

The rate of climb of the loop is given by

$$\nu = \frac{2.\sigma^2.b.\lambda.D}{\mu.k.T} \tag{3}$$

by combining the equations (2) and (3) we obtain a value for R, the generation rate of dislocations at a source,

$$R = \frac{4.\sigma^4.\lambda^2.D}{b.\mu^3.k.t} \tag{4}$$

R originally appeared in the low stress creep rate equation

$$\dot{\varepsilon} = M.\pi.\zeta^2.b.R \tag{5}$$

where M is the density of sources and ζ the maximum radius.

ζ is defined as

$$\zeta = \sqrt{\tfrac{1}{2}.M.h} \tag{6}$$

If the last equations (4), (5) and (6) are combined the creep rate at high stress is

$$\dot{\varepsilon} = \frac{2.\pi.\sigma^4.\lambda^2.D}{h.\mu^3.k.T} \tag{7}$$

Which is valid up to stresses where $n.\sigma.b^3/k.T$ becomes greater than one. At this stage the velocity ν changes and is given by

$$\nu = \left(\frac{D}{2b}\right) \exp\left(\frac{n.\sigma.b^3}{k.T}\right) \tag{8}$$

resulting in a modified expression for $\dot{\varepsilon}$ which is not applicable to these results.